Shape Selection in the non-Euclidean Model of Elasticity

by

John Gemmer

A Dissertation Submitted to the Faculty of the

Graduate Interdisciplinary Program in Applied Mathematics

In Partial Fulfillment of the Requirements
For the Degree of

Doctor of Philosophy

In the Graduate College

The University of Arizona

2 0 1 2

THE UNIVERSITY OF ARIZONA
GRADUATE COLLEGE

As members of the Dissertation Committee, we certify that we have read the dissertation prepared by John Gemmer entitled Shape Selection in the Non-Euclidean Model of Elasticity and recommend that it be accepted as fulfilling the dissertation requirement for the Degree of Doctor of Philosophy.

_____ Date: April 16, 2012
Shankar Venkataramani

_____ Date: April 16, 2012
Michael Tabor

_____ Date: April 16, 2012
David Glickenstein

_____ Date: April 16, 2012
Alan Newell

Final approval and acceptance of this dissertation is contingent upon the candidate's submission of the final copies of the dissertation to the Graduate College.

I hereby certify that I have read this dissertation prepared under my direction and recommend that it be accepted as fulfilling the dissertation requirement.

_____ Date: April 16, 2012
Shankar Venkataramani

Statement by Author

This dissertation has been submitted in partial fulfillment of requirements for an advanced degree at The University of Arizona and is deposited in the University Library to be made available to borrowers under rules of the Library.

Brief quotations from this dissertation are allowable without special permission, provided that accurate acknowledgment of source is made. Requests for permission for extended quotation from or reproduction of this manuscript in whole or in part may be granted by the head of the major department or the Dean of the Graduate College when in his or her judgment the proposed use of the material is in the interests of scholarship. In all other instances, however, permission must be obtained from the author.

Signed: John Alan Gemmer

Dedication

This dissertation is dedicated to my mother, Aretta, who taught me humility and patience and whose passion for history encouraged me to pursue a life of learning; my father, Daniel, who instilled upon me a strong work ethic, a desire to always better myself, and the courage to ask questions; and most of all to Nichole, who has always supported and encouraged me throughout college and graduate school.

Acknowledgments

I am very lucky to have travelled this far academically and there are many who deserve to be acknowledged for helping me along the way. I strongly believe that without these individuals guidance I would have never succeeded in mathematics.

First, I must graciously thank and acknowledge Mr. Myron Price. In a high school were there were no advanced placement courses, where proficiency in typing consisted of mastering the intricacies of an actual typewriter, and computer science meant learning Applesoft on a 1986 Apple IIgs, Mr. Price taught a course in Calculus. This has and always will be the best mathematics course I have ever taken. Although he and I were unaware of it at the time, this course awakened in me a burning desire to pursue a career in mathematics and science. I must also apologize for all of the immature pranks I played on him. I was bored.

Second, I would like to acknowledge the wonderful instructors in mathematics and physics I had at Millersville University of Pennsylvania. The courses and independent studies I took from Drs. Robert Buchanan, Zenaida Uy, Michael Nolan, Zhoude Shao, Ron Umble, John Dooley, Patrick Cooney, Ximena Catepillan, Bruce Ikenaga, Dorothy Blum, and Noel Heitmann were a wonderful source of intellectual stimulation and I will forever treasure them. I would also like to especially acknowledge Drs. Ron Umble and Michael Nolan who served as mentors for my undergraduate thesis, a truly invaluable experience that introduced me to research in the mathematical sciences.

Third, I would like to thank Dr. Michael Tabor and the Interdisciplinary Program in Applied Mathematics at the University of Arizona. Dr. Tabor works tirelessly behind the scenes to provide financial support for students in the applied mathematics program and is our greatest advocate.

Finally, and most importantly, I acknowledge and thank my advisor Dr. Shankar Venkataramani. I have learned an incredible amount from Dr. Venkataramani and I

am very blessed to have had an adviser in the mathematics department who has the same broad interests in mathematics and physics that I have. I also feel very lucky to have had an adviser who had the patience and understanding to work with me as my mathematical and professional skills developed.

Table of Contents

TABLE OF CONTENTS—*Continued*

List of Figures

List of Tables

Abstract

In this dissertation we investigate the behavior of radially symmetric non-Euclidean plates of thickness t with constant negative Gaussian curvature. We present a complete study of these plates using the Föppl-von Kármán and Kirchhoff reduced theories of elasticity. Motivated by experimental results, we focus on deformations with a periodic profile.

For the Föppl-von Kármán model, we prove rigorously that minimizers of the elastic energy converge to saddle shaped isometric immersions. In studying this convergence, we prove rigorous upper and lower bounds for the energy that scale like the thickness t squared. Furthermore, for deformation with n-waves we prove that the lower bound scales like nt^2 while the upper bound scales like n^2t^2. We also investigate the scaling with thickness of boundary layers where the stretching energy is concentrated with decreasing thickness.

For the Kichhoff model, we investigate isometric immersions of disks with constant negative curvature into $\mathbb{R}^3$, and the minimizers for the bending energy, i.e. the L^2 norm of the principal curvatures over the class of $W^{2,2}$ isometric immersions. We show the existence of smooth immersions of arbitrarily large geodesic balls in $\mathbb{H}^2$ into $\mathbb{R}^3$. In elucidating the connection between these immersions and the non-existence/singularity results of Hilbert and Amsler, we obtain a lower bound for the L^∞ norm of the principal curvatures for such smooth isometric immersions. We also construct piecewise smooth isometric immersions that have a periodic profile, are globally $W^{2,2}$, and numerically have lower bending energy than their smooth counterparts. The number of periods in these configurations is set by the condition that the principal curvatures of the surface remain finite and grow approximately exponentially with the radius of the disc.

Chapter 1
Introduction

1.1 The non-Euclidean Model of Differential Growth

Laterally swelling and shrinking thin elastic sheets are ubiquitous in nature and industry and are capable of forming complex surfaces of various geometries. The examples shown in figure 1.1 include shapes formed by differential growth, thermal expansion, and the inhomogeneous swelling of hydrogels. The morphology of these structures is a result of "incompatible" growth in which the growing body adds regions of local tension or compression to prevent cavitation and interpenetration of the material (Goriely & Ben Amar, 2005; Amar & Goriely, 2005; McMahon, 2009). The regions of tension and compression manifest themselves as residual stress in the body, that is stresses that remain in the body in the absence of external forces.

Because of the large deformations possible during the growth or swelling process, many mathematical models of such processes are set within the framework of finite elasticity. One such model, which we call the growth tensor model, borrows from elasto-plasticity theory and decomposes the overall deformation of the body into a growth step and an elastic response (Rodriguez et al., 1994). The growth step is characterized by a tensor G that measures how the infinitesimal material lines of the original body change during the growth. The elastic response is a tensor A that distorts the grown body so that the product $A \cdot G$ forms the gradient of a true deformation of the body. In this model the growth is incompatible if G is not a deformation gradient and the residual stresses in the body depend only on the elastic response A.

The growth tensor model has been placed on a more rigorous foundation inde-

(a) (b)

(c)

FIGURE 1.1. (a) A hybrid species of the Echeveria plant. The rippling near the boundary is caused by local differential growth and has been the focus of several works (Marder et al., 2003; Audoly & Boudaoud, 2002, 2003; Liang & Mahadevan, 2009) (Image of Stuart Kent). (b) The heating and subsequent drying of potato chips generates shapes with a hyperbolic geometry. (c) N-isopropylacrylamide (NIPA) hydrogel disk that has undergone controlled shrinking (Klein et al., 2007) (Image courtesy of Rebecca Stockbridge). Hydrogels replicate many of the characteristic features present in differential growth and are excellent tools for studying such processes quantitatively.

pendent of its origin in elasto-plasticity theory (Hoger, 1997; Chen & Hoger, 2000; Lubarda & Hoger, 2002; DiCarlo & Quiligotti, 2002) and has been successfully used to study morphogenesis in growing soft tissue. In particular it has been used to study buckling patterns in growing shells (Goriely & Ben Amar, 2005; Amar & Goriely, 2005), growing cylinders (Vandiver & Goriely, 2008; Goriely et al., 2008), and growing thin sheets (Dervaux & Ben Amar, 2008).

Another model of such swelling bodies hypothesizes that the equilibrium configuration is the minimum of a "non-Euclidean" free energy functional $E_{3d} : W^{1,2}(\mathcal{D}_{3d}, \mathbb{R}^3) \to \mathbb{R}$ defined by

$$E_{3d}[\mathbf{x}_{3d}] = \int_{\mathcal{D}_{3d}} \| \left(\nabla \mathbf{x}_{3d}\right)^T \cdot \nabla \mathbf{x}_{3d} - \mathbf{g}_{3d} \|^2 \, dV, \tag{1.1.1}$$

that measures strains from a fixed three-dimensional Riemannian metric $\mathbf{g}_{3d}$ defined on a simply connected domain $\mathcal{D}_{3d} \subset \mathbb{R}^3$ (Audoly & Boudaoud, 2003; Marder et al., 2003; Sharon et al., 2004; Marder & Papanicolaou, 2006; Efrati et al., 2007, 2009; Lewicka & Pakzad, 2011). The metric $\mathbf{g}_{3d}$ encodes how the swelling changes the intrinsic distance between nearby material points and this model is essentially the same as the growth tensor formalism with the correspondence between the models given by $\sqrt{\mathbf{g}_{3d}} = G$ (Lewicka & Pakzad, 2011). The intuition behind the non-Euclidean model is that the deformation of the growing body is described by a map $\mathbf{x}_{3d} \in W^{1,2}(\mathcal{D}_{3d}, \mathbb{R}^3)$ that is "close as possible" to an isometric immersion of the metric $\mathbf{g}_{3d}$ (see figure 1.2). Furthermore, the energy E_{3d} can vanish if and only if the Riemannian curvature tensor $\mathcal{R}$ corresponding to $\mathbf{g}_{3d}$ vanishes and thus the growth is "incompatible" if and only if $\mathcal{R} \neq 0$ (McMahon, 2009; Lewicka & Pakzad, 2011).

Laterally swelling thin elastic sheets of thickness t can be modelled in the non-Euclidean framework by a two dimensional Riemannian metric $\mathbf{g}$ defined on the mid-surface of the sheet $\mathcal{D} \subset \mathbb{R}^2$. That is, $\mathcal{D}_{3d}$ can be decomposed as $\mathcal{D}_{3d} = \mathcal{D} \times (-t/2, t/2)$ and in an appropriate coordinate system $\mathbf{g}_{3d}$ is given by

$$\mathbf{g}_{3d} = \begin{pmatrix} \mathbf{g} & 0 \\ 0 & 1 \end{pmatrix}. \tag{1.1.2}$$

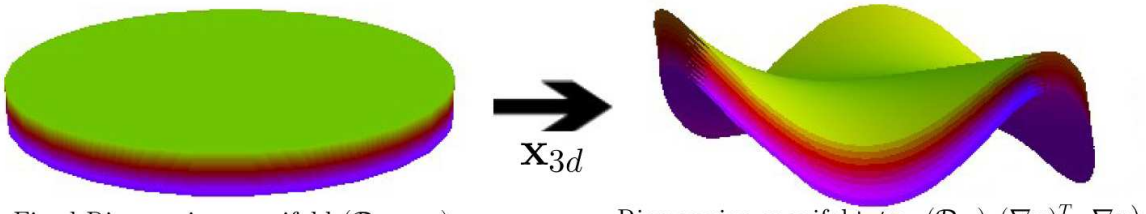

Fixed Riemannian manifold $(\mathcal{D}_{3d}, \mathbf{g}_{3d})$.

Riemannian manifold $(\mathbf{x}_{3d}(\mathcal{D}_{3d}), (\nabla \mathbf{x})^T \cdot \nabla \mathbf{x})$ with induced Riemannian metric from $\mathbb{R}^3$.

FIGURE 1.2. In the non-Euclidean model of elasticity the deformed body selects a configuration that minimizes a strain energy functional measuring the difference between the deformation's induced metric from $\mathbb{R}^3$ and a fixed metric $\mathbf{g}_{3d}$. The metric $\mathbf{g}_{3d}$ measures the intrinsic infinitesimal length between material coordinates induced by the growth.

Furthermore, for this form of the metric, "incompatible growth" corresponds to when the Gaussian curvature K corresponding to $\mathbf{g}$ satisfies $K \neq 0$ (Lewicka & Pakzad, 2011).

The non-Euclidean model of elasticity has grown out of experiments that studied the self-similar rippling patterns observed along the edges of torn elastic sheets and leaves (Sharon et al., 2002). This rippling pattern was studied in the rectangular strip geometry by applying the non-Euclidean model with a metric $\mathbf{g}$ defined on the mid-surface that only differs substantially from the Euclidean metric in a small region near one edge of the strip (Marder et al., 2003; Audoly & Boudaoud, 2002, 2003). In particular, it was shown numerically that the self similar patterns could be explained as being approximate isometric immersions of the abstract Riemannian manifold $(\mathcal{D}, \mathbf{g})$ that minimize a bending energy functional (Audoly & Boudaoud, 2003).

1.2 Reduced Theories of non-Euclidean Elasticity

In many applications the thickness of latterly swelling sheets is much smaller then the diameter of $\mathcal{D}$. Consequently, there is considerable interest in obtaining reduced

energy functionals E_t defined on a suitable space of mappings of the mid-surface $\mathcal{D}$ into $\mathbb{R}^3$ such that minimizers of E_t approximate minimizers E_{3d} in an appropriate asymptotic limit of vanishing thickness. For the classical theory of plates, i.e., when $\mathbf{g}$ is the Euclidean metric, one such reduced model is the so called Föppl-von Kármán equations that reduce the full three dimensional equations of elasticity to a coupled system of partial differential equations defined on the mid-surface of the plate (Föppl, 1907). These equations are valid in an asymptotic limit of vanishing thickness in which the thickness scales in a particular manner with external loadings (Ciarlet, 1980) and different scalings lead to a hierarchy of plate models that includes Föppl-von Kármán (Friesecke et al., 2006). For non-Euclidean plates, there are two reduced theories that have recently been rigorously obtained as asymptotic limits using the technique of Gamma-convergence: the Kirchhoff model (Lewicka & Pakzad, 2011) and the (non-Euclidean) Föppl-von Kármán (FvK) model (Lewicka et al., 2011).

In the Kirchhoff model, if the set of $W^{2,2}$ isometric immersions of the mid-surface is non-empty, that is $\mathcal{A}_{\mathrm{Ki}} = \{\mathbf{x} \in W^{2,2}(\mathcal{D}, \mathbb{R}^3) : (D\mathbf{x})^T \cdot D\mathbf{x} = \mathbf{g}\} \neq \emptyset$, then

$$\Gamma - \lim_{t \to 0} \frac{1}{t^2} E_{3d} = E_{\mathrm{Ki}},$$

with the curvature functional $E_{Ki} : W^{2,2}(\mathcal{D}, \mathbb{R}^3) \to \mathbb{R}$ defined by

$$E_{Ki}[\mathbf{x}] = \begin{cases} \dfrac{Y}{24(1+\nu)} \displaystyle\int_{\mathcal{D}} \left[\frac{4H^2}{1-\nu} - 2K \right] dA_{\mathbf{g}} & \text{if } \mathbf{x} \in \mathcal{A}_{Ki} \\ \infty & \text{if } \mathbf{x} \notin \mathcal{A}_{Ki} \end{cases},$$

where Y and ν are the Young's modulus and Poisson ratio of the material respectively, H and K mean and Gaussian curvatures of the surface $\mathbf{x}(\mathcal{D})$ respectfully, and $dA_{\mathbf{g}}$ the area form induced by $\mathbf{g}$ (Lewicka & Pakzad, 2011). This reduced theory captures the intuition that in the vanishing thickness limit if a $W^{2,2}(\mathcal{D}, \mathbb{R}^3)$ isometric immersion of the mid-surface $\mathcal{D}$ exists then in the vanishing thickness limit the mid-surface should deform into an isometric immersion with a low amount of bending energy. The Kirchhoff model has been used to generate pseudospherical surfaces of

constant negative Gaussian curvature from closed curves (Trejo et al., 2009) which has applications to the modelling of growing bodies with a tubular topology.

The FvK model, which is sometimes called the *small slope approximation*, has also been rigorously derived as a Γ-limit when the following assumptions are met:

1. The metric $\mathbf{g}$ satisfies the following scaling $\mathbf{g} = \mathbf{g}_0 + t^2\mathbf{g}_1$, where $\mathbf{g}_0$ is the Euclidean metric.

2. The deformation of the mid-surface $\mathbf{x} : \mathcal{D} \to \mathbb{R}^3$ satisfies an "in-plane" and "out-of-plane" decomposition of the form

$$\mathbf{x} = i + ti_\perp \circ \eta + t^2 i \circ \chi,$$

where $\chi \in W^{1,2}(\mathcal{D}, \mathbb{R}^2)$, $\eta \in W^{2,2}(\mathcal{D}, \mathbb{R})$, $i : \mathbb{R}^2 \to \mathbb{R}^3$ is the standard immersion and $i_\perp$ maps into the orthogonal compliment of $i(\mathbb{R}^2)$.

In this context it is natural to define the FvK admissible set by $\mathcal{A}_{FvK} = W^{1,2}(\mathcal{D}, \mathbb{R}^2) \times W^{2,2}(\mathcal{D}, \mathbb{R})$ with the understanding that when we write that a deformation $\mathbf{x} : \mathcal{D} \to \mathbb{R}^3$ satisfies $\mathbf{x} \in \mathcal{A}_{FvK}$ we mean that there exists $(\chi, \eta) \in \mathcal{A}_{FvK}$ such that $\mathbf{x} = i + ti_\perp \circ \eta + t^2 i \circ \chi$. The *in-plane strain tensor* $\gamma : \mathcal{A}_{FvK} \to \mathbb{R}^{2\times 2}$ is defined in this approximation by

$$\gamma(\chi, \eta) = (D\chi)^T + D\chi + (D\eta)^T \cdot D\eta - \mathbf{g}_1, \tag{1.2.1}$$

which measures to $\mathcal{O}(t^2)$ the deviation of $\mathbf{x}$ from being an isometric immersion.

The reduced energy under the above assumptions is given by the following Γ-limit:

$$\Gamma - \lim_{t\to 0} \frac{1}{t^4} E_{3d} = E_{FvK},$$

with $E_{FvK} : \mathcal{A}_{FvK} \to \mathbb{R}$ defined by

$$E_{FvK}[\mathbf{x}] = \frac{Y}{8(1+\nu)} \int_{\mathcal{D}} Q(\gamma)\, dA + \frac{Y}{24(1+\nu)} \int_{\mathcal{D}} Q(D^2\eta)\, dA, \tag{1.2.2}$$

where $Q : \mathbb{R}^{2\times 2} \to \mathbb{R}$ is the quadratic form

$$Q(A) = (1-\nu)^{-1}\mathrm{tr}(A)^2 - 2\det(A),$$

$D^2\eta$ the Hessian matrix of second derivatives of η and dA the Euclidean area form (Lewicka et al., 2011). This energy can be interpreted as approximating E_{3d} by an energy that is the additive decomposition of a *stretching energy functional* S_{FvK} : $\mathcal{A}_{FvK} \to \mathbb{R}$ measuring the lowest order elastic energy of the in-plane components of the in-plane strain $(D\mathbf{x})^T \cdot D\mathbf{x} - \mathbf{g}$ and a *bending energy functional* $B_{FvK} : \mathcal{A}_{FvK} \to \mathbb{R}$ measuring the lowest order approximation of E_{Ki}. Additionally, in this approximation, the terms $\Delta\eta$ and $\det(D^2\eta)$ correspond to the mean and Gaussian curvatures respectfully. The Euler-Lagrange equations generated by the variation of E_{FvK} are a modified version of the classical FvK equations that have been used to model morphogenesis in soft tissue (Dervaux & Ben Amar, 2008; Liang & Mahadevan, 2009). Moreover, the FvK equations have been used to study the following phenomenon observed in thin elastic sheets: crumpling (Lobkovsky, 1996; Venkataramani, 2004; Conti & Maggi, 2008), blistering (Jin & Sternberg, 2001; Jin & Sternberg, 2002), and wrinkling (Cerda & Mahadevan, 2003; Davidovitch et al., 2011).

1.3 Hydrogels and the Hyperbolic Plane

There is considerable interest in using the non-Euclidean elasticity to model the equilibrium shapes of swelling hydrogels. Hydrogels have received a lot of attention because of their ability to undergo large reversible deformations by differentially swelling when activated by external stimuli such as pH (Feil et al., 1992), light (Juodkazis et al., 2000), warm water (Klein et al., 2007) and solvents (Holmes et al., 2011). This type of activated morphogenesis has already been used in applications ranging from site specific delivery of drugs (Brndsted & Kopecek, 1991), scaffolding in cellular engineering (Rowley et al., 1999), and the construction of microfluidic devices such as valves (Arndt et al., 2000; Yu et al., 2003), pumps (Richter et al., 2004), and actuators (Richter et al., 2008; Carpi & Smela, 2009). Moreover, hydrogels are being explored as candidates for self assembling devices at the micro and nanoscale

(Schmidt & Eberl, 2001; Alben & Brenner, 2007; Zhang et al., 2010). Furthermore, because of their high water content and elastic properties swelling hydrogels are capable of mimicking the growth of soft tissue (Mora & Boudaoud, 2006; Klein et al., 2007) making them excellent experimental tools to explore the complex morphologies that can be generated by differential growth.

Recently, environmentally responsive hydrogel disks and annuli have been created using a Hele-Shaw cell to inject water, N-isopropylacrylamide (NIPA), bisacrylamide, and polymerization agents to create a cross-linked polymer gel with a radially symmetric variation of the mixture (Klein et al., 2007). These hydrogels undergo a shape transition at $T_c = 33°C$ at which point the material ejects water and shrinks differentially according to the variation of the concentration of NIPA (see figure 1.3). In terms of the non-Euclidean model the shrinking specifies a metric $\mathbf{g}$ on the mid-plane of the disk which in components is given in geodesic polar coordinates (ρ, θ) by

$$g_{11} = 1, \quad g_{12} = g_{21} = 0, \quad g_{22} = \rho^2 f(\rho), \tag{1.3.1}$$

where f is a positive function that can be controlled experimentally by varying the concentration of NIPA.

The Gaussian curvature K_0 corresponding to $\mathbf{g}$ can also be controlled and satisfies

$$K_0 = -\frac{1}{\rho f(\rho)} \frac{\partial^2}{\partial \rho^2} \left[\rho f(\rho)\right]. \tag{1.3.2}$$

Therefore, by controlling the concentration of NIPA the Gaussian curvature can be controlled as well. Regions in which $K_0 < 0$ are shrinking faster then the center of the disk and form a rippling pattern while regions in which $K_0 > 0$ shrink slower and obtain a spherical dome like shape (see figure 1.4.a). Curiously, Hydrogel disks with constant negative Gaussian curvature K_0 obtain a periodic profile of one wavelength with a refinement of the number of waves with decreasing thickness (see figure 1.4.b). The number of waves in these profiles is well fit by the power law $n \sim t^{-1/2}$ and the bending energy E_{Ki} diverges according to the scaling $E_{Ki} \sim t^{-1}$ (Klein et al., 2011).

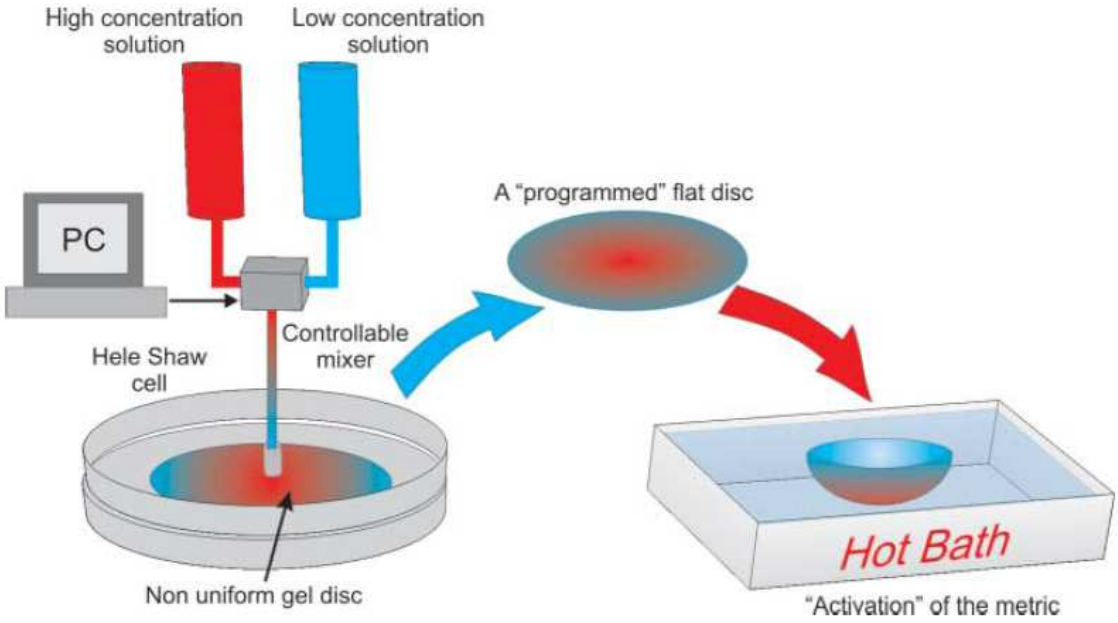

FIGURE 1.3. Non-Euclidean disks with a prescribed radially symmetric metric **g** are creating by a using hydrogels that differentially shrink when activated in a warm water bath (Klein et al., 2007). The amount of shrinking can be controlled by a computer allowing for the creation of non-Euclidean disks of various geometries.

This is in sharp contrast to the case when K_0 is constant and positive where the profile seems to be converging with decreasing thickness to a fixed shape (see figure 1.4.c), with the bending energy scaling like $E_{Ki} \sim t^0$ (Klein et al., 2011).

The observed refinement of the number of waves with decreasing thickness for non-Euclidean gels with $K_0 < 0$ constant and negative is a puzzle. In terms of the Kirchhoff model, the observed refinement seems to imply that there does not exist $W^{2,2}$ isometric immersions of bounded connected domains of the hyperbolic plane $\mathbb{H}^2$ into $\mathbb{R}^3$. Indeed, it is a classical result that there does not exist a real analytic isometric immersion of the entire hyperbolic plane $\mathbb{H}^2$ into $\mathbb{R}^3$ (Hilbert, 1901; Holmgren, 1902) but there does exist C^1 isometric immersions of $\mathbb{H}^2$ (Nash, 1954; Kuiper, 1955). Furthermore, by Efimov's theorem there does not exist C^2 isometric immersions of $\mathbb{H}^2$ (Efimov, 1964) and this difference in the regularity of isometric immersions is sometimes used to explain the rippling morphology of hydrogels with $K_0 < 0$ (Santangelo, 2009). But, for bounded domains of $\mathbb{H}^2$ there exists smooth and hence $W^{2,2}$ isometric immersions (Poznyak, 1973; Han & Hong, 2006) and thus the Kirchhoff model would seem to imply that there can be no refinement of the number of waves.

1.4 Structure of Dissertation and Summary of Main Results

In this dissertation we present a study of non-Euclidean plates in both the FvK and Kirchhoff models. Motived by the experiments on hydrogels, we focus on domains with a disk or annular geometry and metric $\mathbf{g}_{K_0}$ with corresponding constant negative Gaussian curvature K_0. The body of the dissertation is naturally organized into two chapters that present the detailed studies of these two models. In appendix A we provide a catalogue of the main definitions, equations, and theorems from the classical theory of the differential geometry of surfaces that are used throughout the dissertation.

(a) (b) (c)

FIGURE 1.4. (a) By controlling the Gaussian curvature K_0, non-Euclidean plates of different shapes can be constructed (Klein et al., 2007). In the top two images $K_0 < 0$ leading to rippled shapes. In the third image from the top $K_0 > 0$ leading to a spherical dome like shape. The hydrogel in the bottom image is a combination of an interior region with $K_0 > 0$ and an outer region with $K_0 < 0$. (b) The equilibrium shapes of hydrogel disks of constant radius of $R = 14mm$ and varying thickness ($t = .75mm$, $.6mm$, $.25mm$, and $.19mm$ from top to bottom) with a constant Gaussian curvature $K = .0011mm^{-2}$ (Klein et al., 2011). (c) The equilibrium shapes of hydrogel disks of constant radius of $R = 14mm$ and varying thickness ($t = .75mm$, $.6mm$, $.25mm$, and $.19mm$ from top to bottom) with a constant Gaussian curvature $K = -.0011mm^{-2}$ (Klein et al., 2011).

1.4.1 Main Results from the FvK Model

In chapter 2 we study the behavior of minimizers in the FvK approximation for a domain $\mathcal{D}$ that is an annulus with inner radius ρ and outer radius R over the admissible set $\mathcal{A}_n \subset \mathcal{A}_{FvK}$ of deformations with an out-of-plane displacement that has n-fold rotational symmetry for $n \in \{2, 3, \ldots\}$. The FvK elastic energy in this geometry is formulated by approximating the metric by $\mathbf{g}_{K_0} = \mathbf{g}_0 + \epsilon^2 \mathbf{g}_1$, where $\epsilon = \sqrt{-K_0}R$ is a dimensionless curvature, and assuming an in-plane and out-of-plane decomposition of the deformation in the form

$$\mathbf{x} = i + \epsilon i_\perp \circ \eta + \epsilon^2 i \circ \chi.$$

For simplicity, we then repose the resulting variational problem as the minimum of a dimensionless functional $\mathcal{E}_\tau = \mathcal{S} + \tau^2 \mathcal{B}$, where $\tau = t/(\sqrt{3}R\epsilon)$ is a dimensionless thickness.

As a basic tool for studying the minimizers of $\mathcal{E}_\tau$ we derive the Euler-Lagrange equations and its natural boundary conditions for $\mathcal{E}_\tau$. The resulting governing equations are nonlinear and in general finding exact solutions to the resulting equations is impractical. Instead, we study the convergence and scaling of minimizers through Γ-convergence techniques, direct numerical simulation, ansatz free lower and upper bounds, and asymptotic analysis.

In sections 2.3 and 2.4 we construct minimizers over the admissible sets $\mathcal{A}_f = \{\mathbf{x} \in \mathcal{A}_n : \mathcal{B}[\mathbf{x}] = 0\}$ and $\mathcal{A}_0 = \{\mathbf{x} \in \mathcal{A}_n : \mathcal{S}[\mathbf{x}] = 0\}$. The set $\mathcal{A}_f$ consists of flat deformations and the minimum is obtained by solving the Euler-Lagrange equations and its natural boundary conditions when $\eta = 0$. The set $\mathcal{A}_0$ consists of isometric immersions in the Föppl-von Kármán approximation and can be obtained by solving the following Monge-Ampere equation:

$$\det(D^2\eta) = -1. \tag{1.4.1}$$

The global minimum of $\mathcal{B}$ over solutions to (1.4.1) are obtained by the approximate

minimal surfaces $\eta = xy$ and thus we can rigorously prove using Γ-convergence techniques the following theorem:

Theorem 1.4.1. Let $\mathbf{x}_\tau^* \in \mathcal{A}_{FvK}$ be a sequence with corresponding out-of-plane displacement η_τ^* such that $\inf_{\mathbf{x}\in\mathcal{A}_{FvK}} \mathcal{E}_\tau[\mathbf{x}] = \mathcal{E}_\tau[\mathbf{x}_\tau^*]$. Then,

1. $\liminf_{\tau\to 0} \inf_{\mathbf{x}\in\mathcal{A}} \frac{1}{\tau^2}\mathcal{E}_\tau[\mathbf{x}] = \lim_{\tau\to 0} \frac{1}{\tau^2}\mathcal{E}_\tau[\mathbf{x}_\tau^*] = \inf_{\mathbf{x}\in\mathcal{A}_0} \mathcal{B}[\mathbf{x}] = 2\pi(1-\rho_0^2 R^{-2})$.
2. There exists a subsequence $\eta_{\tau_k}^*$ and $\mathbf{x}^* \in \mathcal{A}_0$ with corresponding out-of-plane displacement η^* such that $\eta_{\tau_k}^* \rightharpoonup \eta^*$. Moreover, there exists $A \in SO(2)$ and $b \in \mathbb{R}$ such that $\eta^*(A(x,y)) + b = xy$.

Furthermore, in section 2.4 we construct weak solutions to (1.4.1) with n-fold symmetry and thus $\mathcal{A}_n \cap \mathcal{A}_0 \neq \emptyset$. Using these constructions as test functions we have the following result:

Lemma 1.4.2. Let $\mathbf{x}^* \in \mathcal{A}_n$ such that $\mathcal{E}_\tau[\mathbf{x}^*] = \inf_{\mathbf{x}\in\mathcal{A}_n} \mathcal{E}_\tau[\mathbf{x}]$, then

$$\mathcal{E}_\tau[\mathbf{x}^*] \leq \min\left\{Cn^2\tau^2, \mathcal{F}\right\},$$

where $\mathcal{F} = \inf_{\mathbf{x}\in\mathcal{A}_f} \mathcal{E}_\tau[\mathbf{x}]$ and C is a constant independent of n and τ.

This lemma captures the difference in scaling of $\mathcal{E}_\tau$ with τ for flat deformations and isometric immersions by using specific test functions on $\mathcal{E}_\tau$.

In section 2.5 we numerically minimize $\mathcal{E}_\tau$ over $\mathcal{A}_n$ using a Rayleigh-Ritz type method. The results of the numerics indicate that minimizers transition from flat deformations to buckled shapes such that with decreasing thickness the deformations converge to $\mathbf{x} \in \mathcal{A}_n \cap \mathcal{A}_0$. In the bulk of the domain the stretching energy of these buckled shapes is approximately zero with regions near the edges and, for $n \geq 3$, along the lines of inflection in which stretching energy is concentrated. These results indicate that with decreasing thickness the stretching energy is concentrated in

shrinking boundary layers in which the bending energy of the isometric immersion is reduced by adding some small localized amount of stretching.

In section 2.6 we improve on lemma 1.4.2 and rigorously prove ansatz free lower bounds on $\mathcal{E}_\tau$. Specifically, we prove using Sobolev estimates the following theorem:

Theorem 1.4.3. Suppose $n \in \{2, 3, \ldots\}$ and $\tau > 0$. There exists constants c and C independent of n such that

$$\min\left\{cn\tau^2, \frac{\mathcal{F}}{2}\right\} \leq \inf_{\mathbf{x}\in\mathcal{A}_n} \mathcal{E}[\mathbf{x}] \leq \min\{Cn^2\tau^2, \mathcal{F}\}.$$

This theorem confirms the numerical results that with decreasing thickness the elastic energy of the minimizers scales like that of an isometric immersion. Furthermore, since both the upper and lower bounds in the theorem grow with n it quantifies how the elastic energy is penalized by adding more waves to a deformation.

In section 2.7 we determine the scaling with τ of the width of the boundary layers in which the stretching energy is significantly non-zero. Near the edges of the annulus the out of plane displacement can be additively decomposed into two terms that separately lower contributions to the bending energy from the mean and Gaussian curvatures. The width of the regions in which these terms are relevant satisfies the following scaling:

1. The boundary layer in which one term lowers the magnitude of the *Gaussian curvature* has the following scaling

$$\text{width}(\theta)_{\rho=\rho_0,R} \sim t^{\frac{1}{2}}|K_0|^{-1/4} \csc\left(\frac{\pi}{n}\right)\cos(\theta)\cos(\pi/n - \theta).$$

2. For $n \geq 3$, the boundary layer in which one term lowers the magnitude of the *mean curvature* has the following scaling

$$\text{width}(\theta)_{\rho=\rho_0,R} \sim t^{\frac{1}{2}}|K_0|^{-1/4}\sqrt{\sin\left(\frac{\pi}{n}\right)\sec(\theta)\sec\left(\frac{\pi}{n} - \theta\right)}.$$

The overlap of these two regions forms the complete boundary layer in which the total bending energy is lowered by allowing localized stretching. The width of these boundary layers has the same scaling in thickness obtained by Lamb in the context of vibrating shells (Lamb, 1889) and Efrati et. al. for non-Euclidean plates with $K_0 > 0$ (Efrati et al., 2007). The fact that there is no boundary layer to reduce the mean curvature in the case $n = 2$ is a consequence of the fact that $\eta = xy$ is a minimal surface in the FvK approximation.

The width of the boundary layers near the lines of inflection scale like

$$\text{width}(\rho)_{\eta=0} \sim \tau^{\frac{1}{3}} \rho^{\frac{1}{3}} |K_0|^{-\frac{1}{6}},$$

which has the same scaling with thickness, but not ρ, for minimal ridges formed by crumpling (Lobkovsky, 1996). In this boundary layer the mean curvature is locally reduced by correcting a jump discontinuity in the azimuthal curvature. This reduction of energy near this type of singularity is different from the regularization near a ridge singularity in which the bending energy diverges while the stretching converges to zero with decreasing thickness (Venkataramani, 2004; Conti & Maggi, 2008).

1.4.2 Main Results from the Kirchhoff Model

In chapter 3 we study the Kirchhoff model for the metric $\mathbf{g}_{K_0}$ over a domain $\mathcal{D}$ that is a disk of radius R. Since the admissible set of deformations is exact $W^{2,2}$ isometric immersions of $\mathbf{g}_{K_0}$ in the Kirchhoff model, we reformulate the variational problem as the problem of minimizing the Willmore energy

$$\mathcal{W}[\mathbf{x}] = \int_{\mathcal{D}} \left(k_1^2 + k_2^2\right) dA_{\mathbf{g}_{K_0}},$$

where k_1 and k_2 are the principal curvatures of the deformation, over $W^{2,2}$ isometric immersions. Furthermore, we use a particular parametrization of hyperbolic surfaces, called Chebychev nets, which encodes all of the geometric information about the

surface in terms of the angle $\phi \in (0, \pi)$ between the asymptotic curves of the surface. In particular, solutions to the sine-Gordon equation

$$\frac{\partial^2 \phi}{\partial u \partial v} = -K_0 \sin(\phi) \tag{1.4.2}$$

generate Chebychev nets which provides us with a method for constructing hyperbolic surfaces.

In section 3.2 we use the Chebychev net structure to construct isometric immersions by cutting out subsets of the pseudosphere. These isometric immersions have large bending energy even away from the singular rim of the pseudosphere and moreover do not have the rotational $n-$fold symmetry observed in the experiments on hydrogels (see figure 1.4.c). Nevertheless, this section is valuable in that it illustrates the process of how the elastic energy of geodesic disks is calculated and also illustrates the large amount of bending energy present in smooth isometric immersions of $\mathbf{g}_{K_0}$.

In section 3.3 we use the sine-Gordon equation to construct a direct numerical minimization scheme for minimizing the Willmore energy. Using this scheme we provide numerical evidence that the principal curvatures of smooth isometric immersions satisfy

$$\max\{|k_1|, |k_2|\} \geq \frac{1}{64} \exp(2R),$$

with the surfaces that realize the bound being geodesic disks lying on hyperboloids of revolution. This result illustrates that the bending energy of smooth isometric immersions grows exponentially with the size of the domain, a phenomenon that is not captured by the FvK model.

In section 3.4 we show that (weak) $W^{2,2}$ isometric immersions with a periodic profile exist. The bending content of these surfaces is concentrated in small regions near the edge of the disk and along lines of inflection. These surfaces have lower bending content then their smooth counterparts lying on the pseudosphere or hyperboloids of revolution and qualitatively resemble what is observed experimentally. Additionally, for each $n \geq 2$, there is a radius $R_n \sim \log(n)$ such that the $n-$periodic

isometric immersions only exist for radii satisfying $0 < R < R_n$. This gives a natural geometric mechanism for the refinement of the wavelength of the buckling pattern with increasing radius of the disk.

Chapter 2

Minimizers in the Föppl-von Kármán Approximation

In this chapter we study the convergence and scaling of minimizers of the FvK energy with decreasing values of the thickness t for a metric $\mathbf{g}_{K_0}$ that has corresponding constant negative Gaussian curvature K_0. Motivated by experimental results, we focus on studying on minimizers with a periodic profile when the domain $\mathcal{D}$ is an annulus with inner and outer radius ρ_0 and R respectively. To be precise, for $n \in \{2, 3 \ldots\}$, we study minimizers over the admissible set of **n-periodic deformations** $\mathcal{A}_n \subset \mathcal{A}_{FvK}$ defined by $(\chi, \eta) \in \mathcal{A}_n$ if and only if in polar coordinates (ρ, θ) the out-of-plane displacement η satisfies

1. η is periodic in θ with period $2\pi/n$,
2. η vanishes along the lines $\theta = 0$ and $\theta = \pi/n$,
3. $\eta\left(\theta - \pi/n\right) = -\eta(\theta)$.

We call the lines $\theta = m\pi/n$, $m \in \{0, \ldots, 2n-1\}$, **lines of inflection**.

2.1 Linearized Geometry and the Föppl-von Kármán Energy

In geodesic polar coordinates (ρ, θ), the metric on $\mathcal{D}$ is

$$\mathbf{g} = d\rho^2 + \frac{\sinh^2(\epsilon\rho/R)}{|K_0|}\, d\theta^2,$$

where $\epsilon = \sqrt{|K_0|}R \ll 1$ is the *dimensionless curvature* (Spivak, 1979). Therefore, expanding in ϵ, $\mathbf{g}_{K_0}$ can be approximated to order ϵ^2 by $\mathbf{g}_{K_0} = \mathbf{g}_0 + \epsilon^2 \mathbf{g}_1$ where g_0 is the Euclidean metric on $\mathbb{R}^2$ and

$$\mathbf{g}_1 = \frac{\rho^4}{3R^2}\, d\theta^2 = \frac{1}{3R^2}\left(v^2\, du^2 - 2uv\, dudv + u^2\, dv^2\right),$$

with the "Cartesian" coordinates $u = \rho\cos(\theta)$ and $v = \rho\sin(\theta)$.

A deformation $\mathbf{x} : \mathcal{D} \to \mathbb{R}^3$ can be constructed that is an isometric immersion of $\mathbf{g}$ to order $\mathcal{O}(\epsilon)$ by assuming the so called "linearized geometry" approximation. That is we assume

$$\mathbf{x} = i + \epsilon i_\perp \circ \eta + \epsilon^2 i \circ \chi, \tag{2.1.1}$$

where $\chi \in W^{1,2}(\mathcal{D}, \mathbb{R}^2)$ and $\eta \in W^{2,2}(\mathcal{D}, \mathbb{R})$ and we calculate all geometric quantities to $\mathcal{O}(\epsilon^2)$. In the linearized approximation to the geometry, when we write that a deformation $\mathbf{x} : \mathcal{D} \to \mathbb{R}^3$ satisfies $\mathbf{x} \in \mathcal{A}_{FvK}$ we mean that there exists $(\chi, \eta) \in \mathcal{A}_{FvK}$ such that $\mathbf{x} = i + \epsilon i_\perp \circ \eta + \epsilon^2 i \circ \chi$.

If we let $\chi = (\chi_1, \chi_2)$ denote the components of χ then the induced Riemannian metric $\mathbf{g}' = (\nabla \mathbf{x})^T \cdot \nabla \mathbf{x}$ from the mapping $\mathbf{x}$ has the following components in the linearized geometry:

$$\mathbf{g}'_{11} = \frac{\partial \mathbf{x}}{\partial u} \cdot \frac{\partial \mathbf{x}}{\partial u} = 1 + \epsilon^2 \left(2\frac{\partial \chi_1}{\partial u} + \left(\frac{\partial \eta}{\partial u} \right)^2 \right),$$

$$\mathbf{g}'_{12} = \mathbf{g}'_{21} = \frac{\partial \mathbf{x}}{\partial u} \cdot \frac{\partial \mathbf{x}}{\partial v} = \epsilon^2 \left(\frac{\partial \chi_1}{\partial v} + \frac{\partial \chi_2}{\partial u} + \frac{\partial \eta}{\partial u}\frac{\partial \eta}{\partial v} \right),$$

$$\mathbf{g}'_{22} = \frac{\partial \mathbf{x}}{\partial v} \cdot \frac{\partial \mathbf{x}}{\partial v} = 1 + \epsilon^2 \left(2\frac{\partial \chi_2}{\partial v} + \left(\frac{\partial \eta}{\partial v} \right)^2 \right).$$

The unit normal vector field N to $\mathbf{x}(\mathcal{D})$ can be found in this approximation by simply computing the cross product of the coordinate tangent vectors $\frac{\partial \mathbf{x}}{\partial u}$ and $\frac{\partial \mathbf{x}}{\partial v}$:

$$\begin{aligned} N &= \frac{\left(-\epsilon \frac{\partial \eta}{\partial u}, -\epsilon \frac{\partial \eta}{\partial v}, 1 + \epsilon^2 \left(\frac{\partial \chi_1}{\partial u} + \frac{\partial \chi_2}{\partial v} \right) \right)}{\sqrt{1 + \epsilon^2 \left(\frac{\partial \eta}{\partial u} \right)^2 + \epsilon^2 \left(\frac{\partial \eta}{\partial v} \right)^2}} \\ &= \left(-\epsilon \frac{\partial \eta}{\partial u}, -\epsilon \frac{\partial \eta}{\partial v}, 1 - \epsilon^2 \left(\frac{1}{2} \left(\frac{\partial \eta}{\partial u} \right)^2 + \frac{1}{2} \left(\frac{\partial \eta}{\partial v} \right)^2 - \frac{\partial \chi}{\partial u} - \frac{\partial \chi_2}{\partial v} \right) \right). \end{aligned}$$

Consequently, the components of the second fundamental form $\mathbf{h}'$ are

$$\mathbf{h}'_{11} = N \cdot \frac{\partial^2 \mathbf{x}}{\partial u^2} = \epsilon \frac{\partial^2 \eta}{\partial u^2},$$

$$\mathbf{h}'_{12} = \mathbf{h}'_{21} = N \cdot \frac{\partial^2 \mathbf{x}}{\partial u \partial v} = \epsilon \frac{\partial^2 \eta}{\partial u \partial v},$$
$$\mathbf{h}'_{22} = N \cdot \frac{\partial^2 \mathbf{x}}{\partial v^2} = \epsilon \frac{\partial^2 \eta}{\partial v^2}.$$

Therefore, the Gaussian K and mean H curvatures are given by:

$$K = \det\left((\mathbf{g}')^{ik}\mathbf{h}'_{kj}\right) = \frac{\det(\mathbf{h}')}{\det(\mathbf{g}')} = \epsilon^2 \det(D^2\eta),$$

$$H = \frac{1}{2}\mathrm{tr}\left(\mathbf{g}'\right)^{ik}\mathbf{h}'_{kj}\big) = \frac{1}{2}\frac{\mathbf{h}'_{11}\mathbf{g}'_{22} - 2\mathbf{h}'_{12}\mathbf{g}'_{12} + \mathbf{h}'_{22}\mathbf{g}'_{11}}{\det(\mathbf{g}')} = \frac{1}{2}\epsilon\Delta\eta,$$

where we are using the Einstein summation convention of summing over repeated indices and raised indices correspond to contravariant components (Spivak, 1979).

Based on (1.2.2) we define the elastic energy $E_t : \mathcal{A} \to \mathbb{R}$ by

$$\begin{aligned} E_t[\mathbf{x}] &= \frac{Y\epsilon^4}{8(1+\nu)}\int_{\mathcal{D}}\left[\left(\frac{1}{1-\nu}\mathrm{tr}(\gamma)^2 - 2\det(\gamma)\right)\right. && (2.1.2)\\ &\quad \left. + \frac{t^2}{3R^2\epsilon^2}\left(\frac{1}{1-\nu}\mathrm{tr}(D^2\eta)^2 - 2\det(D^2\eta)\right)\right] dudv. && (2.1.3)\end{aligned}$$

A deformation $\mathbf{x} \in \mathcal{A}_{FvK}$ is called an **equilibrium configuration** in the FvK ansatz if

$$E_t[\mathbf{x}] = \inf_{\mathbf{y}\in\mathcal{A}_{FvK}} E_t[\mathbf{y}].$$

Now, define the dimensionless variables x, y, χ', and η' by

$$u = Rx, \quad v = Ry, \quad r = R\rho, \quad \chi = R\chi', \quad \eta = R\eta',$$

and $(D^2)'$ the Hessian operator in the coordinates x and y. Then, $(D^2)'\eta' = D^2\eta$ and thus introducing the *dimensionless thickness* $\tau = t/\left(\sqrt{3}R\epsilon\right)$ and dropping the $'$ notation we have that

$$\begin{aligned} \frac{8(1+\nu)}{Y\epsilon^4R^2}E_t[\mathbf{x}] &= \mathcal{E}_\tau[\mathbf{x}] = \mathcal{S}[\mathbf{x}] + \tau^2\mathcal{B}[\mathbf{x}] \\ &= \int_B\left(\frac{1}{1-\nu}\mathrm{tr}(\gamma)^2 - 2\det(\gamma)\right)dxdy && (2.1.4)\\ &\quad + \tau^2\int_B\left(\frac{1}{1-\nu}\mathrm{tr}\left(D^2\eta\right)^2 - 2\det\left(D^2\eta\right)\right)dxdy,\end{aligned}$$

where B is an annulus with inner radius $r_0 = \rho_0/R$ and unit outer radius. Minimizers of E_t also minimize $\mathcal{E}_\tau$ and therefore we will restrict our attention to the functional $\mathcal{E}_\tau$.

2.2 Föppl - von Kármán Equations

In this section let ∂B denote the boundary of B with outward normal vector field $\mathbf{n}$ and tangent vector field $\mathbf{t}$. Also, assume that $\mathbf{x} \in \mathcal{A}_{FvK}$ with corresponding out-of-plane displacement η and in-plane displacement $\chi = (\chi_1, \chi_2)$ extremizes $\mathcal{E}_\tau$.

2.2.1 First Föppl-von Kármán Equation

Taking the variation with respect to χ_1, we obtain

$$\begin{aligned}
\delta_{\chi_1}\mathcal{E}_\tau[\mathbf{x}] &= \int_B \left[\frac{4}{1-\nu}(\gamma_{11}+\gamma_{22})\frac{\partial}{\partial x}\delta\chi_1 - 4\left(\gamma_{22}\frac{\partial}{\partial x}\delta\chi_1 - \gamma_{12}\frac{\partial}{\partial y}\delta\chi_1\right)\right] dxdy \\
&= 4\int_B \left(\frac{\gamma_{11}+\nu\gamma_{22}}{1-\nu}, \gamma_{12}\right)\cdot\nabla\delta\chi_1\, dxdy \\
&= 4\int_{\partial B}\left(\frac{\gamma_{11}+\nu\gamma_{22}}{1-\nu}, \gamma_{12}\right)\cdot\mathbf{n}\delta\chi_1\, ds - 4\int_B \nabla\cdot\left(\frac{\gamma_{11}+\nu\gamma_{22}}{1-\nu}, \gamma_{12}\right)\delta\chi_1\, dxdy.
\end{aligned}$$

Similarly, the variation with respect to χ_2 yields:

$$\delta\chi_2\mathcal{E}_\tau[\mathbf{x}] = 4\int_{\partial B}\left(\gamma_{12}, \frac{\gamma_{22}+\nu\gamma_{11}}{1-\nu},\right)\cdot\mathbf{n}\delta\chi_2\, ds - 4\int_B \nabla\cdot\left(\gamma_{12}, \frac{\gamma_{22}+\nu\gamma_{11}}{1-\nu},\right)\delta\chi_1\, dxdy.$$

Therefore, the governing equations for the in-plane strain are

$$\nabla\cdot((1-\nu)^{-1}(\gamma_{11}+\nu\gamma_{22}), \gamma_{12}) = 0, \quad \nabla\cdot(\gamma_{12}, (1-\nu)^{-1}(\nu\gamma_{11}+\gamma_{22})) = 0, \tag{2.2.1}$$

with the natural boundary conditions

$$\mathbf{n}\cdot((1-\nu)^{-1}(\gamma_{11}+\nu\gamma_{22}), \gamma_{12})|_{\partial B} = 0, \quad \mathbf{n}\cdot(\gamma_{12}, (1-\nu)^{-1}(\nu\gamma_{11}+\gamma_{22}))|_{\partial B} = 0.$$

Furthermore, the divergence condition (2.2.1) implies that there exists a stress potential function $\Phi \in W^{2,2}(B, \mathbb{R})$ satisfying

$$D^2\Phi = \frac{1}{1-\nu}\begin{pmatrix} \nu\gamma_{11}+\gamma_{22} & -(1-\nu)\gamma_{12} \\ -(1-\nu)\gamma_{12} & \gamma_{11}+\nu\gamma_{22} \end{pmatrix}, \tag{2.2.2}$$

(Landau & Lifshitz, 1986).

Now, assuming γ is second differentiable, differentiating we have that

$$\begin{aligned}\frac{\partial^2\gamma_{11}}{\partial y^2} - 2\frac{\partial^2\gamma_{12}}{\partial x\partial y} + \frac{\partial^2\gamma_{22}}{\partial x^2} &= 2\frac{\partial^3\chi_1}{\partial x\partial y^2} + 2\left(\frac{\partial\eta}{\partial x\partial y}\right)^2 + 2\frac{\partial\eta}{\partial x}\frac{\partial^3\eta}{\partial x\partial y^2} - \frac{2}{3} \\ &\quad -2\frac{\partial^3\chi_1}{\partial x\partial y^2} - 2\frac{\partial^3\chi_2}{\partial x^2\partial y} - 2\frac{\partial^2\eta}{\partial x^2}\frac{\partial\eta}{\partial y^2} - 2\frac{\partial\eta}{\partial x}\frac{\partial^3\eta}{\partial x\partial y^2} \\ &\quad -2\left(\frac{\partial^2\eta}{\partial x\partial y}\right)^2 - 2\frac{\partial\eta}{\partial y}\frac{\partial^2\eta}{\partial y^2\partial x} - \frac{2}{3} \\ &\quad +2\frac{\partial^3\chi_2}{\partial x^2\partial y} + 2\left(\frac{\partial\eta}{\partial x\partial y}\right)^2 + 2\frac{\partial\eta}{\partial y}\frac{\partial^3\eta}{\partial x^2\partial y} - \frac{2}{3}.\end{aligned}$$

Therefore, upon cancelling terms, we have the following *compatibility condition* between γ and η:

$$\frac{\partial^2\gamma_{11}}{\partial y^2} - 2\frac{\partial^2\gamma_{12}}{\partial x\partial y} + \frac{\partial^2\gamma_{22}}{\partial x^2} - 2[\eta,\eta] - 2 = 0, \tag{2.2.3}$$

where the operator $[\cdot,\cdot] : \mathcal{C}^2(B,\mathbb{R}) \times \mathcal{C}^2(B,\mathbb{R}) \to \mathbb{R}$ is defined by

$$[f,g] = \frac{1}{2}\left(\frac{\partial^2 f}{\partial x^2}\frac{\partial g}{\partial y^2} + \frac{\partial^2 f}{\partial y^2}\frac{\partial^2 g}{\partial x^2} - 2\frac{\partial^2 f}{\partial x\partial y}\frac{\partial^2 g}{\partial x\partial y}\right).$$

Therefore, inverting (2.2.2) and substituting into (2.2.3) we have the following proposition.

Proposition 2.2.1. If $\mathbf{x}^* \in \mathcal{A}$ with potential Φ and out-of-plane displacement η such that $\mathcal{E}_\tau[\mathbf{x}^*] = \inf_{\mathbf{x}\in\mathcal{A}} \mathcal{E}_\tau[\mathbf{x}]$, and if Φ is (weakly) four times differentiable then Φ satisfies the **first Föppl - von Kármán** equation:

$$\frac{1}{2(1+\nu)}\Delta^2\Phi + [\eta,\eta] = -1. \tag{2.2.4}$$

Also, Φ satisfies the following **natural boundary conditions**:

$$\mathbf{n}\cdot\left(\tfrac{\partial^2\Phi}{\partial y^2}, -\tfrac{\partial^2\Phi}{\partial x\partial y}\right)\Big|_{\partial B} = 0, \quad \mathbf{n}\cdot\left(-\tfrac{\partial^2\Phi}{\partial x\partial y}, \tfrac{\partial^2\Phi}{\partial x^2}\right)\Big|_{\partial B} = 0. \tag{2.2.5}$$

Furthermore, by (2.2.2) the stretching energy can be expressed in terms of Φ:

$$\mathcal{S}[\mathbf{x}] = \int_B \left(\frac{1}{1+\nu}(\Delta\Phi)^2 - 2[\Phi,\Phi]\right) dxdy.$$

The next proposition allows us to simplify this energy further and will be useful in the next section.

Proposition 2.2.2. If $\mathbf{x}^* \in \mathcal{A}_{FvK}$ with potential Φ and $\inf_{\mathbf{x}\in\mathcal{A}} \mathcal{E}_\tau[\mathbf{x}] = \mathcal{E}_\tau[\mathbf{x}^*]$ then

$$\mathcal{S}[\mathbf{x}^*] = \int_B \frac{1}{1+\nu} \left(\Delta\Phi\right)^2 \, dxdy.$$

Proof. Let $\mathbf{x}^* \in \mathcal{A}_{FvK}$ with corresponding potential function Φ such that $\inf_{\mathbf{x}\in\mathcal{A}} \mathcal{E}_\tau[\mathbf{x}] = \mathcal{E}_\tau[\mathbf{x}^*]$. Using Stokes' theorem and applying the boundary conditions (2.2.5), we have that

$$\begin{aligned}
\int_B [\Phi,\Phi]\, dxdy &= \int_B \left(\frac{\partial^2\Phi}{\partial x^2}\frac{\partial^2\Phi}{\partial y^2} - \frac{\partial^2\Phi}{\partial x\partial y}\frac{\partial^2\Phi}{\partial x\partial y} \right) dxdy \\
&= \int_B \left[\frac{\partial}{\partial x}\left(\frac{\partial\Phi}{\partial x}\frac{\partial^2\Phi}{\partial y^2} - \frac{\partial\Phi}{\partial y}\frac{\partial^2\Phi}{\partial x\partial y} \right) + \frac{\partial}{\partial y}\left(\frac{\partial\Phi}{\partial y}\frac{\partial^2\Phi}{\partial x^2} - \frac{\partial\Phi}{\partial y}\frac{\partial^2\Phi}{\partial x\partial y} \right) \right] dxdy \\
&= \int_{\partial B} \left(\frac{\partial\Phi}{\partial x}\frac{\partial^2\Phi}{\partial y^2} - \frac{\partial\Phi}{\partial y}\frac{\partial^2\Phi}{\partial x\partial y}, \frac{\partial\Phi}{\partial y}\frac{\partial^2\Phi}{\partial x^2} - \frac{\partial\Phi}{\partial x}\frac{\partial^2\Phi}{\partial x\partial y} \right) \cdot \mathbf{n}\, ds \\
&= \int_{\partial B} \frac{\partial\Phi}{\partial x}\left(\frac{\partial^2\Phi}{\partial y^2}, -\frac{\partial^2\Phi}{\partial x\partial y} \right) \cdot \mathbf{n}\, ds + \int_{\partial B} \frac{\partial\Phi}{\partial y}\left(-\frac{\partial^2\Phi}{\partial x\partial y}, \frac{\partial^2\Phi}{\partial x\partial y} \right) \cdot \mathbf{n}\, ds \\
&= 0.
\end{aligned}$$

Therefore,

$$\mathcal{S}[\mathbf{x}^*] = \int_B \left(\frac{1}{1+\nu}\left(\Delta\Phi\right)^2 - 2[\Phi,\Phi] \right) dxdy = \int_B \frac{1}{1+\nu}\left(\Delta\Phi\right)^2 \, dxdy.$$

□

2.2.2 Second Föppl-von Kármán Equation

Now, taking the variation of $\mathcal{S}$ with respect to η and applying the boundary conditions (2.2.5) we have

$$\begin{aligned}
\delta_\eta \mathcal{S}[\mathbf{x}] &= 2\int_B \left[\frac{1}{1-\nu}\left(\gamma_{11}+\gamma_{22}\right)\left(\frac{\partial\eta}{\partial x}\frac{\partial}{\partial x}\delta\eta + \frac{\partial\eta}{\partial y}\frac{\partial}{\partial y}\delta\eta\right)\right. \\
&\quad \left. -\left(\gamma_{11}\frac{\partial\eta}{\partial y}\frac{\partial}{\partial y}\delta\eta + \gamma_{22}\frac{\partial\eta}{\partial x}\frac{\partial}{\partial x}\delta\eta - \gamma_{12}\frac{\partial\eta}{\partial x}\frac{\partial}{\partial y}\delta\eta - \gamma_{12}\frac{\partial\eta}{\partial y}\frac{\partial}{\partial x}\delta\eta\right)\right] dxdy \\
&= 8\int_B \left(\frac{\partial^2\Phi}{\partial y^2}\frac{\partial\eta}{\partial x} - \frac{\partial^2\Phi}{\partial x\partial y}\frac{\partial\eta}{\partial y}, \frac{\partial^2\Phi}{\partial x^2}\frac{\partial\eta}{\partial y} - \frac{\partial^2\Phi}{\partial x\partial y}\frac{\partial\eta}{\partial x}\right)\cdot\nabla\delta\eta\, dxdy \\
&= 8\int_{\partial B}\left[\frac{\partial\eta}{\partial x}\left(\frac{\partial^2\Phi}{\partial y^2}, -\frac{\partial^2\Phi}{\partial x\partial y}\right)\cdot\mathbf{n} + \frac{\partial\eta}{\partial y}\left(-\frac{\partial^2\Phi}{\partial x\partial y}, \frac{\partial^2\Phi}{\partial x\partial y}\right)\cdot\mathbf{n}\right]\delta\eta\, ds \\
&\quad -8\int_B [\Phi,\eta]\delta\eta\, dxdy \\
&= -8\int_B [\Phi,\eta]\delta\eta\, dxdy.
\end{aligned}$$

Furthermore, taking the variation of the mean curvature we have that

$$\begin{aligned}
\delta_\eta \frac{1}{2}\int_B (\Delta\eta)^2\, dxdy &= \int_B \Delta\eta\cdot\Delta\delta\eta\, dxdy \\
&= \int_B \left[\nabla\cdot(\Delta\eta\cdot\nabla\delta\eta) - \nabla(\Delta\eta)\cdot\nabla\delta\eta\right] dxdy \\
&= \int_{\partial B}\Delta\eta\nabla\delta\eta\cdot\mathbf{n}\, ds - \int_{\partial B}\nabla(\Delta\eta)\delta\eta\cdot\mathbf{n}\, ds + \int_B \Delta^2\eta\delta\eta\, dxdy.
\end{aligned}$$

Taking the variation of the Gaussian curvature we have that

$$\begin{aligned}
&\delta_\eta \int_B \det(D^2\eta)\, dxdy \\
&= -\int_D \left[2\frac{\partial^2\eta}{\partial x\partial y}\frac{\partial^2\delta\eta}{\partial x\partial y} - \frac{\partial^2\eta}{\partial x^2}\frac{\partial^2\delta\eta}{\partial y^2} - \frac{\partial^2\delta\eta}{\partial x^2}\frac{\partial^2\eta}{\partial y^2}\right] dxdy \\
&= -\int_B \left[\frac{\partial}{\partial x}\left(\frac{\partial\delta\eta}{\partial y}\frac{\partial^2\eta}{\partial x\partial y} - \frac{\partial\delta\eta}{\partial x}\frac{\partial^2\eta}{\partial y^2}\right) + \frac{\partial}{\partial y}\left(\frac{\partial\delta\eta}{\partial x}\frac{\partial^2\eta}{\partial x\partial y} - \frac{\partial\delta\eta}{\partial y}\frac{\partial^2\eta}{\partial x^2}\right)\right] dxdy \\
&= -\int_{\partial B}\left[\left(\frac{\partial\delta\eta}{\partial y}\frac{\partial^2\eta}{\partial x\partial y} - \frac{\partial\delta\eta}{\partial x}\frac{\partial^2\eta}{\partial y^2}\right)\cos(\phi) + \left(\frac{\partial\delta\eta}{\partial x}\frac{\partial^2\eta}{\partial x\partial y} - \frac{\partial\delta\eta}{\partial y}\frac{\partial^2\eta}{\partial x^2}\right)\sin(\phi)\right] ds \\
&= -\int_{\partial B}\left(2\sin(\phi)\cos(\phi)\frac{\partial^2\eta}{\partial x\partial y} - \sin^2(\phi)\frac{\partial^2\eta}{\partial x^2} - \cos^2(\phi)\frac{\partial^2\eta}{\partial y^2}\right)\frac{\partial\delta\eta}{\partial\mathbf{n}}\, ds \\
&\quad -\int_{\partial B}\left(\sin(\phi)\cos(\phi)\left(\frac{\partial^2\eta}{\partial y^2} - \frac{\partial^2\eta}{\partial x^2}\right) + \left(\cos^2(\phi) - \sin^2(\phi)\right)\frac{\partial^2\eta}{\partial x\partial y}\right)\frac{\partial\delta\eta}{\partial\mathbf{t}}\, ds,
\end{aligned}$$

where ϕ is the angle between $\mathbf{n}$ and the x-axis and we have used the following transformation

$$\begin{aligned}\frac{\partial}{\partial x} &= \cos(\phi)\frac{\partial}{\partial \mathbf{n}} - \sin(\phi)\frac{\partial}{\partial \mathbf{t}} \\ \frac{\partial}{\partial y} &= \sin(\phi)\frac{\partial}{\partial \mathbf{n}} + \cos(\phi)\frac{\partial}{\partial \mathbf{t}}.\end{aligned}$$

The fact that the variation of the Gaussian curvature reduces to integrals on ∂B is a realization of the Gauss-Bonet theorem in the FvK approximation. Since ∂B is a closed contour it follows from integration by parts that

$$\begin{aligned}&\int_{\partial B}\left(\sin(\phi)\cos(\phi)\left(\frac{\partial^2\eta}{\partial y^2}-\frac{\partial^2\eta}{\partial x^2}\right)+\left(\cos^2(\phi)-\sin^2(\phi)\right)\frac{\partial^2\eta}{\partial x\partial y}\right)\frac{\partial\delta\eta}{\partial\mathbf{t}}\,ds \\ &= -\int_{\partial B}\frac{\partial}{\partial\mathbf{t}}\left(\sin(\phi)\cos(\phi)\left(\frac{\partial^2\eta}{\partial y^2}-\frac{\partial^2\eta}{\partial x^2}\right)+\left(\cos^2(\phi)-\sin^2(\phi)\right)\frac{\partial^2\eta}{\partial x\partial y}\right)\delta\eta\,ds.\end{aligned}$$

Therefore, the variation of the total energy with respect to η is given by

$$\begin{aligned}\delta_\eta\mathcal{E}_\tau[\mathbf{x}] &= \int_B\left(-8[\Phi,\eta]+2\frac{\tau^2}{1-\nu}\Delta^2\eta\right)\delta\eta\,dxdy \\ &\quad +2\int_{\partial B}\left(\frac{1}{1-\nu}\Delta\eta-\mathbf{n}^T\cdot D^2\eta\cdot\mathbf{n}\right)\frac{\partial\delta\eta}{\partial\mathbf{n}}\,ds \\ &\quad -\int_{\partial B}\left(\frac{1}{1-\nu}\frac{\partial\Delta\eta}{\partial\mathbf{n}}+\frac{\partial}{\partial\mathbf{t}}\left(\mathbf{n}^T\cdot D^2\eta\cdot\mathbf{t}\right)\right)\delta\eta\,ds.\end{aligned}$$

Proposition 2.2.3. If $\mathbf{x}^* \in \mathcal{A}$ with potential Φ and out-of-plane displacement η, $\mathcal{E}_\tau[\mathbf{x}^*] = \inf_{\mathbf{x}\in\mathcal{A}}\mathcal{E}_\tau[\mathbf{x}]$, and if η is (weakly) four times differentiable then

$$[\Phi,\eta] = \frac{\tau^2}{4(1-\nu)}\Delta^2\eta. \tag{2.2.6}$$

This equation is called the **second Föppl - von Kármán** equation. Furthermore, η satisfies the following **natural boundary conditions**:

$$\left.\frac{1}{1-\nu}\Delta\eta-\mathbf{n}^T\cdot D^2\eta\cdot\mathbf{n}\right|_{\partial B}=0, \tag{2.2.7}$$

$$\left.\frac{1}{1-\nu}\frac{\partial\Delta\eta}{\partial\mathbf{n}}+\frac{\partial}{\partial\mathbf{t}}\left(\mathbf{n}^T\cdot D^2\eta\cdot\mathbf{t}\right)\right|_{\partial B}=0. \tag{2.2.8}$$

The equations (2.2.4) and (2.2.6) along with the boundary conditions (2.2.5), (2.2.7) and (2.2.8) are a complete system of equations governing the deformation of the sheet. For general geometries, the boundary conditions are intractable and in later sections we will use the geometry of B to simplify these equations further.

2.3 Flat Solution

In general finding exact solutions to the FvK equations and its natural boundary conditions is intractable. If we make the assumption that the deformation remains flat, that is the out-of-plane displacement is zero, then the FvK equations can be significantly simplified. Define the **admissible set of flat configurations** $\mathcal{A}_f \subset \mathcal{A}$ by $\mathcal{A}_f = \{\mathbf{x} \in \mathcal{A} : \eta = 0\}$ and define $\mathcal{F} = \inf_{\mathbf{x}\in\mathcal{A}_f} \mathcal{E}_\tau[\mathbf{x}]$. If $\mathbf{x} \in \mathcal{A}_f$ extremizes $\mathcal{E}_\tau$ with potential function Φ then, assuming radial symmetry, we have by (2.2.4) and (2.2.5) that Φ satisfies the following boundary value problem

$$\frac{\partial^4\Phi}{\partial r^4} + \frac{2}{r}\frac{\partial^3\Phi}{\partial r^3} - \frac{1}{r^2}\frac{\partial^2\Phi}{\partial r^2} + \frac{1}{r^3}\frac{\partial\Phi}{\partial r} = -2(1+\nu), \qquad \left.\frac{\partial\Phi}{\partial r}\right|_{r=r_0,1} = 0. \tag{2.3.1}$$

The general solution to this differential equation is

$$\Phi = c_1 + c_2 r^2 + c_3 \ln(r) + c_4 r^2 \ln(r) - (1+\nu)\frac{r^4}{32},$$

where c_1, c_2, c_3 and c_4 are arbitrary constants. Since c_1 and $c_3 \ln(r)$ are harmonic functions it follows from proposition 2.2.2 that we can assume without loss of generality that $c_1 = c_3 = 0$. Consequently, the solution to (2.3.1) is

$$\Phi = \frac{1+\nu}{32\ln(r_0)}\left[\left(r_0^2 - 1 - 2\ln(r_0)\right) r^2 + 2\left(r_0^2 - 1\right) r^2 \ln(r) - \ln(r_0)\, r^4\right].$$

Therefore, we have the following result:

Lemma 2.3.1. Suppose $\mathbf{x}^* \in \mathcal{A}_f$ satisfies $\mathcal{E}_\tau[\mathbf{x}^*] = \inf_{\mathbf{x}\in\mathcal{A}_f} \mathcal{E}_\tau[\mathbf{x}]$. Then,

$$\mathcal{E}_\tau[\mathbf{x}^*] = \mathcal{F} = \frac{(1+\nu)\pi}{32\ln(r_0)^2}\left[\frac{1}{2}\left(r_0^2-1\right)^3 + \left(r_0^2-1\right)^2\left(r_0^2+1\right)\ln(r_0) + \frac{2}{3}\left(1-r_0^6\right)\ln(r_0)^2\right].$$

The quantity $\mathcal{F}$ measures the minimal elastic energy of deformations that undergo pure stretching, i.e. the bending energy of such deformations is zero. Although we have found exact solutions to the FvK equations, as we will see in the next section, we can construct deformations with pure bending energy that have lower elastic energy if the sheet is sufficiently thin.

2.4 Isometric Immersions

In the FvK approximation, define the set of **FvK isometric immersions** by $\mathcal{A}_0 = \{\mathbf{x} \in \mathcal{A} : \gamma = 0\}$. By (2.2.3), it follows that the solvability condition for the equation $\gamma = 0$ is the Monge-Ampere equation

$$[\eta, \eta] = \det\left(D^2\eta\right) = -1, \tag{2.4.1}$$

which is a version of Gauss's Theorema Egregium in the FvK ansatz. Consequently, if $\mathbf{x} \in \mathcal{A}_0$ with corresponding out-of-plane displacement η, it follows that if $\mathbf{x}$ satisfies (2.2.4) and (2.2.6) then $\Delta^2\eta = 0$. Therefore, it is natural to look for solutions to the FvK equations by finding solutions to the above Monge-Ampere equation (2.4.1) satisfying $\Delta^2\eta = 0$.

2.4.1 Saddle Isometric Immersions

By (2.1.4) and (2.4.1) it follows that for all $\mathbf{x} \in \mathcal{A}_0$

$$\frac{1}{\tau^2}\inf_{\mathbf{x}\in\mathcal{A}_0}\mathcal{E}_\tau[\mathbf{x}] = \inf_{\mathbf{x}\in\mathcal{A}_0}\int_B \frac{1}{1-\nu}\left(\Delta\eta\right)^2\, dxdy + 2\pi(1-r_0^2). \tag{2.4.2}$$

Consequently, since $\eta = xy$ satisfies (2.4.1) and is harmonic, it follows that the global minimum of (2.4.2) over $\mathcal{A}_0$ is obtained. Therefore, using this deformation as a test function we can extend lemma 2.3.1 to form the following proposition.

Proposition 2.4.1. Let $\mathbf{x}^* \in \mathcal{A}_{FvK}$ such that $\mathcal{E}_\tau[\mathbf{x}^*] = \inf_{\mathbf{x}\in\mathcal{A}_{FvK}}\mathcal{E}_\tau[\mathbf{x}]$. Then,

$$\mathcal{E}_\tau[\mathbf{x}^*] \leq \min\{2\pi\tau^2(1-r_0^2), \mathcal{F}\}.$$

There are two natural test functions for the elastic energy, flat deformations and isometric immersions, the upper bounds in the above proposition correspond to the minimum of the elastic energy over these two classes of deformations. Moreover, this proposition illustrates that with decreasing thickness minimizers of the elastic energy necessarily must buckle out of the plane.

2.4.2 Convergence of Minimizers

Since the lower bound of the bending energy over $\mathcal{A}_0$ is obtained, we can prove rigorously, using the notion of $\Gamma-$convergence, that in the vanishing thickness limit minimizers should converge to a saddle shaped isometric immersion. Recall the following definition of $\Gamma-$convergence (Braides, 2002):

Definition 2.4.2. On a metric space X a sequence of functionals $F_t : X \to \mathbb{R}$ (weakly) $\Gamma-$converges as $t \to 0$ to a functional $F_0 : X \to \mathbb{R}$, written $\Gamma-\lim_{t\to 0} F_t = F_0$ if for all $\mathbf{x} \in X$ we have that

1. (**Liminf inequality**) - for every sequence $\mathbf{x}_0$ (weakly) converging to $\mathbf{x}$

$$F_0[\mathbf{x}] \leq \liminf_{t\to 0} F_t[\mathbf{x}_t].$$

2. (**Recovery sequence**) - there exists a sequence $\mathbf{x}_t$ (weakly) converging to $\mathbf{x}$ such that

$$F_0[\mathbf{x}] \geq \limsup_{t\to 0} F_t[\mathbf{x}].$$

Lemma 2.4.3. The sequence of functionals $F_\tau : \mathcal{A}_{FvK} \to \mathbb{R}$ defined by $F_\tau = \tau^{-2}\mathcal{E}_\tau$ weakly Γ-converge to the limiting functional $F_0 : \mathcal{A}_{FvK} \to \mathbb{R}$ defined by

$$F_0[\mathbf{x}] = \begin{cases} \mathcal{B}[\mathbf{x}], & \text{if } \mathcal{S}[\mathbf{x}] \neq 0 \\ \infty, & \text{if } \mathcal{S}[\mathbf{x}] = 0. \end{cases}$$

Proof. We first prove the liminf inequality. Let $\mathbf{x}_\tau \in \mathcal{A}_{FvK}$ such that $\mathbf{x}_\tau \overset{\mathcal{A}_{FvK}}{\searrow} \mathbf{x}$, that is if we let (f_τ, g_τ), (f, g) and η_τ, η be the corresponding in-plane and out-of-plane displacements of $\mathbf{x}_\tau$ and $\mathbf{x}$ respectively then

$$f_\tau \overset{W^{1,2}(B,\mathbb{R})}{\searrow} f, \quad g_\tau \overset{W^{1,2}(B,\mathbb{R})}{\searrow} g \quad \eta_\tau \overset{W^{2,2}(B,\mathbb{R})}{\searrow} \eta.$$

To prove the liminf inequality we will show that

$$\mathcal{B}[\mathbf{x}] \leq \liminf_{\tau\to 0} \mathcal{B}[\mathbf{x}_\tau] \text{ and } \mathcal{S}[\mathbf{x}] \leq \liminf_{\tau\to 0} \mathcal{S}[\mathbf{x}_\tau].$$

Since $\eta \overset{W^{2,2}(B,\mathbb{R})}{\searrow} \eta$ it follows that

$$\frac{\partial^2 \eta_\tau}{\partial x^2} \overset{L^2(B,\mathbb{R})}{\searrow} \frac{\partial^2 \eta}{\partial x^2}, \quad \frac{\partial^2 \eta_\tau}{\partial x \partial y} \overset{L^2(B,\mathbb{R})}{\searrow} \frac{\partial^2 \eta}{\partial x \partial y}, \quad \frac{\partial^2 \eta_\tau}{\partial y^2} \overset{L^2(B,\mathbb{R})}{\searrow} \frac{\partial^2 \eta}{\partial y^2}.$$

It is basic property of weak convergence that for all $\psi \in L^2(B, \mathbb{R})$ if $\psi_\tau \overset{L^2(B,\mathbb{R})}{\searrow} \psi$ then we have the following lower semi-continuity property

$$\|\psi\|_{L^2(B,\mathbb{R})} \leq \liminf_{\tau\to 0} \|\psi_\tau\|_{L^2(B,\mathbb{R})}, \tag{2.4.3}$$

and $\exists C > 0$ such that

$$\|\psi_\tau\|_{L^2(B,\mathbb{R})} < C, \tag{2.4.4}$$

(Evans, 1990). Therefore,

$$\begin{aligned}
\mathcal{B}[\mathbf{x}] &= \int_B \left(\frac{1}{1-\nu} (\Delta\eta)^2 - 2\det(D^2\eta) \right) dxdy \\
&= \int_B \left(\frac{\nu}{1-\nu} (\Delta\eta)^2 + |D^2\eta|^2 \right) dxdy \\
&\leq \liminf_{\tau\to 0} \int_B \left(\frac{\nu}{1-\nu} (\Delta\eta_t)^2 + |D^2\eta_t|^2 \right) dxdy \\
&\leq \liminf_{\tau\to 0} \mathcal{B}[\mathbf{x}_t].
\end{aligned}$$

Recall that the stretching energy is given by

$$\begin{aligned}
\mathcal{S}[\mathbf{x}] &= \int_B \left(\frac{1}{1-\nu} (\gamma_{11} + \gamma_{22})^2 - \det(\gamma) \right) dxdy \\
&= \int_B \left(\frac{\nu}{1-\nu} (\gamma_{11} + \gamma_{22})^2 + \gamma_{11}^2 + 2\gamma_{12}^2 + \gamma_{22}^2 \right) dxdy.
\end{aligned}$$

Concentrating on one term we have that

$$\int_B \gamma_{11}^2 \, dxdy = \int_B \left[2\left(\frac{\partial f_\tau}{\partial x}\right)^2 + 4\frac{\partial f_\tau}{\partial x}\left(\frac{\partial \eta_\tau}{\partial x^2}\right)^2 - \frac{2y^2}{3} + \left(\frac{\partial \eta_\tau}{\partial x}\right)^4 \right.$$
$$\left. -2\left(\frac{\partial \eta_\tau}{\partial x}\right)^2 - 2\left(\frac{\partial \eta_\tau}{\partial x}\right)^2 \frac{y^2}{3} + \frac{y^4}{3} \right] dxdy.$$

To understand the limiting behavior of the terms on the right hand of the above equation we will use the following intermediate results:

1. Since B has finite area and $\eta \in W^{2,2}(B, \mathbb{R})$ it follows from an application of Hölder's inequality that $\dfrac{\partial \eta_\tau}{\partial x} \in W^{1,p}(B, \mathbb{R})$ for $1 \leq p \leq 2$. Therefore, by Rellich's compactness theorem (Hunter & Nachtergaele, 2001) it follows that

$$\frac{\partial \eta_\tau}{\partial x} \overset{L^q(B,\mathbb{R})}{\longrightarrow} \frac{\partial \eta}{\partial x}, \tag{2.4.5}$$

   for $1 \leq q < \infty$.

2. Applying the reverse triangle inequality we have that

$$\left| \left\| \frac{\partial \eta_\tau}{\partial x} \right\|_{L^q(B,\mathbb{R})} - \left\| \frac{\partial \eta}{\partial x} \right\|_{L^q(B,\mathbb{R})} \right| \leq \left\| \frac{\partial \eta_\tau}{\partial x} - \frac{\partial \eta}{\partial x} \right\|_{L^q(B,\mathbb{R})}$$

   and thus for $1 \leq q < \infty$ it follows that

$$\lim_{\tau \to 0} \left\| \frac{\partial \eta_\tau}{\partial x} \right\|_{L^q(B,\mathbb{R})} = \left\| \frac{\partial \eta}{\partial x} \right\|_{L^q(B,\mathbb{R})}. \tag{2.4.6}$$

Again since $f_\tau \overset{W^{2,2}(D,\mathbb{R})}{\longrightarrow} f$ it follows that $\dfrac{\partial f_\tau}{\partial x} \overset{L^2(B,\mathbb{R})}{\longrightarrow} \dfrac{\partial f}{\partial x}$ which can be used to show the following limits and inequalities:

i By (2.4.3):

$$\lim_{\tau \to 0} \left\| \frac{\partial f_\tau}{\partial x} \right\|^2_{L^2(B,\mathbb{R})} \geq \left\| \frac{\partial f}{\partial x} \right\|^2_{L^2(B,\mathbb{R})}.$$

ii Rearranging we have that

$$\begin{aligned}
&\int_B \frac{\partial f_\tau}{\partial x}\left(\frac{\partial \eta_\tau}{\partial x}\right)^2 dxdy \\
&\quad = \int_B \frac{\partial f_\tau}{\partial x}\left(\left(\frac{\partial \eta_\tau}{\partial x}\right)^2 - \left(\frac{\partial \eta}{\partial x}\right)^2\right) dxdy + \int_B \frac{\partial f_\tau}{\partial x}\left(\frac{\partial \eta}{\partial x}\right)^2 dxdy \\
&\quad = \int_B \frac{\partial f_\tau}{\partial x}\left(\frac{\partial \eta_\tau}{\partial x} - \frac{\partial \eta}{\partial x}\right)\left(\frac{\partial \eta_\tau}{\partial x} - \frac{\partial \eta}{\partial x}\right) dxdy + \int_B \frac{\partial f_\tau}{\partial x}\left(\frac{\partial \eta}{\partial x}\right)^2 dxdy.
\end{aligned}$$

Applying Hölder's inequality

$$\begin{aligned}
&\int_B \frac{\partial f_\tau}{\partial x}\left(\frac{\partial \eta_\tau}{\partial x} - \frac{\partial \eta}{\partial x}\right)\left(\frac{\partial \eta_\tau}{\partial x} - \frac{\partial \eta}{\partial x}\right) dxdy \\
&\leq \left(\int_B \left(\frac{\partial f_\tau}{\partial x}\right)^2 dxdy\right)^{\frac{1}{2}} \left(\int_B \left(\frac{\partial \eta_\tau}{\partial x} - \frac{\partial \eta}{\partial x}\right)^4 dxdy\right)^{\frac{1}{4}} \left(\int_B \left(\frac{\partial \eta_\tau}{\partial x} + \frac{\partial \eta}{\partial x}\right) dxdy\right)^{\frac{1}{4}}.
\end{aligned}$$

Now, applying the elementary inequality $(a+b)^4 \leq 8(a^4+b^4)$ and (2.4.4) we have that

$$\begin{aligned}
&\int_B \frac{\partial f_\tau}{\partial x}\left(\frac{\partial \eta_\tau}{\partial x} - \frac{\partial \eta}{\partial x}\right)\left(\frac{\partial \eta_\tau}{\partial x} - \frac{\partial \eta}{\partial x}\right) dxdy \\
&\qquad \leq 2^{\frac{3}{4}} C \left\|\frac{\partial \eta_\tau}{\partial x} - \frac{\partial \eta}{\partial x}\right\|_{L^4(B,\mathbb{R})} \left(\left\|\frac{\partial \eta_\tau}{\partial x}\right\|^4_{L^4(B,\mathbb{R})} + \left\|\frac{\partial \eta}{\partial x}\right\|^4_{L^4(B,\mathbb{R})}\right)^{\frac{1}{4}}.
\end{aligned}$$

Taking limits of both sides it follows that

$$\lim_{\tau\to 0} \int_B \frac{\partial f_\tau}{\partial x}\left(\left(\frac{\partial \eta_\tau}{\partial x}\right)^2 - \left(\frac{\partial \eta}{\partial x}\right)^2\right) dxdy = 0.$$

Furthermore, since $\dfrac{\partial f_\tau}{\partial x} \xrightarrow{L^2(B,\mathbb{R})} \dfrac{\partial f}{\partial x}$ and $\left(\dfrac{\partial \eta}{\partial x}\right)^2 \in L^2(B,\mathbb{R})$ we can conclude that

$$\lim_{\tau\to 0} \int_B \frac{\partial f_\tau}{\partial x}\left(\frac{\partial \eta_\tau}{\partial x}\right)^2 dxdy = \int_B \frac{\partial f}{\partial x}\left(\frac{\partial \eta}{\partial x}\right)^2 dxdy.$$

iii Since $\dfrac{\partial f_\tau}{\partial x} \xrightarrow{L^2(B,\mathbb{R})} \dfrac{\partial f}{\partial x}$ it follows that

$$\lim_{\tau\to 0} \int_B \frac{\partial f_\tau}{\partial x}\frac{y^2}{3}\, dA = \int_B \frac{\partial f}{\partial x}\frac{y^2}{3}\, dA.$$

iv By item 2

$$\lim_{\tau\to 0}\left\|\frac{\partial \eta_\tau}{\partial x}\right\|^4_{L^4(B,\mathbb{R})} = \left\|\frac{\partial \eta}{\partial x}\right\|^4_{L^4(B,\mathbb{R})}.$$

v Applying the same techniques as in item ii we have that

$$\lim_{\tau\to 0}\int_B \left(\frac{\partial \eta_\tau}{\partial x}\right)^2 \frac{y^2}{3} dxdy = \int_B \left(\frac{\partial \eta}{\partial x}\right)^2 \frac{y^2}{3} dxdy.$$

Therefore, by items i-v it follows that

$$\liminf_{\tau\to 0}\int_B \left(2\frac{\partial f_\tau}{\partial x} + \left(\frac{\partial \eta_\tau}{\partial x}\right)^2 - \frac{y^2}{3}\right)^2 dxdy \geq \int_B \left(2\frac{\partial f}{\partial x} + \left(\frac{\partial \eta}{\partial x}\right)^2 - \frac{y^2}{3}\right)^2 dxdy.$$

Identical arguments can be applied to the other strain terms to show that

$$\mathcal{S}[\mathbf{x}] \leq \liminf_{\tau\to 0} \mathcal{S}[\mathbf{x}_\tau]$$

Now, we can prove the liminf inequality. First, if $\mathcal{S}[\mathbf{x}] = 0$ then

$$\liminf_{\tau\to 0} F_\tau[\mathbf{x}_\tau] = \liminf_{\tau\to 0} \frac{1}{\tau^2}\mathcal{S}[\mathbf{x}_\tau] + \liminf_{\tau\to 0} \mathcal{B}[\mathbf{x}_\tau] \geq \liminf_{\tau\to 0} B[\mathbf{x}_\tau] \geq \mathcal{B}[\mathbf{x}] = F_0[\mathbf{x}].$$

If $\mathcal{S}[\mathbf{x}] \neq 0$ then

$$\liminf_{\tau\to 0} F_\tau[\mathbf{x}_\tau] \geq \liminf_{\tau\to 0} \frac{1}{\tau^2}\mathcal{S}[\mathbf{x}_\tau] \geq \liminf_{\tau\to 0} \frac{1}{\tau^2}\mathcal{S}[\mathbf{x}] = \infty = F_0[\mathbf{x}].$$

Finally, to construct the recovery sequence for a deformation $\mathbf{y} \in \mathcal{A}_{FvK}$ we simply select $\mathbf{y}_t = \mathbf{y}$. If $\mathcal{S}[\mathbf{y}] = 0$ then

$$\lim_{\tau\to 0} F_\tau[\mathbf{y}_\tau] = \lim_{\tau\to 0}\left(\frac{1}{\tau^2}\mathcal{S}[\mathbf{y}_\tau] + \mathcal{B}[\mathbf{y}_\tau]\right) = \lim_{\tau\to 0}\mathcal{B}[\mathbf{y}] = \mathcal{B}[\mathbf{y}] = F_0[\mathbf{y}].$$

If $\mathcal{S}[\mathbf{y}] \neq 0$ then

$$\lim_{\tau\to 0} F_\tau[\mathbf{y}_\tau] = \lim_{\tau\to 0}\left(\frac{1}{\tau^2}\mathcal{S}[\mathbf{y}_\tau] + \mathcal{B}[\mathbf{y}_\tau]\right) \geq \lim_{\tau\to 0}\frac{1}{\tau^2}\mathcal{S}[\mathbf{y}] = \infty = F_0[\mathbf{y}].$$

□

Lemma 2.4.4. Let $\mathbf{x}_\tau \in \mathcal{A}_{FvK}$ such that $F_\tau[\mathbf{x}_\tau] = \inf_{\mathbf{y}} F_\tau[\mathbf{y}]$. Then, $\lim_{\tau\to 0} F_\tau[\mathbf{x}_\tau]$ exists and $0 \leq \lim_{\tau\to 0} F_\tau[\mathbf{x}_\tau] \leq 2\pi(1 - r_0^2)$.

Proof. Fix $s, t > 0$ such that $s < t$ and let $\mathbf{x}_s, \mathbf{x}_t$ such that $\inf_{\mathbf{x}\in\mathcal{A}_{FvK}} F_t[\mathbf{x}] = F_t[\mathbf{x}]$ and $\inf_{\mathbf{x}\in\mathcal{A}_{FvK}} F_s[\mathbf{x}] = F_s[\mathbf{x}]$. Then,

$$F_t[\mathbf{x}_t] \leq F_t[\mathbf{x}_s] = \frac{1}{t^2}\mathcal{S}[\mathbf{x}_s] + \mathcal{B}[\mathbf{x}_s] < \frac{1}{s^2}\mathcal{S}[\mathbf{x}_s] + \mathcal{B}[\mathbf{x}_s] = F_s[\mathbf{x}_s].$$

Therefore the sequence $\inf_{\mathbf{x}\in\mathcal{A}_{FvK}} F_s[\mathbf{x}]$ is monotone increasing as $s \to 0$ and by lemma (2.4.1), satisfies $0 \leq \inf_{\mathbf{x}\in\mathcal{A}_{FvK}} F_s[\mathbf{x}] \leq 2\pi(1 - r_0^2)$. Therefore, by the Bolzano-Weierstrass theorem $\inf_{\mathbf{x}\in\mathcal{A}_{FvK}} F_\tau[\mathbf{x}]$ converges. □

Definition 2.4.5. Define $\mathcal{A}'_{FvK} \subset \mathcal{A}_{FvK}$ by

$$\mathcal{A}'_{FvK} = \left\{ (f, g, \omega) \in \mathcal{A}_{FvK} : f(0) = g(0) = \eta(0) = 0 \text{ and } \left.\frac{\partial\eta}{\partial x}\right|_{(0,0)} = \left.\frac{\partial\eta}{\partial y}\right|_{(0,0)} = 0 \right\}.$$

The above definition fixes the origin of a deformation and aligns the normal at the origin with the z-axis of $\mathbb{R}^3$ and thus removes the possibility of a minimizing sequence "escaping to infinity". By a rigid translation and rotation any element $\mathbf{x} \in \mathcal{A}_{FvK}$ can naturally be identified with an element of $\mathcal{A}'_{FvK}$.

Theorem 2.4.6. If $\mathbf{x}_\tau \in \mathcal{A}'_{FvK}$ is a sequence such that $\inf_{\mathbf{y}\in\mathcal{A}'_{FvK}} F_\tau[\mathbf{y}] = F_\tau[\mathbf{x}_\tau]$ then

$$2\pi(1 - r_0^2) = \inf_{\mathbf{y}\in\mathcal{A}'_{FvK}} F_0[\mathbf{y}] = \lim_{\tau\to 0} F_\tau[\mathbf{x}_\tau]. \tag{2.4.7}$$

and every limit of convergent subsequence of $\mathbf{x}_t$ is a minimum point for F_0.

Proof. Let $\mathbf{x} = (f, g, \eta) \in \mathcal{A}'_{FvK}$ such that for all $\tau \in (0, 1)$, $F_\tau[\mathbf{x}] \leq 2\pi(1 - r_0^2)$. Consequently, there exists $C_1 > 0$ such that

$$\|\nabla f\|_{L^2(B,\mathbb{R})} < C_1, \quad \|\nabla g\|_{L^2(B,\mathbb{R})} < C_1, \quad \|\nabla\eta\|_{L^4(B,\mathbb{R})} < C_1, \quad \||D^2\eta|^2\|_{L^2(B,\mathbb{R})} < C_1.$$

It follows from Hölder's inequality that there exists a constant $C_2 > 0$ such that $\|\nabla\eta\|_{L^2(B,\mathbb{R})} \leq C_2\|\nabla\eta\|_{L^4(B,\mathbb{R})}$. Therefore, by Poincaré's inequality there exists a constant $C_3 > 0$ such that

$$\|f\|_{L^2(B,\mathbb{R})} < C_3, \quad \|g\|_{L^2(B,\mathbb{R})} < C_3, \quad \|\eta\|_{L^2(B,\mathbb{R})} < C_3,$$

and thus by the Banach-Alaoglu theorem (Hunter & Nachtergaele, 2001) the set $K = \{\mathbf{x} \in \mathcal{A}'_{FvK} : \forall \tau \in (0,1), F_\tau[\mathbf{x}] \leq 2\pi(1-r_0^2)\}$ is weakly compact in $\mathcal{A}'_{FvK}$.

Let $\mathbf{x}_\tau$ be a sequence such that $\inf_{\mathbf{y}\in\mathcal{A}'_{FvK}} F_\tau[\mathbf{y}] = F_\tau[\mathbf{x}_\tau]$. By (2.4.1) it follows that $F_\tau[\mathbf{x}_\tau] \leq 2\pi(1-r_0^2)$ and thus by compactness of K there exists a subsequence $\mathbf{x}_{\tau_k}$ and $\mathbf{x}^* \in \mathcal{A}'_{FvK}$ such that $\mathbf{x}_{\tau_k} \xrightarrow{\mathcal{A}'_{FvK}} \mathbf{x}^*$. Therefore, by lemmas 2.4.3 and 2.4.4 we have that

$$\inf_{\mathbf{y}\in\mathcal{A}'_{FvK}} F_0[\mathbf{y}] \leq F_0[\mathbf{x}^*] \leq \liminf_{k\to 0} F_{\tau_k}[\mathbf{x}_{t_k}] = \lim_{k\to 0} \inf_{\mathbf{y}\in\mathcal{A}'_{FvK}} F_{\tau_k}[\mathbf{y}] = \lim_{\tau\to 0} \inf_{\mathbf{y}\in\mathcal{A}'_{FvK}} F_\tau[\mathbf{y}].$$

Therefore,

$$\inf_{\mathbf{y}\in\mathcal{A}'_{FvK}} F_0[\mathbf{y}] \leq \lim_{\tau\to 0} \inf_{\mathbf{y}\in\mathcal{A}'_{FvK}} F_\tau[\mathbf{y}]. \tag{2.4.8}$$

Now, fix $\delta > 0$ and let $\mathbf{y} \in \mathcal{A}_{FvK}$ such that $F_0[\mathbf{y}] \leq \inf_{\mathbf{z}\in\mathcal{A}'_{FvK}} F_0[\mathbf{z}] + \delta$. Then, if $\mathbf{y}_j$ is recovery sequence for $\mathbf{y}$ then

$$\inf_{\mathbf{z}\in\mathcal{A}'_{FvK}} F_0[\mathbf{z}] + \delta \geq F_0[\mathbf{y}] \geq \limsup_{\tau\to 0} F_\tau[\mathbf{y}_\mathbf{t}] \geq \limsup_{\tau\to 0} \inf_{\mathbf{z}\in\mathcal{A}'_{FvK}} F_\tau[\mathbf{z}] = \lim_{\tau\to 0} \inf_{\mathbf{z}\in\mathcal{A}'_{FvK}} F_\tau[\mathbf{z}].$$

By the arbitrariness of δ if follows that

$$\inf_{\mathbf{z}\in\mathcal{A}'_{FvK}} F_0[\mathbf{z}] \geq \lim_{\tau\to 0} \inf_{\mathbf{z}\in\mathcal{A}'_{FvK}} F_\tau[\mathbf{z}]. \tag{2.4.9}$$

Therefore, by (2.4.8) and (2.4.9) we have proved that

$$\inf_{\mathbf{z}\in\mathcal{A}'_{FvK}} F_0[\mathbf{z}] = \lim_{\tau\to 0} \inf_{\mathbf{z}\in\mathcal{A}'_{FvK}} F_\tau[\mathbf{z}].$$

Furthermore, if $\mathbf{y}_\tau$ is the sequence as defined above and $\mathbf{y}_{\tau_k}$ is a subsequence such that $\mathbf{y}_{\tau_k} \xrightarrow{\mathcal{A}'_{FvK}} \mathbf{y}^*$ then

$$\lim_{\tau\to 0} \inf_{\mathbf{z}\in\mathcal{A}'_{FvK}} F_\tau[\mathbf{z}] = \inf_{\mathbf{z}\in\mathcal{A}'_{FvK}} F_0[\mathbf{z}] \leq F_0[\mathbf{y}^*] \leq \lim_{\tau\to 0} \inf_{\mathbf{z}\in\mathcal{A}'_{FvK}} F_\tau[\mathbf{z}],$$

which proves that

$$\inf_{\mathbf{z}\in\mathcal{A}'_{FvK}} F_0[\mathbf{z}] = F_0[\mathbf{y}^*].$$

□

2.4.3 Periodic Isometric Immersions

The saddle shaped isometric immersion with out-of-plane displacement $\eta = xy$ is not the only solution to the Monge-Ampere equation (2.4.1). The one parameter family of quadratic functions

$$\overline{\eta}_n = y\left(x - \cot\left(\frac{\pi}{n}\right)y\right) = \frac{r^2}{2}\csc\left(\frac{\pi}{n}\right)\left[\cos\left(\frac{\pi}{n} - 2\theta\right) - \cos\left(\frac{\pi}{n}\right)\right], \tag{2.4.10}$$

satisfy (2.4.1) and $\Delta^2\overline{\eta} = 0$ as well (Polyanin & Zaitsev, 2004). Furthermore, this family of surfaces vanish along the lines $\theta = \pi/n$ and $\theta = 0$. Therefore, if $n \in \{2, 3, 4, \ldots\}$, a deformation with a periodic profile can be constructed by odd periodic extensions (see figure 2.1). It is a basic result of Fourier analysis that η_n has continuous first partial derivatives but a jump in the second partial derivative with respect to θ at integer multiples of π/n. Consequently, these lines of inflection are singularities in the sense that the deformation is not smooth along these lines but $\eta_n \in W^{2,2}(B, \mathbb{R})$ and the bending energy remains continuous and is finite. Therefore, these surfaces are valid isometric immersions in the FvK approximation and thus $\mathcal{A}_n \cap \mathcal{A}_0 \neq \emptyset$ and by calculating the energy of this configuration we have the following result which agrees with proposition 2.4.1 when $n = 2$.

Lemma 2.4.7. Let $\mathbf{x}^* \in \mathcal{A}_n$ such that $\mathcal{E}_\tau[\mathbf{x}^*] = \inf_{\mathbf{x}\in\mathcal{A}_n}\mathcal{E}_\tau[\mathbf{x}]$, then

$$\mathcal{E}_\tau[\mathbf{x}^*] \leq \min\left\{\tau^2\left(\frac{4\pi\cot^2(\pi/n)}{1-\nu} + 2\pi\right)(1 - r_0^2), \mathcal{F}\right\} \leq \min\left\{Cn^2\tau^2, \mathcal{F}\right\},$$

where C is a constant independent of n and τ.

Proof. The middle term in the chain of inequalities is the bending energy of the deformation η_n and the calculation is omitted. Expanding near $n = \infty$ we have that

$$\frac{4\pi\cot^2\left(\frac{\pi}{n}\right)}{1-\nu} + 2\pi = \frac{4n^2}{\pi(1-\nu)} + \left(2\pi - \frac{8\pi}{3(1-nu)}\right) + \ldots .$$

Consequently there exists $M > 0$ and $K_1 > 0$ such that if $n \geq M$ then

$$\frac{4\pi\cot^2\left(\frac{\pi}{n}\right)}{1-\nu} + 2\pi \leq K_1 n^2.$$

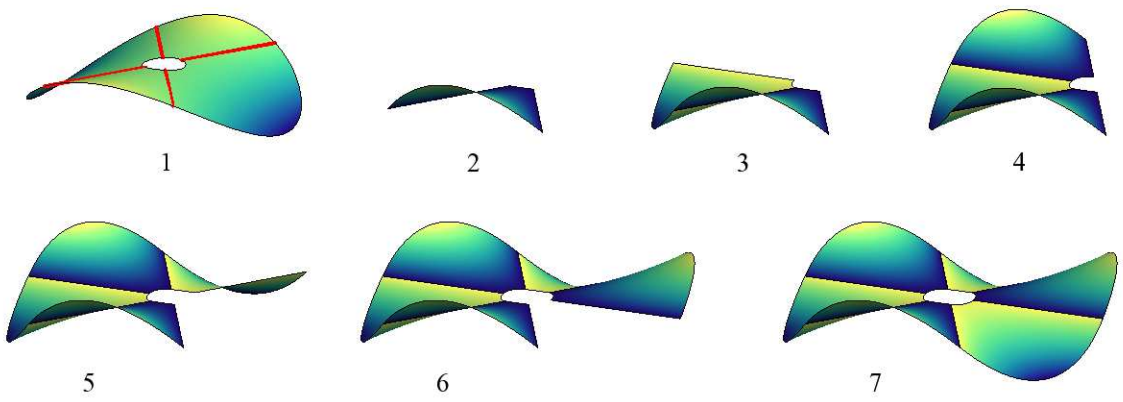

FIGURE 2.1. **1.** The one parameter family of isometric immersions with out-of-plane displacement $\eta = y\,(x - \cot\,(\pi/n))$ parametrized by $n \in \{2, 3, \ldots\}$ vanishes along the lines $\theta = 0$ and $\theta = \pi/n$. **2.** We can "cut out" the section of the surface bounded between these two lines. **3.** We can take the odd reflection of this isolated piece of the surface about the the line $\theta = 0$. **4-7.** By continually taking the odd reflection of sectors about lines where the surface vanishes we can construct a periodic isometric immersion.

Differentiating we have that

$$\frac{d}{dn}\cot^2\left(\frac{\pi}{n}\right) = \frac{2\cot^2\left(\frac{\pi}{n}\right)\csc\left(\frac{\pi}{n}\right)}{n^2}$$

and thus $\cot^2\left(\frac{\pi}{n}\right)$ is monotone increasing. Consequently, on the interval $[2, M]$ we have that

$$\frac{4\pi\cot^2\left(\frac{\pi}{n}\right)}{1-\nu} + 2\pi \leq \left(\frac{\pi\cot^2\left(\frac{\pi}{M}\right)}{1-\nu} + \frac{\pi}{2}\right) n^2 = K_2 n^2.$$

Therefore, if we set $C = \max\{K_1, K_2\}$ then the result follows. □

The preceding lemma shows that the elastic energy of periodic isometric immersions grows like n^2, and thus the two wave isometric immersion is energetically preferred over isometric immersions with more waves. Furthermore, by theorem 2.4.6 minimizers of the elastic energy converge to a saddle shaped deformation with decreasing thickness. But, the periodic isometric immersions we constructed are qualitatively

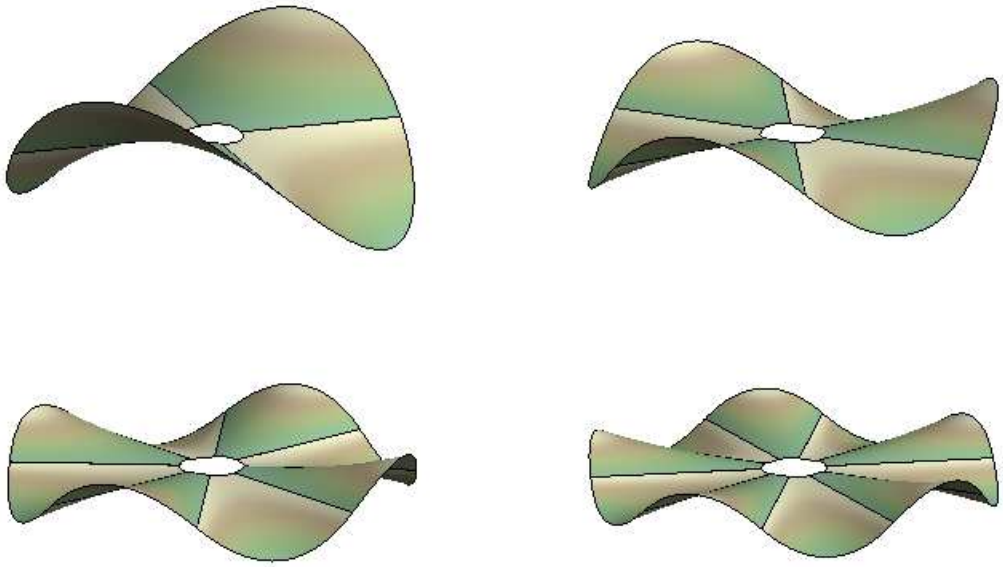

FIGURE 2.2. Periodic isometric immersions in the FvK ansatz

similar to what is observed in experiments (see figure 2.2) and thus we will continue to study them in future sections.

2.5 Numerical Solutions

Beyond the flat solution, exact solutions to the Föppl-von Kármán equations are largely unknown. In this section we construct numerical solutions to illustrate the transition of the flat solutions to ones that are approximately isometric immersions. The boundary value problem given by (2.2.4-2.2.8) can be approximately solved by numerically minimizing $\mathcal{E}_\tau$ using a Rayleigh-Ritz type algorithm (Szilard, 2004). To do this, it is convenient to write the energy in the form

$$\begin{aligned}\mathcal{E}_\tau[\mathbf{x}] = &\int_B \left[\frac{\nu}{1-\nu}\left(\gamma_{11}^2+\gamma_{22}\right)^2+\gamma_{11}^2+2\gamma_{12}^2+\gamma_{22}^2\right] dxdy \\ &+\tau^2\int_B \left[\frac{\nu}{1-\nu}\left(\Delta\eta\right)^2+\left(\frac{\partial^2\eta}{\partial x^2}\right)^2+2\left(\frac{\partial^2\eta}{\partial x\partial y}\right)^2+\left(\frac{\partial^2\eta}{\partial y^2}\right)^2\right] dxdy. \quad (2.5.1)\end{aligned}$$

$\mathcal{E}_\tau[\mathbf{x}]$ can then be discretized using a finite difference scheme to approximate the integrand and a composite quadrature rule to approximate the integrals. This discretization of (2.5.1) generates a sum of quadratic terms that can then be minimized using Matlab's minimization routine lsqnonlin (MATLAB, 2010).

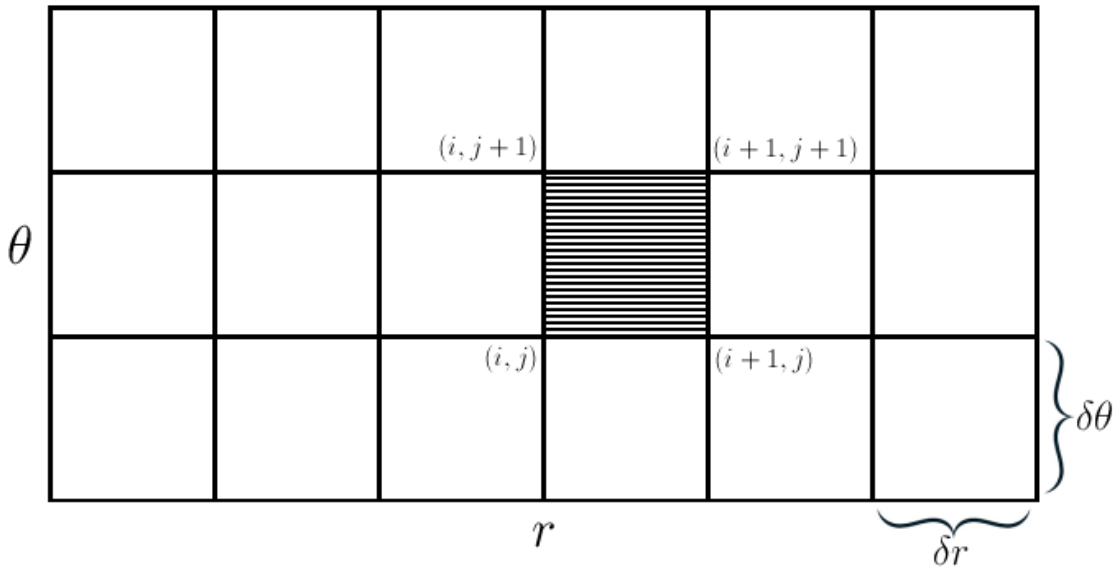

FIGURE 2.3. Stencil of the domain.

To be specific, we use a uniform discretization in the variables r and θ with spacing δr and $\delta\theta$ respectively and approximate the integral (2.5.1) in a coordinate rectangle $B_{i,j}$ with lower left index (i, j) (see figure 2.3) by

$$\mathcal{E}_\tau^{i,j}[\mathbf{x}] = \frac{\delta r \delta\theta}{4} \sum_{l=0}^{1} \sum_{k=0}^{1} \left[\frac{\nu}{1-\nu} \left(\gamma_{11}^{i,j} + \gamma_{22}^{i,j}\right)^2 + \left(\gamma_{11}^{i,j}\right)^2 + 2\left(\gamma_{12}^{i,j}\right)^2 + \left(\gamma_{22}^{i,j}\right)^2 \right] r^{i,j}$$
$$+\tau^2 \frac{\delta r \delta\theta}{4} \sum_{l=0}^{1} \sum_{k=0}^{1} \left[\frac{\nu}{1-\nu} \left(\Delta\eta^{i,j}\right)^2 + \left(\frac{\partial^2 \eta^{i,j}}{\partial x^2}\right)^2 + 2\left(\frac{\partial^2 \eta^{i,j}}{\partial x \partial y}\right)^2 + \left(\frac{\partial^2 \eta^{i,j}}{\partial y^2}\right)^2 \right] r^{i,j}.$$

The derivatives are then approximated by a fourth order finite differences with appropriate forward and backward schemes near the boundary (see appendix B). Summing

over i and j the elastic energy is approximated by

$$\mathcal{E}[\mathbf{x}] = \sum_i \sum_j \mathcal{E}^{i,j}[\mathbf{x}] + \mathcal{O}(\delta r^2 + \delta\theta^2).$$

This discrete sum of quadratic terms can then be directly minimized.

It is important to note that we used a fourth order difference schemes to approximate derivatives. This is critical to obtain an accurate approximation in that for lower order schemes the error in the stretching energy may be significantly bounded away from zero. That is, the numerical algorithm will not detect the existence of an isometric immersion. Furthermore, as the thickness decreases the bending content of an isometric immersion will be lower than the error in approximating the stretching energy. Therefore, the algorithm will break down at a critical thickness τ^* which can be estimated by

$$\tau^* = \sqrt{\delta r^4 + \delta\theta^4}.$$

In figure 2.4 we plot the elastic energy of numerical minimizers of $\mathcal{E}_\tau$ for decreasing values of τ with $r_0 = 1$ and $\nu = 1/2$. The data in this figure was generated using the algorithm outlined above with a 40×40 mesh. The solid line corresponds to the upper bound in lemma 2.3.1 for flat deformations while the dashed line is the upper bound in proposition 2.4.1 for isometric immersions. In this figure three representative minimizers are plotted and colored by the Gaussian curvature $K = \det(D^2\eta)$ for various values of τ. These three surfaces and the scaling of the energy illustrate that with decreasing thickness the minimizing surface transitions from being flat to one that is close to the isometric immersion $\eta = xy$. For the left most surface, the regions in which the Gaussian curvature is substantially different from -1 are localized to the edges of the annulus and shrink with decreasing thickness. This indicates that with decreasing thickness the stretching energy is being concentrated in boundary layers in which the bending energy of the isometric energy is slightly reduced.

In figure 2.5 we again plot the numerical minimizers of $\mathcal{E}_\tau$ using the same parameters and discretization used to generate figure 2.4 but with the boundary conditions

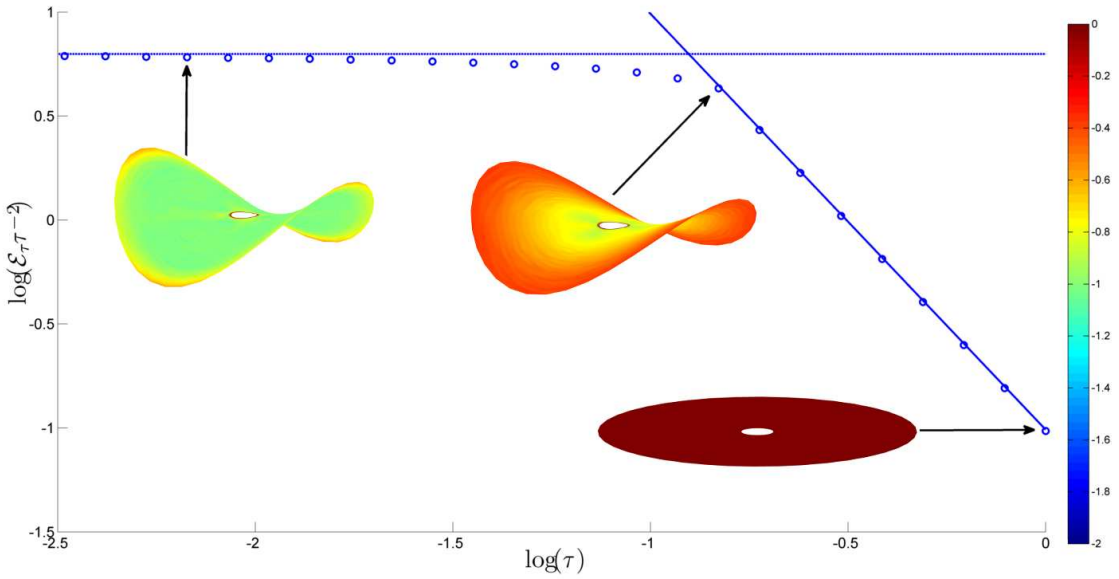

FIGURE 2.4. The normalized elastic energy of numerical minimizers of $\mathcal{E}_\tau$ with $\nu = 1/2$ and $r_0 = 10^{-1}$ for decreasing values of τ. The solid line corresponds to the elastic energy of minimizers over the set of flat deformations given by lemma 2.3.1. The dashed line corresponds to the elastic energy over the set of deformations satisfying $\gamma = 0$ given in lemma 2.4.1. The three configurations plotted are colored by the approximate Gaussian curvature $K = [\eta, \eta]$. These three surfaces illustrate that with decreasing thickness the surface transitions from being a flat surface to one that is close to the isometric immersion $\eta = xy$ with localized regions of stretching near the inner and outer radius of the disk.

$\eta = 0$ along the lines $\theta = 0, \pi/n, 2\pi/n, \ldots$ for $n \in \{2, 3, 4, 5\}$. These boundary conditions were selected to generate numerical minimizers over $\mathcal{A}_n$. The dashed lines correspond to the upper bounds for n-periodic isometric immersions given by lemma 2.4.7 while the solid line is again the upper bound in lemma 2.3.1. The four plotted surfaces are colored by the approximate Gaussian curvature $K = [\eta, \eta]$ and were selected to compare the geometry of the boundary layers for $n \geq 3$ with the case $n = 2$. For $n \geq 3$ additional boundary layers form around the lines of inflection in which the surface stretches to reduce the local mean curvature of the surface. Notice also that for $n \geq 3$ the Gaussian curvature within the boundary layers near the edge of the disk satisfies $[\eta, \eta] < -1$ which is in contrast to the case when $n = 2$ where $[\eta, \eta] > -1$.

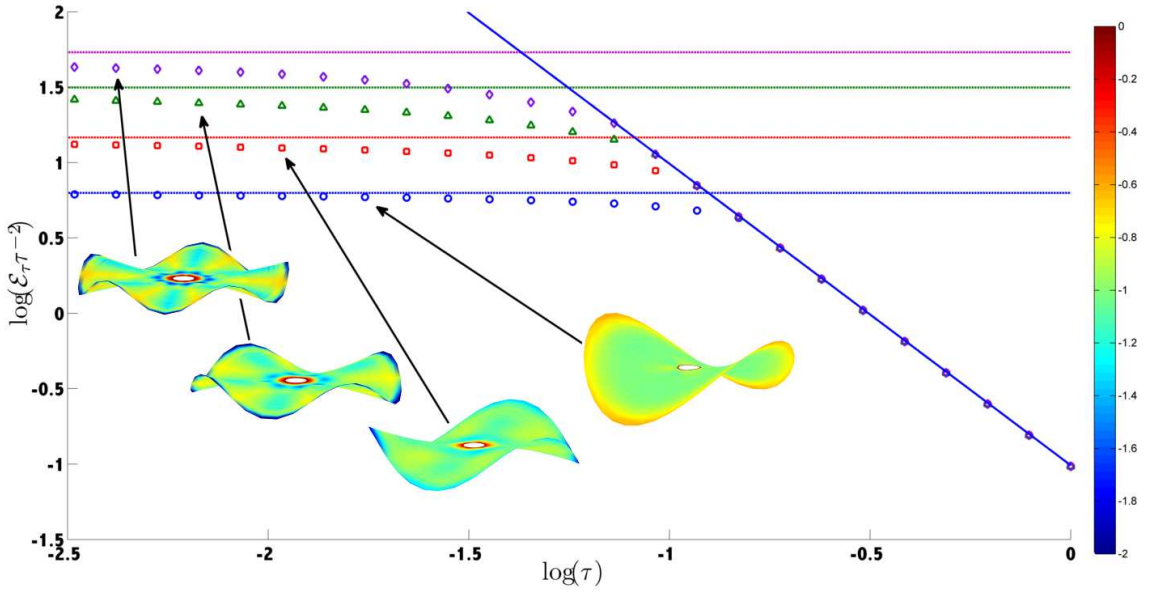

FIGURE 2.5. The normalized elastic energy of numerical minimizers of $\mathcal{E}_\tau$ over $\mathcal{A}_n$ with $r_0 = 10^{-1}$ and $\nu = 1/2$. The dashed lines correspond to the upper bounds given by lemma 2.4.7 while the solid line corresponds to the upper bound in lemma 2.3.1. The configurations plotted are colored by the approximate Gaussian curvature $[\eta, \eta]$. In the vanishing thickness limit minimizers of $\mathcal{E}_\tau$ converge to an n-periodic isometric immersion. The numerical minimizers have localized regions of stretching near the inner and outer radius and along the lines of inflection. The existence of these regions indicate that the minimizers are perturbations of an isometric immersion with boundary layers to account for the natural boundary conditions.

2.6 Scaling Laws for the Elastic Energy of Periodic Deformations

In this section we derive ansatz free lower bounds for n-periodic configurations. The essential idea of this section is that the bending energy near the edge of the annulus controls the stretching energy in the bulk of the annulus. Before we state and prove this lower bound we need several intermediate results. Let $n \in \{2, 3, \ldots\}$ and define the following sets:

1. S_n is the sector in $\mathbb{R}^2$ bounded between $\theta = 0$ and $\theta = \pi/n$,

2. For $z > r_0$, $B^z \subset B$ is the annular region defined by $B^z = \{(r, \theta) \in B : r_0 \leq$

$z \leq r \leq 1\}$,

3. $B_n^z = S_n \cap B^z$ is a wedge shaped region bounded between $\theta = 0$, $\theta = \pi/n$, $r = 1$, and $r = z$.

Furthermore, let $r^* = \max\{.95, r_0\}$.

Lemma 2.6.1. If $\mathbf{x} \in \mathcal{A}_n$ with corresponding out-of-plane displacement η then

1.
$$\int_{B_n^z} \left(\frac{\partial \eta}{\partial r}\right)^2 dA \leq \frac{1}{n^2} \int_{B_n^z} \left(\frac{\partial^2 \eta}{\partial r \partial \theta}\right)^2 dA \tag{2.6.1}$$

2.
$$\int_{B_n^z} \eta^2 \, dA \leq \frac{\pi^4}{48n^4} \int_{B_n^z} \left(\frac{\partial^2 \eta}{\partial \theta^2}\right)^2 dA \tag{2.6.2}$$

3.
$$\int_{B_n^z} \left(\frac{\partial \eta}{\partial \theta}\right)^2 dA \leq \frac{\pi^2}{12n^2} \int_{B_n^z} \left(\frac{\partial^2 \eta}{\partial \theta^2}\right)^2 dA \tag{2.6.3}$$

Proof. Since $\mathbf{x} \in \mathcal{A}_n$ we have that $\eta = 0$ along the lines $\theta = 0, \pi/n$ and thus

$$\left.\frac{\partial \eta}{\partial r}\right|_{\theta = 0, \frac{\pi}{n}} = 0.$$

Consequently it follows from Poincare's inequality with the optimal constant that

$$\int_0^{\frac{\pi}{n}} \left(\frac{\partial \eta}{\partial r}\right)^2 d\theta \leq \frac{1}{n^2} \int_0^{\frac{\pi}{n}} \left(\frac{\partial^2 \eta}{\partial r \partial \theta}\right)^2 d\theta,$$

(Payne & Weinberger, 1960). Therefore, integrating we have that

$$\int_{B_n^z} \left(\frac{\partial \eta}{\partial r}\right)^2 dA \leq \frac{1}{n^2} \int_{B_n^z} \left(\frac{\partial^2 \eta}{\partial r \partial \theta}\right)^2 dA,$$

proving item 1.

Constructing the Green's function $G(\theta, \phi)$ for the operator $\frac{\partial^2}{\partial \theta^2}$ with Dirichlet boundary conditions on $[0, \pi/n]$ we have that

$$\eta(r, \theta) = \int_0^{\frac{\pi}{n}} G(\theta, \phi) \frac{\partial^2 \eta}{\partial \phi^2} d\phi,$$

where

$$G(\theta,\phi)=\begin{cases}\frac{n}{\pi}\phi(\theta-\pi/n), & \text{if } \theta<\phi\\ \frac{n}{\pi}\theta(\phi-\pi/n), & \text{if } \phi<\theta\end{cases}.$$

Therefore,

$$\begin{aligned}\eta^2(r,\theta) &\leq \left(\int_0^{\frac{\pi}{n}} G^2(\theta,\phi)dA\right)\left(\int_0^{\frac{\pi}{n}}\left(\frac{\partial^2\eta}{\partial\theta^2}\right)^2 d\theta\right)\\ &= \frac{\theta^2(\pi-n\theta)^2}{3n\pi}\int_0^{\frac{\pi}{n}}\left(\frac{\partial^2\eta}{\partial\theta^2}\right)^2 d\theta\\ &\leq \frac{\pi^3}{48n^3}\int_0^{\frac{\pi}{n}}\left(\frac{\partial^2\eta}{\partial\theta^2}\right)^2 d\theta.\end{aligned}$$

Integrating we have that

$$\int_{B_n^z}\eta^2 dA\leq\frac{\pi^4}{48n^4}\int_{B_n^z}\left(\frac{\partial^2\eta}{\partial\theta^2}\right)^2 dA,$$

proving item 2.

Differentiating, we have that

$$\frac{\partial\eta}{\partial\theta}=\int_0^{\frac{\pi}{n}}\frac{\partial G}{\partial\theta}\frac{\partial^2\eta}{\partial\phi^2}d\phi.$$

Therefore,

$$\begin{aligned}\left(\frac{\partial\eta}{\partial\theta}\right)^2 &\leq \left(\int_0^{\frac{\pi}{n}}\left(\frac{\partial G}{\partial\theta}\right)^2 d\phi\right)\left(\int_0^{\frac{\pi}{n}}\left(\frac{\partial^2\eta}{\partial\theta^2}\right)^2 d\theta\right)\\ &= \left(\frac{\pi}{3n}-\theta+\frac{n\theta^2}{\pi}\right)\int_0^{\frac{\pi}{n}}\left(\frac{\partial^2\eta}{\partial\phi^2}\right)^2 d\phi\\ &\leq \frac{\pi}{12n}\int_0^{\frac{\pi}{n}}\left(\frac{\partial^2\eta}{\partial\phi}\right)^2 d\phi.\end{aligned}$$

Integrating we have that

$$\int_{B_n^z}\left(\frac{\partial\eta}{\partial\theta}\right)^2 dA\leq\frac{\pi^2}{12n^2}\int_{B_n^z}\left(\frac{\partial^2\eta}{\partial\theta^2}\right)^2 dA,$$

proving item 3. □

Lemma 2.6.2. Let $\mathbf{x} \in \mathcal{A}_n$ with corresponding out-of-plane displacement η. If $\mathcal{B}[\mathbf{x}] \leq \mathcal{B}_0$ and $n > 2$ then there exists a constant C independent of n and $\mathbf{x}$ such that

$$\int_{B_n^{r^*}} \left[\left(\frac{\partial^2 \eta}{\partial \theta^2} \right)^2 + \left(\frac{\partial^2 \eta}{\partial r \partial \theta} \right)^2 \right] dA \leq C \frac{\mathcal{B}_0}{n}.$$

Proof. Since $\mathcal{B}[\mathbf{x}] < \mathcal{B}_0$ it follows that

$$\begin{aligned} \int_{B_n^{r_0}} |D^2 \eta|^2 dA &= \int_{B_n^{r_0}} \left[\frac{1}{r^2} \left(\frac{1}{r} \frac{\partial \eta}{\partial \theta} - \frac{\partial^2 \eta}{\partial r \partial \theta} \right)^2 + \frac{1}{r^4} \left(\frac{\partial^2 \eta}{\partial \theta^2} + r \frac{\partial \eta}{\partial r} \right)^2 + \left(\frac{\partial \eta}{\partial r} \right)^2 \right] dA \\ &\leq \frac{\mathcal{B}_0}{2n}. \end{aligned}$$

Therefore,

$$\int_{B_n^{r^*}} \left[\left(\frac{1}{r} \frac{\partial \eta}{\partial \theta} - \frac{\partial^2 \eta}{\partial r \partial \theta} \right)^2 + \left(\frac{\partial^2 \eta}{\partial \theta^2} + r \frac{\partial \eta}{\partial r} \right)^2 \right] dA \leq \frac{\mathcal{B}_0}{2n}$$

and thus applying the elementary inequality $(a+b)^2 \geq \frac{1}{2}a^2 - 2b^2$ we have that

$$\frac{1}{2} \int_{B_n^{r^*}} \left[\left(\frac{\partial^2 \eta}{\partial \theta^2} \right)^2 + \left(\frac{\partial^2 \eta}{\partial r \partial \theta} \right)^2 \right] dA - 2 \int_{B_n^{r^*}} \left[\frac{1}{r^2} \left(\frac{\partial \eta}{\partial \theta} \right)^2 + r^2 \left(\frac{\partial \eta}{\partial r} \right)^2 \right] dA \leq \frac{\mathcal{B}_0}{2n}.$$

Consequently, applying lemma 2.6.1 we have that

$$\begin{aligned} \int_{B_n^{r^*}} \left[\left(\frac{\partial^2 \eta}{\partial \theta^2} \right)^2 + \left(\frac{\partial^2 \eta}{\partial r \partial \theta} \right)^2 \right] dA &\leq \frac{\mathcal{B}_0}{n} + 4 \int_{B_n^{r^*}} \left[\frac{1}{(r^*)^2} \left(\frac{\partial \eta}{\partial \theta} \right)^2 + \left(\frac{\partial \eta}{\partial r} \right)^2 \right] dA \\ &\leq \frac{\mathcal{B}_0}{n} + \frac{\pi^2}{3n^2 (r^*)^2} \int_{B_n^{r^*}} \left(\frac{\partial^2 \eta}{\partial \theta^2} \right)^2 dA + \frac{4}{n^2} \int_{B_n^{r^*}} \left(\frac{\partial^2 \eta}{\partial r \partial \theta} \right)^2 dA. \end{aligned}$$

Therefore, since $r^* > \pi/(2\sqrt{3})$ and $n > 2$ the result follows. □

Lemma 2.6.3. Let $\mathbf{x} \in \mathcal{A}_n$ with corresponding out-of-plane displacement η. If $\mathcal{B}[\mathbf{x}] \leq \mathcal{B}_0$ and $n > 2$ then there exists a constant C independent of $\mathbf{x}$ and n such that

$$\int_{B^{r^*}} |\nabla \eta|^4 dA \leq C \frac{\mathcal{B}_0}{n^2}.$$

Proof. By lemmas 2.6.1 and 2.6.2 it follows that

$$\int_{B_n^{r^*}} \eta^2 \, dA \leq \frac{\pi^4}{48n^4} \int_{B_n^{r^*}} \left(\frac{\partial^2 \eta}{\partial \theta^2} \right)^2 dA \leq C_1 \frac{\mathcal{B}_0}{n^5}$$

and

$$\begin{aligned}\int_{B_n^{r^*}} |\nabla\eta|^2 dA &= \int_{B_n^{r^*}} \left[\left(\frac{\partial^2\eta}{\partial r}\right)^2 + \frac{1}{r^2}\left(\frac{\partial\eta}{\partial\theta}\right)^2\right] dA \\ &\leq \int_{B_n^{r^*}} \left[\left(\frac{\partial^2\eta}{\partial r}\right)^2 + \frac{1}{(r^*)^2}\left(\frac{\partial\eta}{\partial\theta}\right)^2\right] dA \\ &\leq C_2\frac{\mathcal{B}_0}{n^3}.\end{aligned}$$

By rotational symmetry of $\mathcal{A}_n$ we have that

$$\int_{B^{r^*}} \eta^2\, dA \leq C_1\frac{\mathcal{B}_0}{n^4} \text{ and } \int_{B^{r^*}} |\nabla\eta|^2 dA \leq C_2\frac{\mathcal{B}_0}{n^2}$$

and therefore by a multiplicative inequality (Maz'ya, 2011) it follows that there exists a constant C_3 independent of $\mathbf{x}$ and n such that

$$\begin{aligned}\int_{B^{r^*}} |\nabla\eta|^4 dA &\leq C_3\left(\int_{B^{r^*}} \eta^2 dA\right)^{\frac{1}{2}}\left(\int_{B^{r^*}} \left(\eta^2 + |\nabla\eta|^2 + |D^2\eta|^2\right) dA\right)^{\frac{3}{2}} \\ &\leq C\frac{\mathcal{B}_0^{\frac{1}{2}}}{n^2}\left(C_1\frac{\mathcal{B}_0}{n^4} + C_2\frac{\mathcal{B}_0}{n^2} + \mathcal{B}_0\right)^{\frac{3}{2}} \\ &\leq C\frac{\mathcal{B}_0^2}{n^2}.\end{aligned}$$

□

Lemma 2.6.4. Let $\mathbf{x} \in \mathcal{A}_2$ with corresponding out-of-plane displacement η. If $\mathcal{B}_\tau[\mathbf{x}] \leq \mathcal{B}_0$ then there exists a constant C independent of $\mathbf{x}$ such that

$$\int_{B^{r^*}} |\nabla\eta|^4 dA \leq C\frac{\mathcal{B}_0^2}{4}$$

Proof. Since $\mathbf{x} \in \mathcal{A}_2$ it follows that the means of the functions η, $\frac{\partial\eta}{\partial x}$, and $\frac{\partial\eta}{\partial y}$ satisfy

$$\begin{aligned}\langle\eta\rangle &= \frac{1}{\pi(1-(r^*)^2)}\int_{B^{r^*}} \eta\, dA = 0, \\ \left\langle\frac{\partial\eta}{\partial x}\right\rangle &= \frac{1}{\pi(1-(r^*)^2)}\int_{B^{r^*}} \frac{\partial\eta}{\partial x}\, dA = 0, \\ \left\langle\frac{\partial\eta}{\partial y}\right\rangle &= \frac{1}{\pi(1-(r^*)^2)}\int_{B^{r^*}} \frac{\partial\eta}{\partial y}\, dA = 0.\end{aligned}$$

Therefore, by Poincare's inequality it follows that there exists constants C_1 and C_2 independent of $\mathbf{x}$ such that

$$\int_{B^{r^*}} \left(\frac{\partial \eta}{\partial x}\right)^2 dA \leq C_1 \int_{B^{r^*}} |\nabla \eta|^2 dA \text{ and } \int_{B^{r^*}} |\nabla \eta|^2 dA \leq C_2 \int_{B^{r^*}} |D^2 \eta|^2 dA.$$

Consequently, by applying the same multiplicative inequality as in the proof of lemma 2.6.3 the result follows. □

Lemma 2.6.5. Let $\mathbf{x} \in \mathcal{A}_n$. If $\mathcal{B}[\mathbf{x}] \leq \mathcal{B}_0$ then there exists a constant $C > 0$ independent of $\mathbf{x}$ and n such that

$$\mathcal{S}[\mathbf{x}] \geq \frac{1}{2}\mathcal{F}^* - C\frac{\mathcal{B}_0^2}{n^2},$$

where $\mathcal{F}^*$ is the infimum in lemma 2.3.1 with $r_0 = r^*$

Proof. Let η be the out-of-plane displacement corresponding to $\mathbf{x}$ and $\chi = (f, g)$ the in-plane displacement with component functions $f, g \in W^{1,2}(\mathbb{B}, \mathbb{R})$. Then, by lemmas 2.6.3 and 2.6.4 it follows that there exists a constant C independent of $\mathbf{x}$ and n such that

$$\int_{B^{r^*}} |\nabla \eta|^4 dA \leq \int_B |\nabla \eta|^4 dA \leq C\frac{\mathcal{B}_0}{n^2}.$$

Therefore, the following inequalities hold:

1.

$$\begin{aligned}
\int_{B^{r^*}} \gamma_{11}^2 \, dxdy &= \int_{B^{r^*}} \left(2\frac{\partial f}{\partial x} + \left(\frac{\partial \eta}{\partial x}\right)^2 - \frac{y^2}{3}\right) dxdy \\
&\geq \frac{1}{2}\int_{B^{r^*}} \left(2\frac{\partial f}{\partial x} - \frac{y^2}{3}\right)^2 dxdy - 2\int_{B^{r^*}} \left(\frac{\partial \eta}{\partial x}\right)^4 dxdy \\
&\geq \frac{1}{2}\int_{B^{r^*}} \left(2\frac{\partial f}{\partial x} - \frac{y^2}{3}\right)^2 dxdy - 2C\frac{\mathcal{B}_0^2}{n^2}.
\end{aligned}$$

2.

$$\int_{B^{r^*}} \gamma_{22}^2 \, dxdy \geq \frac{1}{2}\int_{B^{r^*}} \left(2\frac{\partial g}{\partial y} - \frac{x^2}{3}\right)^2 dxdy - 2C\frac{\mathcal{B}_0^2}{n^2}.$$

3.

$$\begin{aligned}\int_{B^{r^*}} \gamma_{12}^2\,dxdy &\geq \frac{1}{2}\int_{B^{r^*}} \left(\frac{\partial f}{\partial y}+\frac{\partial g}{\partial x}+\frac{xy}{3}\right)^2 dxdy - 2\int_{B^{r^*}} \left(\frac{\partial \eta}{\partial x}\right)^2\left(\frac{\partial \eta}{\partial y}\right)^2 dxdy \\ &\geq \frac{1}{2}\int_{B^{r^*}} \left(\frac{\partial f}{\partial y}+\frac{\partial g}{\partial x}+\frac{xy}{3}\right)^2 dxdy \\ &\quad -2\left(\int_{B^{r^*}} \left(\frac{\partial \eta}{\partial x}\right)^4 dxdy\right)^{1/2}\left(\int_{B^{r^*}} \left(\frac{\partial \eta}{\partial y}\right)^4 dxdy\right)^{1/2} \\ &\geq \frac{1}{2}\int_{B^{r^*}} \left(\frac{\partial f}{\partial y}+\frac{\partial g}{\partial x}+\frac{xy}{3}\right)^2 dxdy - 2C\frac{\mathcal{B}_0^2}{n^2}.\end{aligned}$$

4.

$$\int_{B^{r^*}} (\gamma_{11}+\gamma_{22})^2\,dxdy \geq \frac{1}{2}\int_{B^{r^*}} \left(2\frac{\partial f}{\partial x}+2\frac{\partial g}{\partial y}-\frac{x^2}{3}-\frac{y^2}{3}\right)^2 dxdy - 8C\frac{\mathcal{B}_0^2}{n^2}.$$

Therefore, since $\mathcal{S}[\mathbf{x}]$ can be rewritten in the following form

$$\begin{aligned}\mathcal{S}[\mathbf{x}] &= \int_B \left(\frac{1}{1-\nu}\mathrm{tr}(\gamma)^2 - 2\det(\gamma)\right) dxdy \\ &= \int_B \left(\frac{\nu}{1-\nu}(\gamma_{11}+\gamma_{22})^2 + \gamma_{11}^2 + 2\gamma_{12}^2 + \gamma_{22}^2\right) dxdy \\ &\geq \int_{B^{r^*}} \left(\frac{\nu}{1-\nu}(\gamma_{11}+\gamma_{22})^2 + \gamma_{11}^2 + 2\gamma_{12}^2 + \gamma_{22}^2\right) dxdy\end{aligned}$$

it follows by items 1-4 that there exists a constant C independent of n and $\mathbf{x}$ such that

$$\mathcal{S}[\mathbf{x}] \geq \frac{1}{2}\mathcal{F}^* - C\frac{\mathcal{B}_0^2}{n^2}.$$

□

The preceding lemma is the essential estimate that quantifies the trade off between bending and stretching energy. Furthermore, it shows that in the limit $n \to \infty$ that $\mathcal{S}$ is bounded away from zero. That is, as the bending energy increases by adding more waves there is no reduction in the stretching energy. This is in contrast to the behavior of a minimal ridge in which with decreasing thickness the bending energy diverges while the stretching energy converges to zero (Venkataramani, 2004; Conti & Maggi, 2008).

Theorem 2.6.6. Suppose $n \in \{2, 3, \ldots\}$ and $\tau > 0$. There exists constants $c, C > 0$ independent of n such that

$$\min\{cn\tau^2, \mathcal{F}^*/2\} \leq \inf_{\mathbf{x}\in\mathcal{A}_n} \mathcal{E}[\mathbf{x}] \leq \min\{Cn^2\tau^2, \mathcal{F}\}.$$

Proof. By lemma 2.6.5 there exists a constant c_1 independent of n and $\mathbf{x}$ such that

$$\mathcal{S}[\mathbf{x}] \geq \frac{1}{2}\mathcal{F}^* - c_1\frac{\mathcal{B}[\mathbf{x}]^2}{n^2}.$$

Therefore, minimizing the function $\mathcal{E} = \mathcal{S} + \tau^2\mathcal{B}$ subject to the constraints

$$\mathcal{S} \geq 0, \quad \tau^2\mathcal{B} \geq 0, \quad \mathcal{S} \geq \tfrac{1}{2}\mathcal{F}^* - c_1\tfrac{\mathcal{B}}{n^2},$$

it follows that there exists a constant c independent of n and $\mathbf{x}$ such that

$$\min\left\{cn\tau^2, \mathcal{F}^*/2\right\} \leq \inf_{\mathbf{x}\in\mathcal{A}_n} \mathcal{E}[\mathbf{x}]$$

The upper bound follows from lemma 2.4.7. □

Corollary 2.6.7. There exists $n^* \geq 2$ such that if $\tau < [\mathcal{F}^*/(4\pi(1-r_0^2))]^{1/2}$ and $n > n^*$ then

$$\inf_{\mathbf{x}\in\mathcal{A}} \mathcal{E}_\tau[\mathbf{x}] < \inf_{\mathbf{x}\in\mathcal{A}_n} \mathcal{E}_\tau[\mathbf{x}].$$

Proof. By theorem 2.6.6 it follows that there exists a constant c independent of n and τ such that $\min\{cn\tau^2, \mathcal{F}^*/2\} \leq \inf_{\mathbf{x}\in\mathcal{A}_n} \mathcal{E}_\tau[\mathbf{x}]$. Furthermore, if $\tau < [\mathcal{F}^*/(4\pi(1-r_0^2))]^{1/2}$ then $2\pi(1-r_0^2)\tau^2 < \mathcal{F}^*/2$ and if $n > 2\pi(1-r_0^2)/c$ then $2\pi(1-r_0)^2 < cn$. Therefore, letting $n^* = 2\pi(1-r_0^2)/c$ it follows that if $\tau < [\mathcal{F}^*/(4\pi(1-r_0^2))]^{1/2}$ and $n > n^*$ then by proposition 2.4.1

$$\inf_{\mathbf{x}\in\mathcal{A}} \mathcal{E}_\tau[\mathbf{x}] \leq 2\pi(1-r_0^2)\tau^2 \leq \min\{\mathcal{F}^*/2, cn\tau^2\} < \inf_{\mathbf{x}\in\mathcal{A}_n} \mathcal{E}_\tau[\mathbf{x}].$$

By theorem 2.6.6 and the fact that the upper bound in proposition 2.4.1 corresponds to the elastic energies of deformations in $\mathcal{A}_2$ it follows that $\min\{2c\tau^2, \mathcal{F}^*/2\} \leq 2\pi(1-r_0)^2\tau^2$. Therefore, $c \leq \pi(1-r_0^2)$ and consequently $n^* = 2\pi(1-r_0^2)/c \geq 2$. □

Corollary 2.6.8. Let $n \in \{2, 3, \ldots\}$. There exists constants $c, C > 0$ independent of n and τ such that if $\tau < \mathcal{F}^*/(2c)n^{-1/2}$ then

$$cn\tau^2 \leq \inf_{\mathbf{x}\in\mathcal{A}_n} \mathcal{E}_\tau[\mathbf{x}] \leq Cn^2\tau^2.$$

Proof. By theorem 2.6.6 it follows that there exists constants $c, C > 0$ such that

$$\min\{cn\tau^2, \mathcal{F}^*/2\} \leq \inf_{\mathbf{x}\in\mathcal{A}_n} \mathcal{E}[\mathbf{x}] \leq \min\{Cn^2\tau^2, \mathcal{F}\} \leq Cn^2\tau^2$$

Therefore, if $\tau < \mathcal{F}^*/(2c)n^{-1/2}$ it follows that $\min\{cn\tau^2, \mathcal{F}^*/2\} = cn\tau^2$ and the result follows. □

The previous corollaries 2.6.7 and 2.6.8 extend the results of theorem 2.6.6 and quantify different "crossover regimes" in n and τ. Specifically, corollary 2.6.7 gives a critical wave number $n^* \geq 2$ such that energetically there can be no refinement with decreasing thickness of the number of waves greater than n^*. Corollary 2.6.8 gives a crossover condition for when minimizers transition from being close to a flat deformation to one whose elastic energy scales with τ like an isometric immersion. In figure 2.6 we plot a schematic of these crossover regimes.

2.7 Boundary Layer Analysis

The n-periodic isometric immersions constructed in section 2.4 satisfy the governing equations (2.2.4) and (2.2.6) but not the boundary conditions (2.2.7) and (2.2.8). But, in figure 2.5 we see that in the vanishing thickness limit numerical minimizers of $\mathcal{E}_\tau$ over $\mathcal{A}_n$ converge to an isometric immersion. In figure 2.7 we color the annulus by the Gaussian curvature of numerical minimizers over the set $\mathcal{A}_n$. We can see that the Gaussian curvature is significantly different from -1 in regions near the edge of the annulus and along the lines of inflection. Thus, by the Monge-Ampere equation 2.4.1 the stretching energy is non-zero in these regions and we expect the sheet to be a perturbation of an isometric immersion that introduces boundary layers near

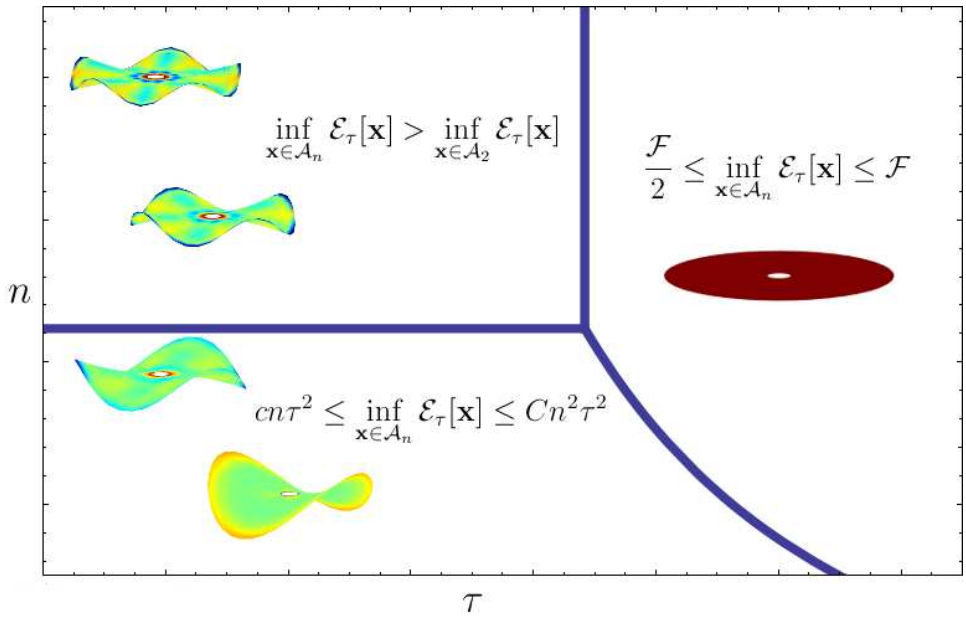

FIGURE 2.6. A schematic of regions in the $n - \tau$ plane in which minimizing deformations in $\mathcal{A}_n$ "crossover" to different scaling regimes. In the upper left region minimizing deformations in $\mathcal{A}_n$ have larger energy than minimizers over $\mathcal{A}$. the existence of this upper bound means that there can be no refinement with decreasing thickness of the number of waves for minimizers in $\mathcal{A}$. In the lower left region the minimizing deformations scale in energy like that of an isometric immersion. In the region on the right the minimizing deformations are either a flat deformation or are close to being a flat deformation. It is important to note that this figure is just a schematic drawn for a specific values of the constant c in theorem 2.6.6. Different values of c will change the positions of the boundaries between the regions but will not change the qualitative form of the figure.

the edge of the disk and along the lines of inflection. By theorem 2.6.6 the scaling in these regions will be selected so that the energy in these regions scales like τ^2 or smaller.

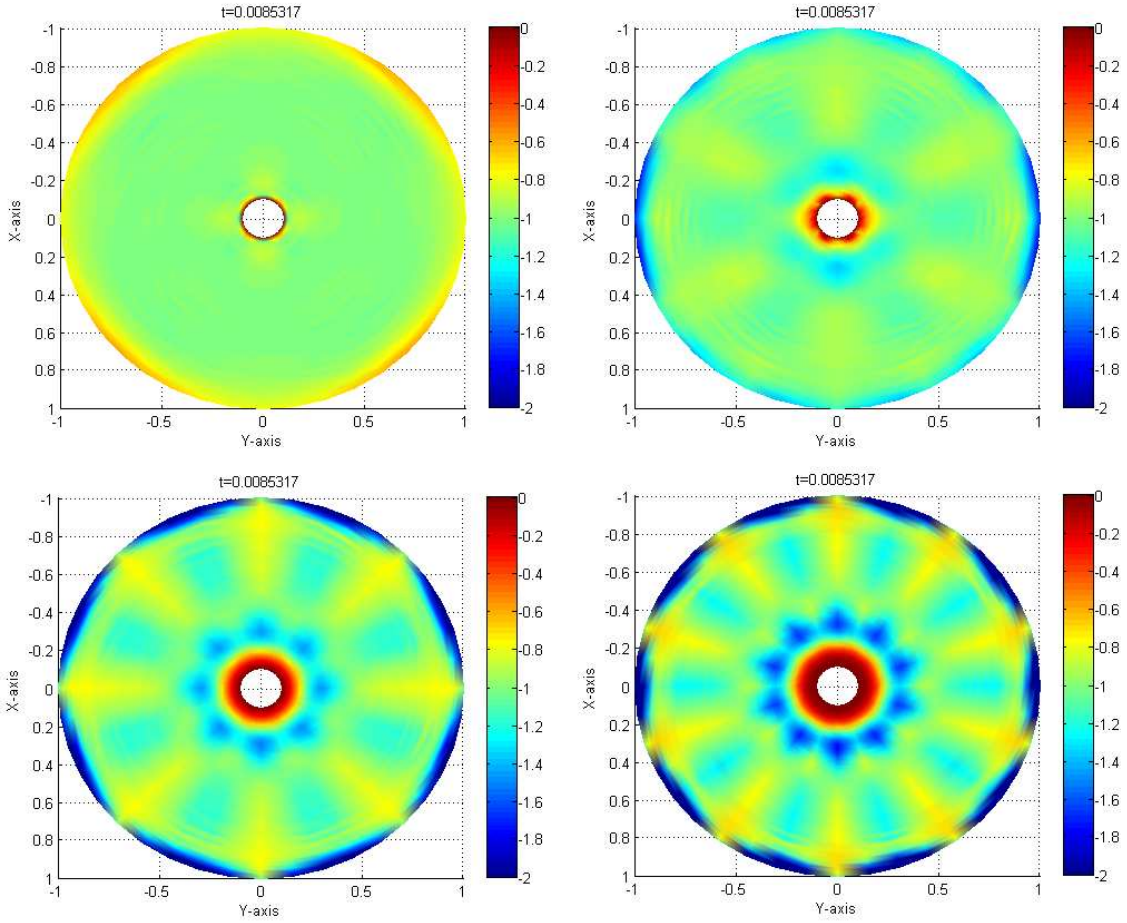

FIGURE 2.7. The annular domain colored by the Gaussian curvature of numerical minimizers over $\mathcal{A}_n$, with $n = 2, 3, 4, 5$ clockwise from upper left. The plots indicate that the minimizers are close to isometric immersions with localized regions of stretching near the edge of the annulus and the lines of inflection .

2.7.1 Governing Equations of Perturbations

Again, let $n \in \{2, 3, \ldots\}$. Define S_n to be the sector in $\mathbb{R}^2$ bounded between $\theta = 0$ and $\theta = \pi/n$ and define $B_n = B \cap S_n$. Let $\mathbf{x} \in \mathcal{A}_n$ with corresponding out-of-plane

displacement η given by and potential Φ and suppose η and Φ are perturbations of an n-periodic isometric immersion. That is, on B_n assume η and Φ are of the form

$$\eta = y\left(x - \cot\left(\frac{\pi}{n}\right) y\right) + \tilde{\eta}, \tag{2.7.1}$$

$$\Phi = \tilde{\Phi}, \tag{2.7.2}$$

for some perturbations $\tilde{\Phi}$ and $\tilde{\eta}$. Furthermore, since $\mathbf{x} \in \mathcal{A}_n$ we enforce the Dirichlet boundary conditions $\tilde{\eta} = 0$ along the lines $\theta = 0$ and $\theta = \frac{\pi}{n}$.

The elastic energy of this perturbation is

$$\mathcal{E}_\tau[\mathbf{x}] = 2n\int_{B_n} \frac{1}{1+\nu}\left(\Delta\tilde{\Phi}\right)^2 dxdy + 2n\tau^2\int_{B_n}\left[\frac{1}{1-\nu}\left(\Delta\tilde{\eta} - 2\cot\left(\frac{\pi}{n}\right)\right)^2 + 4\cot\left(\frac{\pi}{n}\right)\frac{\partial^2\tilde{\eta}}{\partial x^2} + 4\frac{\partial^2\tilde{\eta}}{\partial x\partial y} - 2[\tilde{\eta},\tilde{\eta}] + 2\right] dxdy. \tag{2.7.3}$$

If $\tilde{\eta}$ and $\tilde{\Phi}$ extremize (2.7.3) then by (2.2.4-2.2.8), and the fact that $\delta\eta = 0$ along the lines $\theta = 0$ and $\theta = \pi/n$, it follows that $\tilde{\eta}$ and $\tilde{\Phi}$ satisfy the following boundary value problem

$$\frac{1}{2(1+\nu)}\Delta^2\tilde{\Phi} - 2\cot\left(\frac{\pi}{n}\right)\frac{\partial^2\tilde{\eta}}{\partial x^2} - 2\frac{\partial^2\tilde{\eta}}{\partial x\partial y} + [\tilde{\eta},\tilde{\eta}] = 0, \tag{2.7.4}$$

$$\frac{\tau^2}{4(1-\nu)}\Delta^2\tilde{\eta} + \cot\left(\frac{\pi}{n}\right)\frac{\partial^2\tilde{\Phi}}{\partial x^2} + \frac{\partial^2\tilde{\Phi}}{\partial x\partial y} + [\tilde{\Phi},\tilde{\eta}] = 0, \tag{2.7.5}$$

$$\left.\frac{1}{r}\frac{\partial^2\tilde{\Phi}}{\partial\theta^2} + \frac{\partial\tilde{\Phi}}{\partial r}\right|_{r=r_0,1} = 0, \quad \left.\frac{\partial^2\tilde{\Phi}}{\partial r\partial\theta} - \frac{1}{r}\frac{\partial\tilde{\Phi}}{\partial\theta}\right|_{r=r_0,1} = 0, \tag{2.7.6}$$

$$\left.\frac{1}{1-\nu}\Delta\tilde{\eta} - \mathbf{n}^T\cdot D^2\tilde{\eta}\cdot\mathbf{n}\right|_{r=r_0,1} = -\csc\left(\frac{\pi}{n}\right)\left(\frac{(\nu-2)\cos\left(\frac{\pi}{n}\right) + \nu\cos\left(\frac{\pi}{n} - 2\theta\right)}{1-\nu}\right), \tag{2.7.7}$$

$$\left.\frac{1}{1-\nu}\frac{\partial\Delta\tilde{\eta}}{\partial\mathbf{n}} + \frac{\partial}{\partial\mathbf{t}}\left(\mathbf{n}^T\cdot D^2\tilde{\eta}\cdot\mathbf{t}\right)\right|_{r=r_0,1} = \left.\frac{2}{r}\csc\left(\frac{\pi}{n}\right)\cos\left(\frac{\pi}{n} - 2\theta\right)\right|_{r=r_0,1}, \tag{2.7.8}$$

$$\left.\mathbf{n}\cdot\left(\frac{\partial^2\tilde{\Phi}}{\partial y^2}, -\frac{\partial^2\tilde{\Phi}}{\partial x\partial y}\right)\right|_{\theta=0,\frac{\pi}{n}} = 0, \quad \left.\mathbf{n}\cdot\left(-\frac{\partial^2\tilde{\Phi}}{\partial x\partial y}, \frac{\partial^2\tilde{\Phi}}{\partial x^2}\right)\right|_{\theta=0,\frac{\pi}{n}} = 0, \tag{2.7.9}$$

$$\tilde{\eta}|_{\theta=0,\pi/n} = 0, \quad \left.\frac{\partial^2\tilde{\eta}}{\partial\theta^2}\right|_{\theta=0,\pi/n} = 2r^2\cot\left(\frac{\pi}{n}\right). \tag{2.7.10}$$

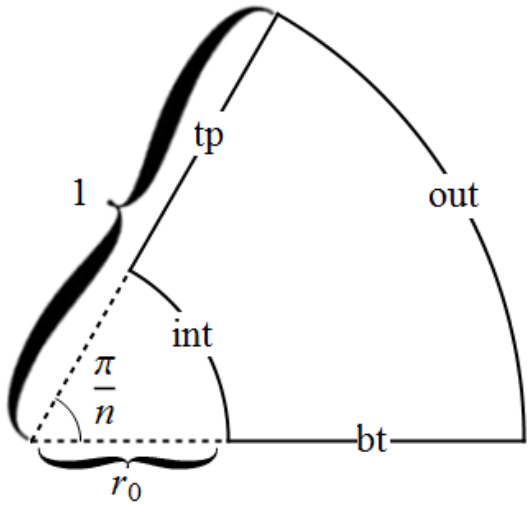

FIGURE 2.8. The domain for the governing equations of the perturbation from an isometric immersion is $B_n = \{(r, \theta) : r_0 < r < 1, 0 < \theta < \pi/n\}$.

Remark 2.7.1. So far no approximations have taken place. The boundary value problem (2.7.4-2.7.10) is the Euler-Lagrange equations corresponding to the ansatz (2.7.1) and (2.7.2).

Remark 2.7.2. The boundary value problem (2.7.4-2.7.10) for $n = 2$ is different from the other cases since $\cot(\pi/2) = 0$. We will see that for the case $n = 2$ there is no need to introduce a boundary layer near the lines of inflection. Furthermore, the boundary layers near the edges of the annulus will have a different geometry as well.

We look for approximate solutions of (2.7.4) and (2.7.5) that are linear combinations of boundary layer solutions near the interior radius (int), outer radius (out), bottom of the sector (bt), and the top of the sector (tp) (see figure 2.8). That is we assume

$$\tilde{\eta} = \tilde{\eta}_{int} + \tilde{\eta}_{out} + \tilde{\eta}_{bt} + \tilde{\eta}_{\text{tp}} \text{ and } \tilde{\Phi} = \tilde{\Phi}_{int} + \tilde{\Phi}_{out} + \tilde{\Phi}_{bt} + \tilde{\Phi}_{\text{tp}}, \tag{2.7.11}$$

where each term is found by an appropriate asymptotic expansion. The full configuration with domain B can then be obtained by taking odd extensions of η and even

extensions of Φ.

Remark 2.7.3. To construct a complete asymptotic solution of the boundary value problem (2.7.5-2.7.10) we would also need to analyse regions where boundary layers overlap. In this dissertation we are interested only in the scaling of the width of the boundary layer and do not analyse these overlap regions in this work.

2.7.2 Boundary Layer Near Outer Radius

Define the rescaled radius $\tilde{r}_{out}$ and functions $\tilde{\eta}'_{out}$ and $\tilde{\Phi}'_{out}$ by

$$\tilde{r}_{out} = \tau^{\alpha}(1-r), \quad \tilde{\eta}_{out} = \tau^{\beta}\tilde{\eta}'_{out}, \quad \tilde{\Phi}_{out} = \tau^{\gamma}\tilde{\Phi}'_{out}$$

where $-\alpha, \beta, \gamma \in \mathbb{R}^{+}$. To lowest order the stretching and bending energies near the outer radius are

$$\begin{aligned}
\frac{\mathcal{S}[\mathbf{x}]}{2n} &= \tau^{2\gamma+4\alpha} \int_{B_n} \frac{1}{1+\nu} \left(\frac{\partial^2 \tilde{\Phi}'_{out}}{\partial \tilde{r}^2_{out}} \right)^2 dxdy, \\
\frac{\tau^2 \mathcal{B}[\mathbf{x}]}{2n} = \tau^2 \int_{B_n} \Bigg[& \frac{1}{1-\nu} \left(\tau^{\beta+2\alpha} \frac{\partial^2 \tilde{\eta}'_{out}}{\partial \tilde{r}^2_{out}} - 2\cot\left(\frac{\pi}{n}\right) \right)^2 \\
& + 4\tau^{\beta+2\alpha} \cos(\theta) \left(\cot\left(\frac{\pi}{n}\right) + \sin(\theta) \right) \frac{\partial^2 \tilde{\eta}'_{out}}{\partial \tilde{r}^2_{out}} + 2 \Bigg] dxdy,
\end{aligned}$$

and the compatibility condition is

$$\frac{1}{2(1+\nu)} \tau^{\gamma+4\alpha} \frac{\partial^4 \tilde{\Phi}'_{out}}{\partial \tilde{r}^4_{out}} - 2\tau^{\beta+2\alpha} \cos(\theta) \left(\cot(\pi/n) + \sin(\theta) \right) \frac{\partial^2 \tilde{\eta}'_{out}}{\partial \tilde{r}^2_{out}} = 0.$$

To ensure that the elastic energy is $\mathcal{O}(\tau^2)$ and the compatibility condition is non-trivial we must have that

$$\beta + 2\alpha = 0, \quad 2\gamma + 4\alpha = 2, \quad \gamma + 4\alpha = \beta + 2\alpha.$$

The solution to these equations gives us the following scaling

$$\alpha = -\tfrac{1}{2}, \quad \beta = 1, \quad \gamma = 2,$$

which motivates the asymptotic expansion

$$\tilde{\eta}_{out} = \tau\eta^{(0)}_{out} + \tau^{\frac{3}{2}}\eta^{(1)}_{out} + \tau^2\eta^{(2)}_{out} + \dots,$$
$$\tilde{\Phi}_{out} = \tau^2\Phi^{(0)}_{out} + \tau^{\frac{5}{2}}\Phi^{(1)}_{out} + \tau^3\Phi^{(2)}_{out} + \dots.$$

Therefore, to lowest order (2.7.4) and (2.7.5) become

$$\frac{\partial^4\Phi^{(0)}_{out}}{\partial\tilde{r}^4_{out}} - 4(1+\nu)\csc\left(\frac{\pi}{n}\right)\cos(\theta)\cos\left(\frac{\pi}{n}-\theta\right)\frac{\partial^2\eta^{(0)}_{out}}{\partial\tilde{r}^2_{out}} = 0, \tag{2.7.12}$$

$$\frac{\partial^4\eta^{(0)}_{out}}{\partial\tilde{r}^4_{out}} + 4(1-\nu)\csc\left(\frac{\pi}{n}\right)\cos(\theta)\cos\left(\frac{\pi}{n}-\theta\right)\frac{\partial^2\Phi^{(0)}_{out}}{\partial\tilde{r}^2_{out}} = 0. \tag{2.7.13}$$

Furthermore, by (2.7.6), (2.7.7) and (2.7.8) the boundary conditions to lowest order are

$$\left.\frac{\partial\Phi^{(0)}_{out}}{\partial\tilde{r}_{out}}\right|_{\tilde{r}=0} = 0, \qquad \left.\frac{\partial^3\eta^{(0)}_{out}}{\partial\tilde{r}^3_{out}}\right|_{\tilde{r}=0} = 0, \tag{2.7.14}$$

$$\left.\frac{\partial^2\eta^{(0)}_{out}}{\partial\tilde{r}^2_{out}}\right|_{\tilde{r}_{out}=0} = -2\nu\csc\left(\frac{\pi}{n}\right)\cos(\theta)\cos\left(\frac{\pi}{n}-\theta\right) + 2\cot\left(\frac{\pi}{n}\right). \tag{2.7.15}$$

To solve the boundary value problem (2.7.12-2.7.15) we make the following ansatz

$$\eta^{(0)}_{out} = \lambda_n^3(\theta)A(\tilde{r}_{out}\lambda_n^{-1}(\theta)) - B(\tilde{r}_{out},\theta),$$

$$\Phi^{(0)}_{out} = \lambda_n^6(\theta)C(\tilde{r}_{out}\lambda_n^{-1}(\theta)) - D(\tilde{r}_{out},\theta),$$

where $\lambda_n : \left(0,\frac{\pi}{n}\right) \to \mathbb{R}$ is defined by

$$\lambda_n(\theta) = \csc\left(\frac{\pi}{n}\right)\cos(\theta)\cos\left(\frac{\pi}{n}-\theta\right).$$

This ansatz transforms the boundary value problem (2.7.12-2.7.15) into the following form

$$\frac{\partial^4 C}{\partial\tilde{r}^4_{out}} - 4(1+\nu)\frac{\partial^2 A}{\partial\tilde{r}^2_{out}} = 0, \tag{2.7.16}$$

$$\frac{\partial^4 A}{\partial\tilde{r}^4_{out}} + 4(1-\nu)\frac{\partial^2 C}{\partial\tilde{r}^2_{out}} = 0, \tag{2.7.17}$$

$$\frac{\partial^4 D}{\partial \tilde{r}_{out}^4} - 4(1+\nu)\lambda_n(\theta)\frac{\partial^2 B}{\partial \tilde{r}_{out}^2} = 0, \tag{2.7.18}$$

$$\frac{\partial^4 B}{\partial \tilde{r}_{out}^4} + 4(1-\nu)\lambda_n(\theta)\frac{\partial^2 D}{\partial \tilde{r}_{out}^2} = 0, \tag{2.7.19}$$

$$\left.\frac{\partial C}{\partial \tilde{r}_{out}}\right|_{\tilde{r}=0} = 0, \qquad \left.\frac{\partial D}{\partial \tilde{r}_{out}}\right|_{\tilde{r}=0} = 0, \tag{2.7.20}$$

$$\left.\frac{\partial^2 A}{\partial \tilde{r}_{out}^2}\right|_{\tilde{r}_{out}=0} = -2\nu, \qquad \left.\frac{\partial^2 B}{\partial \tilde{r}_{out}^2}\right|_{\tilde{r}_{out}=0} = -2\cot(\pi/n). \tag{2.7.21}$$

$$\left.\frac{\partial^3 A}{\partial \tilde{r}_{out}^3}\right|_{\tilde{r}_{out}=0} = 0, \qquad \left.\frac{\partial^3 B}{\partial \tilde{r}_{out}^3}\right|_{\tilde{r}_{out}=0} = 0. \tag{2.7.22}$$

The solution to (2.7.16-2.7.22) containing only exponentially decaying terms is given by

$$A(\tilde{r}_{out}\lambda_n^{-1}(\theta)) = \frac{\nu}{\sqrt{2(1-\nu^2)}}\exp\left(-\frac{\sqrt{2}\tilde{r}_{out}(1-\nu^2)^{\frac{1}{2}}}{\lambda_n(\theta)}\right)\sin\left(\frac{\sqrt{2}\tilde{r}_{out}(1-\nu^2)^{\frac{1}{4}}}{\lambda_n(\theta)} - \frac{\pi}{4}\right),$$

$$B(\tilde{r}_{out},\theta) = \frac{\cot(\pi/n)}{\lambda_n(\theta)\sqrt{2(1-\nu^2)}}\exp\left(-\sqrt{2}\tilde{r}_{out}(1-\nu^2)^{\frac{1}{4}}\lambda_n^{\frac{1}{2}}(\theta)\right) \times \sin\left(\sqrt{2}\tilde{r}_{out}(1-\nu^2)^{\frac{1}{4}}\lambda_n^{\frac{1}{2}}(\theta) - \frac{\pi}{4}\right),$$

$$C(\tilde{r}_{out}\lambda_n^{-1}(\theta)) = \frac{\nu}{2(1-\nu)}\exp\left(-\frac{\sqrt{2}\tilde{r}_{out}(1-\nu^2)^{\frac{1}{4}}}{\lambda_n(\theta)}\right)\cos\left(\frac{\sqrt{2}\tilde{r}(1-\nu^2)^{\frac{1}{4}}}{\lambda_n(\theta)} - \frac{\pi}{4}\right),$$

$$D(\tilde{r}_{out},\theta) = \frac{\cot(\pi/n)}{\lambda_n(\theta)\sqrt{2}(1-\nu)}\exp\left(-\sqrt{2}\tilde{r}(1-\nu^2)^{\frac{1}{4}}\lambda_n^{\frac{1}{2}}(\theta)\right) \times \cos\left(\sqrt{2}\tilde{r}_{out}(1-\nu^2)^{\frac{1}{4}}\lambda_n^{\frac{1}{2}}(\theta) - \frac{\pi}{4}\right).$$

The terms $\lambda_n^3(\theta)A(\tilde{r}_{out}\lambda_n^{-1}(\theta))$ and $\lambda_n^6(\theta)C(\tilde{r}_{out}\lambda_n^{-1}(\theta))$ can be interpreted as terms that alone reduce the magnitude of the Gaussian curvature in a thin boundary layer while $B(\tilde{r}_{out},\theta)$ and $D(\tilde{r}_{out},\theta)$ alone locally reduce the mean curvature in a separate boundary layer with a different geometry. In the overlap of these two boundary layers the bending energy is reduced through the combination of these two effects. By expressing $\eta_{out}^{(0)}$ and $\Phi_{out}^{(0)}$ in terms of the actual radius $\rho = Rr = R\tau^{1/2}\tilde{r}$ we have the following results for the scaling of the width of these boundary layers:

1. The width of the *boundary layer in which the Gaussian curvature is significantly reduced* satisfies the following scaling

$$\text{width}(\theta)_{\rho=R} \sim t^{\frac{1}{2}}|K_0|^{-1/4}\csc(\pi/n)\cos(\theta)\cos(\pi/n-\theta). \tag{2.7.23}$$

2. For $n \geq 3$, the width of the *boundary layer in which the mean curvature is significantly reduced* satisfies the following scaling

$$\text{width}(\theta)_{\rho=R} \sim t^{\frac{1}{2}}|K_0|^{-1/4}\sqrt{\sin(\pi/n)\sec(\theta)\sec(\pi/n-\theta)}. \tag{2.7.24}$$

The width of these boundary layers has the same scaling in thickness for a vibrating shell (Lamb, 1889) and non-Euclidean plates with $K_0 > 0$ (Efrati et al., 2007). What is unique to the case when $K_0 < 0$ is this existence of two overlapping boundary layers that arises from the competition between Gaussian and mean curvatures in the bending energy.

2.7.3 Boundary Layer Near Interior Radius

The boundary layer near $r = r_0$ is completely analogous to the one near $r = 1$. Define the rescaled radius $\tilde{r}_{int}$ by

$$\tilde{r}_{int} = \tau^{-\frac{1}{2}}(r - r_0)$$

and consider the asymptotic expansion

$$\tilde{\eta}_{int} = \tau\eta_{int}^{(0)} + \tau^{\frac{3}{2}}\eta_{int}^{(1)} + \tau^2\eta_{int}^{(2)} + \dots$$
$$\tilde{\Phi}_{int} = \tau^2\Phi_{int}^{(0)} + \tau^{\frac{5}{2}}\Phi_{int}^{(1)} + \tau^3\Phi_{int}^{(2)} + \dots.$$

This yields identical governing and boundary equations as the outer radius and thus

$$\eta_{int}^{(0)} = \lambda_n^3(\theta)A(\tilde{r}_{int}, \lambda_n^{-1}(\theta)) - B(\tilde{r}_{int}, \theta)$$

$$\Phi_{int}^{(0)} = \lambda_n^6(\theta)A(\tilde{r}_{int}), \lambda_n^{-1}(\theta) - D(\tilde{r}_{int}, \theta),$$

where A, B, C, D are defined as in the previous subsection.

2.7.4 Boundary Layer Near the Bottom of the Sector

From the observations in the remark 2.7.2 we will assume in this section that $n \in \{3, 4, \ldots\}$. Define the rescaled coordinate $\tilde{y}_{bt}$ and functions $\tilde{\eta}'_{bt}$ and $\tilde{\Phi}'_{bt}$ by

$$\tilde{y}_{bt} = \tau^{\alpha} y, \quad \tilde{\eta}_{bt} = \tau^{\beta} \tilde{\eta}'_{bt}, \quad \tilde{\Phi}_{bt} = \tau^{\gamma} \tilde{\Phi}'_{bt}$$

where $-\alpha, \beta, \gamma \in \mathbb{R}^+$. To lowest order the stretching and bending energies near the outer radius are

$$\begin{aligned} \frac{\mathcal{S}[\mathbf{x}]}{2n} &= \tau^{2\gamma+4\alpha} \int_{B_n} \frac{1}{1+\nu} \left(\frac{\partial^2 \tilde{\Phi}'_{bt}}{\partial \tilde{y}_{bt}^2} \right)^2 dxdy, \\ \frac{\tau^2 \mathcal{B}[\mathbf{x}]}{2n} &= \tau^2 \int_{B_n} \left[\frac{1}{1-\nu} \left(\tau^{\beta+2\alpha} \frac{\partial^2 \tilde{\eta}'_{bt}}{\partial \tilde{y}_{bt}^2} - 2\cot\left(\frac{\pi}{n}\right) \right)^2 + 2 \right] dxdy, \end{aligned}$$

and the compatibility condition is

$$\frac{1}{2(1+\nu)} \tau^{\gamma+4\alpha} \frac{\partial^4 \tilde{\Phi}'_{bt}}{\partial \tilde{y}_{bt}^4} - 2\tau^{\beta+\alpha} \frac{\partial^2 \tilde{\eta}_{bt}}{\partial x \partial \tilde{y}_{bt}} = 0.$$

Therefore, the scaling that ensures the elastic energy is $\mathcal{O}(\tau^2)$ and the compatibility equation is non-trivial is

$$\alpha = -\tfrac{1}{3}, \quad \beta = \tfrac{2}{3}, \quad \gamma = \tfrac{5}{3},$$

which is a different scaling then the one near the edges of the annulus. This scaling motivates the asymptotic expansion

$$\begin{aligned} \tilde{\eta}_{bt} &= \tau^{\frac{2}{3}} \eta_{bt}^{(0)} + \tau \eta_{bt}^{(1)} + \tau^{\frac{4}{3}} \eta_{bt}^{(2)} + \ldots \\ \tilde{\Phi}_{bt} &= \tau^{\frac{5}{3}} \Phi_{bt}^{(0)} + \tau^2 \Phi_{bt}^{(1)} + \tau^{\frac{7}{3}} \Phi_{bt}^{(2)} + \ldots . \end{aligned}$$

Consequently, to lowest order (2.7.4) and (2.7.5) become

$$\frac{\partial}{\partial \tilde{y}_{bt}} \left(\frac{\partial^3 \Phi_{bt}^{(0)}}{\partial \tilde{y}_{bt}^3} - 4(1+\nu) \frac{\partial \eta_{bt}^{(0)}}{\partial x} \right) = 0, \tag{2.7.25}$$

$$\frac{\partial}{\partial \tilde{y}_{bt}}\left(\frac{\partial^3 \eta_{bt}^{(0)}}{\partial \tilde{y}_{bt}^3}+4(1-\nu)\frac{\partial \Phi_{bt}^{(0)}}{\partial x}\right)=0. \tag{2.7.26}$$

Furthermore, by (2.7.9) and (2.7.10) the boundary conditions are

$$\left.\frac{\partial^2 \Phi_{bt}^{(0)}}{\partial x^2}\right|_{\tilde{y}_{bt}=0}=0, \qquad \left.\frac{\partial^2 \Phi_{bt}^{(0)}}{\partial x \partial \tilde{y}_{bt}}\right|_{\tilde{y}_{bt}=0}=0, \tag{2.7.27}$$

$$\left.\eta_{bt}^{(0)}\right|_{\tilde{y}_{bt}=0}=0, \qquad \left.\frac{\partial^2 \eta_{bt}^{(0)}}{\partial \tilde{y}_{bt}^2}\right|_{\tilde{y}_{bt}=0}=2\cot\left(\frac{\pi}{n}\right). \tag{2.7.28}$$

To solve this boundary value problem we make the following ansatz

$$\begin{array}{l}\tilde{\eta}_{bt}^{(0)}=\psi_1(x)+\tilde{y}_{bt}^2\cot\left(\frac{\pi}{n}\right)f(x,\tilde{y}_{bt}),\\ \tilde{\Phi}_{bt}^{(0)}=\psi_2(x)+\tilde{y}_{bt}^2\cot\left(\frac{\pi}{n}\right)g(x,\tilde{y}_{bt}),\end{array} \tag{2.7.29}$$

which transforms equations (2.7.25) and (2.7.26) into

$$\begin{array}{l}\frac{\partial}{\partial \tilde{y}_{bt}}\left(\tilde{y}_{bt}^2\frac{\partial^3 g}{\partial \tilde{y}_{bt}^3}+6\tilde{y}_{bt}\frac{\partial^2 g}{\partial \tilde{y}_{bt}^2}+6\frac{\partial g}{\partial \tilde{y}_{bt}}-4(1+\nu)\tilde{y}_{bt}^2\frac{\partial f}{\partial x}\right)=0,\\ \frac{\partial}{\partial \tilde{y}_{bt}}\left(\tilde{y}_{bt}^2\frac{\partial^3 f}{\partial \tilde{y}_{bt}^3}+6\tilde{y}_{bt}\frac{\partial^2 f}{\partial \tilde{y}_{bt}^2}+6\frac{\partial f}{\partial \tilde{y}_{bt}}+4(1-\nu)\tilde{y}_{bt}^2\frac{\partial g}{\partial x}\right)=0.\end{array} \tag{2.7.30}$$

If we integrate with respect to $\tilde{y}_{bt}$ and make the similarity transformation $z=\tilde{y}_{bt}^3/x$, we obtain the system of ordinary differential equations given by

$$\begin{array}{l}27z^2\frac{d^3 g}{dz^3}+108z\frac{d^2 g}{dz^2}+60\frac{dg}{dz}+4(1+\nu)z\frac{df}{dz}=0,\\ 27z^2\frac{d^3 f}{dz^3}+108z\frac{d^2 f}{dz^2}+60\frac{df}{dz}-4(1-\nu)z\frac{dg}{dz}=0.\end{array}$$

Solving for $\frac{dg}{dz}$ we obtain the following single differential equation

$$4(1+\nu)z\frac{df}{dz}+\frac{1}{1-\nu}\left(\frac{90}{z}\frac{df}{dz}+2430\frac{d^2 f}{dz^2}+4455z\frac{d^3 f}{dz^3}+\frac{3645}{2}z^2\frac{d^4 f}{dz^4}+\frac{729}{4}z^3\frac{d^5 f}{dz^5}\right)=0. \tag{2.7.31}$$

The general solution to equation (2.7.31) that does not contain exponentially growing terms is

$$\begin{aligned}f(z) \;=\; & \int\Big[c_1 z^{-\frac{3}{2}}\mathrm{Ker}_{\frac{1}{3}}\left(4\cdot 3^{-\frac{3}{2}}\cdot(1-\nu^2)^{\frac{1}{4}}\sqrt{z}\right)\\ & +c_2 z^{-\frac{3}{2}}\mathrm{Kei}_{\frac{1}{3}}\left(4\cdot 3^{-\frac{3}{2}}\cdot(1-\nu^2)^{\frac{1}{4}}\sqrt{z}\right)\Big]\,dz+c_3,\end{aligned}$$

where $\mathrm{Ker}_{1/3}$ and $\mathrm{Kei}_{1/3}$ denote Kelvin functions of the second kind and c_1, c_2 and c_3 are arbitrary constants (Abramowitz & Stegun, 1964). Therefore, we have that

$$\begin{aligned}\eta_{bt}^{(0)} = \psi_1(x) + \tilde{y}_{bt}^2 \cot(\pi/n) \left(\int \left[c_1 z^{-\frac{3}{2}} \mathrm{Ker}_{\frac{1}{3}} \left(4 \cdot 3^{-\frac{3}{2}} \cdot (1-\nu^2)^{\frac{1}{4}} \sqrt{z} \right) \right.\right. \\ \left.\left. + c_2 z^{-\frac{3}{2}} \mathrm{Kei}_{\frac{1}{3}} \left(4 \cdot 3^{-\frac{3}{2}} \cdot (1-\nu^2)^{\frac{1}{4}} \sqrt{z} \right) \right] dz + c_3 \right), \\ \Phi_{bt}^{(0)} = \psi_2(x) + \tilde{y}_{bt}^2 \cot(\pi/n) \left(\sqrt{\frac{1+\nu}{1-\nu}} \int \left[c_2 z^{-\frac{3}{2}} \mathrm{Ker}_{\frac{1}{3}} \left(4 \cdot 3^{-\frac{3}{2}} \cdot (1-\nu^2)^{\frac{1}{4}} \sqrt{z} \right) \right.\right. \\ \left.\left. - c_1 z^{-\frac{3}{2}} \mathrm{Kei}_{\frac{1}{3}} \left(4 \cdot 3^{-\frac{3}{2}} \cdot (1-\nu^2)^{\frac{1}{4}} \sqrt{z} \right) \right] dz + c_4 \right),\end{aligned}$$

where c_4 is an arbitrary constant.

Now, near $y = 0$, we have that

$$\begin{aligned}\eta_{bt}^{(0)} &= \psi_1(x) + \tilde{y}_{bt}^2 \cot\left(\frac{\pi}{n}\right) \left[2^{-\frac{17}{6}} 3^{\frac{3}{2}} \Gamma\left(\frac{1}{3}\right) (1-\nu^2)^{-\frac{1}{12}} (c_2 - c_1) \frac{x^{\frac{2}{3}}}{\tilde{y}_{bt}^2} \right. \\ &\quad \left. - 2^{-\frac{13}{6}} 3^{\frac{1}{2}} \Gamma\left(-\frac{1}{3}\right) (1-\nu^2)^{\frac{1}{12}} \left(c_1 \left(1+\sqrt{3}\right) + c_2 \left(1-\sqrt{3}\right) \right) \frac{x^{\frac{1}{3}}}{\tilde{y}_{bt}} + c_3 + \ldots \right], \\ \Phi_{bt}^{(0)} &= \Psi_2(x) + \tilde{y}_{bt}^2 \cot\left(\frac{\pi}{n}\right) \left[-2^{-\frac{17}{6}} 3^{\frac{3}{2}} \Gamma\left(\frac{1}{3}\right) (1-\nu^2)^{-\frac{7}{12}} (1-\nu) (c_1 + c_2) \frac{x^{\frac{2}{3}}}{\tilde{y}_{bt}^2} \right. \\ &\quad - 2^{-\frac{13}{6}} 3^{\frac{1}{3}} \Gamma\left(-\frac{1}{3}\right) \left(1-\nu^2\right)^{\frac{7}{12}} (1-\nu)^{-1} \left(\left(-1+\sqrt{3}\right) c_1 + \left(1+\sqrt{3}\right) c_2 \right) \frac{x^{\frac{1}{3}}}{\tilde{y}_{bt}} \\ &\quad \left. + c_4 \ldots \right].\end{aligned}$$

Furthermore,

$$\begin{aligned}\lim_{z\to\infty} \int z^{-\frac{3}{2}} \mathrm{Ker}_{\frac{1}{3}} \left(4 \cdot 3^{-\frac{3}{2}} (1-\nu^2)^{\frac{1}{4}} \sqrt{z} \right) dz &= \frac{\pi}{2} \sqrt{2+\sqrt{3}}, \\ \lim_{z\to\infty} \int z^{-\frac{3}{2}} \mathrm{Kei}_{\frac{1}{3}} \left(4 \cdot 3^{-\frac{3}{2}} (1-\nu^2)^{\frac{1}{4}} \sqrt{z} \right) dz &= \frac{\pi}{2} \sqrt{2-\sqrt{3}}.\end{aligned}$$

Therefore, to satisfy the boundary conditions (2.7.27) and (2.7.28) we must have that

$$\begin{aligned}&\psi_1(x) = -\frac{3^{\frac{3}{2}} \Gamma\left(\frac{1}{3}\right) \cot\left(\frac{\pi}{n}\right)}{2^{7/3} (1-\nu^2)^{\frac{1}{3}} \pi} x^{\frac{2}{3}}, && \psi_2(x) = -\frac{3(1-\nu^2)^{\frac{1}{6}} \Gamma\left(\frac{1}{3}\right) \cot\left(\frac{\pi}{n}\right)}{2^{\frac{7}{3}} (1-\nu) \pi} x^{\frac{2}{3}}, \\ &c_1 = -\frac{1+\sqrt{3}}{\sqrt{6}(1-\nu^2)^{\frac{1}{4}} \pi}, && c_2 = \frac{-1+\sqrt{3}}{3^{\frac{3}{4}} (1-\nu^2)^{\frac{1}{4}} \pi}, \\ &c_3 = 1, && c_4 = -\sqrt{\frac{1+\nu}{3(1-\nu)}}.\end{aligned} \tag{2.7.32}$$

By expressing $\eta_{bt}^{(0)}$ and $\Phi_{bt}^{(0)}$ in terms of the actual Cartesian coordinates $u = Rx$ and $v = Ry$ and approximating ρ and θ near $y = 0$ by $\rho \approx u$ and $\theta \approx \ v/u$, it follows that the width of the boundary layer in this region scales like

$$\text{width}(\rho)_{\eta=0} \sim \tau^{\frac{1}{3}} \rho^{\frac{1}{3}} |K_0|^{-\frac{1}{6}}. \tag{2.7.33}$$

This boundary layer can be interpreted as a region in which the mean curvature is locally reduced while the change in energy contributed from the Gaussian curvature of the perturbation is of the order $\mathcal{O}(\tau^{5/3})$. This reduction of energy near this type of singularity is different from the regularization near a ridge singularity in which the bending energy diverges while the stretching energy converges to zero with decreasing thickness (Venkataramani, 2004; Conti & Maggi, 2008).

2.7.5 Boundary Layer Near the Top of the Sector

To construct the boundary layer near $\theta = \pi/n$ we can simply rotate the asymptotic expansion for $\tilde{\eta}_{bt}$ and $\tilde{\Phi}_{bt}$ through the angle $\theta = \pi/n$ and then evenly reflect about the line $\theta = \pi/n$. That is, in polar coordinates we set

$$\tilde{\eta}_{tp}(r, \theta) = \tilde{\eta}_{bt}\left(r, \pi/n - \theta\right) \text{ and } \tilde{\Phi}_{tp}(r, \theta) = \tilde{\Phi}_{bt}\left(r, \pi/n - \theta\right).$$

In figure 2.9 we color the annulus by the different boundary layers using the characteristic widths (2.7.23), (2.7.24), and (2.7.33).

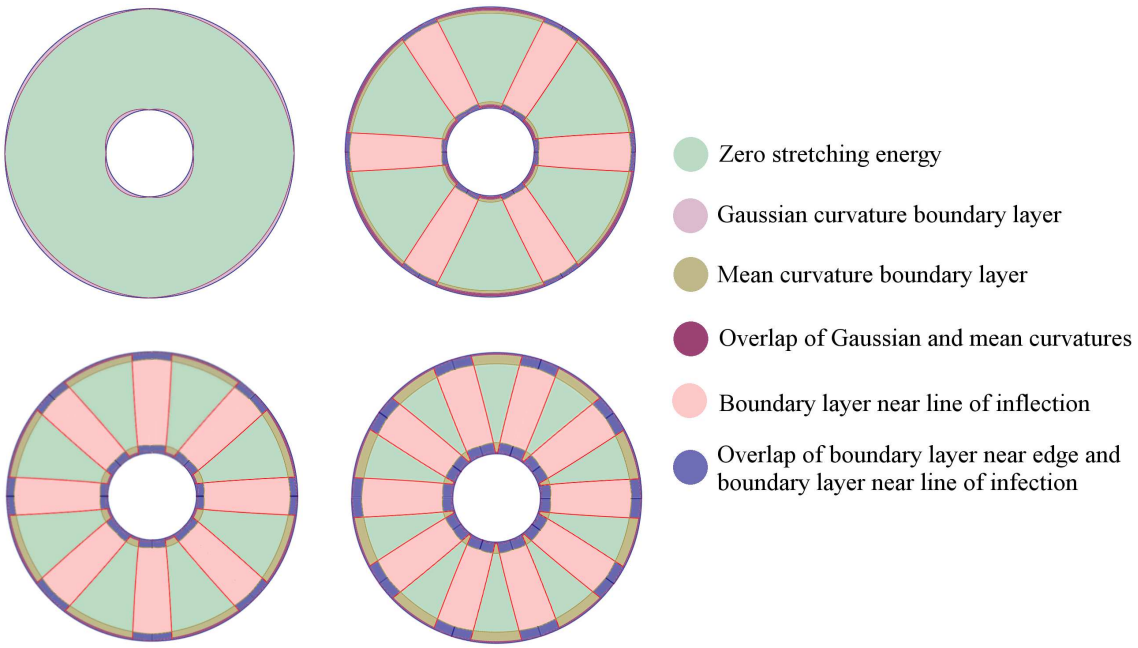

FIGURE 2.9. Schematic of the various boundary layers in n-periodic deformations, $n = 2, 3, 4, 5$ clockwise from upper left corner. The annulus is colored by the effect of different boundary layers on the elastic energy.

Chapter 3

Isometric Immersions and the Kirchhoff Model

In this chapter we study the Kirchhoff model of non-Euclidean plates when the metric $\mathbf{g}_{K_0}$ has corresponding constant negative Gaussian curvature $K_0 < 0$ and the domain $\mathcal{D}$ is now a disk of radius R. Recall that in the Kirchhoff model the elastic energy $E_{Ki} : W^{2,2}(\mathcal{D}, \mathbb{R}^3) \to \mathbb{R}^3$ is given by

$$E_{Ki}[\mathbf{x}] = \begin{cases} \dfrac{Y}{24(1+\nu)} \displaystyle\int_{\mathcal{D}} \left[\frac{4H^2}{1-\nu} - 2K \right] dA_{\mathbf{g}_{K_0}} & \text{if } \mathbf{x} \in \mathcal{A}_{Ki} \\ \infty & \text{if } \mathbf{x} \notin \mathcal{A}_{Ki} \end{cases},$$

where Y and ν are the Young's modulus and Poisson ratio of the material respectively, H and K mean and Gaussian curvatures of the surface $\mathbf{x}(\mathcal{D})$ respectfully, and $dA_{\mathbf{g}_{K_0}}$ the area form induced by $\mathbf{g}_{K_0}$. We assume without loss of generality that $K_0 = -1$, since if $K_0 \neq -1$ we can always non-dimensionalize by setting the units of length as $(-K_0)^{-1/2}$. That is, if a mapping $\mathbf{x} : \mathcal{D} \to \mathbb{R}^3$ is initially parametrized by the variables u, v then the dimensionless variables $u' = \sqrt{-K_0}u$ and $v' = \sqrt{-K_0}$ are the dimensionless parametrization variables and $R' = \sqrt{-K_0}R$ is the dimensionless radius. Furthermore, we will drop the subscript notation and simply write $\mathbf{g}$ instead of $\mathbf{g}_{K_0}$.

To study the Kirchhoff model for our metric and domain it is necessary to construct $W^{2,2}$ isometric immersions of subsets of the hyperbolic plane $\mathbb{H}^2$, that is solutions to the differential equation $(\nabla \mathbf{x})^T \cdot \nabla \mathbf{x} = \mathbf{g}$. In general finding solutions to this equation for an arbitrary metric is a non-trivial problem. But, by Minding's theorem, which states that any two abstract surfaces having the same *constant* Gaussian curvature are locally isometric, we can "cut out" subsets of surfaces of constant negative curvature which will be isometric to pieces of $\mathbb{H}^2$ (Minding, 1839). In particular, if S is a surface of constant negative curvature and $p \in S$ then $U = \{q \in S : d(p, q) < R\}$,

where d is the distance function inherited from $\mathbf{g}$, is isometric to a disk of radius R in $\mathbb{H}^2$, provided U is smooth. But, by the non-existence results of Hilbert (Hilbert, 1901) and Holmgren (Holmgren, 1902) it is known that for a fixed $p \in S$ the set $U = \{q \in S : d(p,q) < R\}$ will fail to be smooth for some critical value of R. The singularities where S fails to be smooth form curves or singular points at infinity that form boundaries on S beyond which no disks locally isometric to $\mathbb{H}^2$ can be cut out of the surface (Amsler, 1955).

Now, if we assume that $\mathbf{x} : \mathcal{D} \to U \subset \mathbb{R}^3$ forms a surface of constant Gaussian curvature $K = -1$ with mean curvature H then

$$\begin{aligned} E_{Ki}[\mathbf{x}] &= \frac{Y}{24(1+\nu)} \int_{\mathcal{D}} \left[\frac{4H^2}{1-\nu} - 2K \right] dA_{\mathbf{g}} \\ &= \frac{Y}{24(1+\nu)} \int_{\mathcal{D}} \frac{k_1^2 + k_2^2}{1-\nu} \, dA_{\mathbf{g}} - \frac{Y}{24(1-\nu)} \int_{\mathcal{D}} k_1 k_2 \, dA_{\mathbf{g}} \\ &= \frac{Y}{24(1-\nu)^2} \int_{\mathcal{D}} \left(k_1^2 + k_2^2 \right) \, dA_{\mathbf{g}} + \frac{Y}{24(1-\nu)} \int_{\mathcal{D}} dA_{\mathbf{g}}, \end{aligned}$$

where k_1 and k_2 are the principal curvatures of the surface. Therefore, to study minimizers over $\mathcal{A}_{Ki}$ it is sufficient to study minimizers of the following functional

$$\mathcal{W}[\mathbf{x}] = \int_{\mathcal{D}} (k_1^2 + k_2^2) \, dA_{\mathbf{g}}, \tag{3.0.1}$$

over $\mathcal{A}_{Ki}$ which is equivalent to a Willmore functional in this geometry (Willmore, 1982).

Remark 3.0.4. It is important to point out that in the above calculation we showed that the terms involving the Gaussian curvature are immaterial since $k_1 k_2 = K = -1$, but for more general metrics, in which the Gaussian curvature is not constant, the same term can be removed as a consequence of the Theorema Egregium.

Since we are integrating over a geodesic circle it is convenient to work in geodesic polar coordinates (r, Ψ) which are the natural analogs of the radial and polar angle

coordinates on a Riemannian manifold. In this coordinate system the metric $\mathbf{g}$ has components

$$g_{11} = 1,\ g_{12} = g_{21} = 0,\ \text{and}\ g_{22} = \sinh(r), \tag{3.0.2}$$

and equation (3.0.1) takes the form:

$$\mathcal{W}[\mathbf{x}] = \int_0^{2\pi} \int_0^R \sinh(r)(k_1^2 + k_2^2)\, dr\, d\Psi. \tag{3.0.3}$$

3.1 Chebychev Nets and the Hyperbolic Plane

To study isometric immersions of $\mathbb{H}^2$ we will use Chebyshev nets (C-nets) which are local parametrizations of a surface whose coordinate curves form quadrilaterals on the surface with opposite sides having equal length (Gray et al., 2006). To be precise, a **Chebyshev net** or a **Chebyshev patch** is defined to be a parametrization $\mathbf{x} : \mathcal{D} \to U \subset \mathbb{R}^3$ in which the induced metric $\mathbf{g}'$ in the parametrization coordinates u and v satisfies,

$$\mathbf{g}' = du^2 + 2\cos(\phi) + dv^2, \tag{3.1.1}$$

where ϕ is the angle between the coordinate curves. The key property of a C-net parametrization is that coordinate curves have unit speed in the parametrization variables.

Originally, Chebyshev used C-nets to describe the arrangement of fibers in clothing and he showed that a sphere must be covered by at least two cuts of cloth (Chebychef, 1878; McLachlan, 1994). As evidenced by the sphere, C-nets in general are only local parametrizations of a surface and a global C-net exists if the integral of the magnitude of the Gaussian curvature over a quadrilateral is less than 2π (Hazzidakis, 1880). In figure 3.1 we plot the pseudosphere covered by two C-nets that meet at the singular rim of the pseudosphere.

C-nets are useful parametrizations in that they lead to a natural way to discretize a surface (Bobenko & Pinkall, 1999) and projections of C-nets onto paper retain the

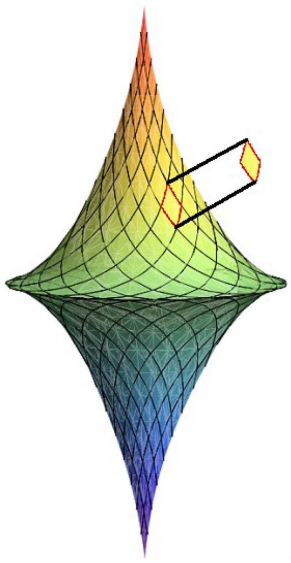

FIGURE 3.1. C-net parametrization of the pseudosphere.

three dimensional properties of the surface (Koenderink & van Doorn, 1998). Moreover, as we shall see in this section all of the geometric properties of the surface are encoded in the angle ϕ and for surfaces of constant negative Gaussian curvature ϕ satisfies the sine-Gordon equation (Gray et al., 2006). For this reason, we call the angle ϕ the **generating angle** of the surface.

3.1.1 Construction of C-nets

To construct C-nets on surfaces of constant negative Gaussian curvature, we will need the concept of an asymptotic curve. A curve α on S is an **asymptotic curve** if for all s:

$$\mathbf{h}\left(\frac{d\alpha}{ds}, \frac{d\alpha}{ds}\right) = 0, \tag{3.1.2}$$

where $\mathbf{h}$ is the second fundamental form of the surface. Thus, by (A.4.1) a curve is asymptotic if its tangent vectors are aligned with the directions of vanishing curvature for the surface. Now, if S is a surface with constant negative Gaussian it follows that

for every point $p \in S$ there are two directions of zero curvature. Therefore a pair of vector fields V and W can be defined on S that are everywhere aligned with the directions of zero curvature and by the fundamental theorem of vector fields and flows it follows that on a surface of constant negative curvature the asymptotic curves can be taken as coordinate curves (Frankel, 2003). We now show that a parametrization of a surface of constant negative Gaussian curvature in which the coordinate curves are asymptotic generates a C-net.

Proposition 3.1.1. If p is a point in a surface S of constant negative Gaussian curvature $K = -1$, then there is a neighborhood of p with the coordinate curves unit speed and asymptotic.

Proof. Let $\mathbf{x} : \Omega \to S$ define a parametrization around p with asymptotic coordinates (u, v). Let $\mathbf{g}$ and $\mathbf{h}$ be the corresponding first and second fundamental forms of this parametrization. It follows from the Mainardi-Codazzi equations (A.5.8) and (A.5.9) that

$$\begin{aligned}
\frac{\partial h_{12}}{\partial u} &= \frac{h_{12}}{\det(g_{ij})}\left(\frac{1}{2}\frac{\partial \det(g_{ij})}{\partial u} + g_{12}\frac{\partial g_{11}}{\partial v} - g_{11}\frac{\partial g_{22}}{\partial u}\right) \\
\frac{\partial h_{12}}{\partial v} &= \frac{h_{12}}{\det(g_{ij})}\left(\frac{1}{2}\frac{\partial \det(g_{ij})}{\partial v} + g_{12}\frac{\partial g_{22}}{\partial u} - g_{11}\frac{\partial g_{11}}{\partial v}\right).
\end{aligned}$$

Furthermore, since the coordinate curves are asymptotic it follows that $h_{11} = h_{22} = 0$ and consequently the Gaussian curvature satisfies

$$-1 = K = \frac{-h_{12}^2}{\det(g_{ij})}.$$

Therefore, differentiating with we have that

$$2\frac{\partial h_{12}}{\partial u}h_{12} = \frac{\partial \det(g_{ij})}{\partial u} \text{ and } 2\frac{\partial h_{12}}{\partial v}h_{12} = \frac{\partial \det(g_{ij})}{\partial v}.$$

Substituting these expressions for $\frac{\partial h_{12}}{\partial u}$ and $\frac{\partial h_{12}}{\partial v}$ into the Mainairdi-Codazzi equations we obtain

$$g_{12}\frac{\partial g_{11}}{\partial v} = g_{11}\frac{\partial g_{22}}{\partial u} \text{ and } g_{12}\frac{\partial g_{22}}{\partial u} = g_{22}\frac{\partial g_{11}}{\partial v}.$$

Therefore,

$$g_{12}^2\frac{\partial g_{11}}{\partial v} = g_{11}g_{12}\frac{\partial g_{22}}{\partial u} = g_{11}g_{22}\frac{\partial g_{11}}{\partial v} \text{ and } g_{12}^2\frac{\partial g_{22}}{\partial u} = g_{12}g_{22}\frac{\partial g_{11}}{\partial v} = g_{11}g_{22}\frac{\partial g_{22}}{\partial u}.$$

Consequently,

$$\det(g_{ij})\frac{\partial g_{11}}{\partial v} = 0 \text{ and } \det(g_{ij})\frac{\partial g_{22}}{\partial u} = 0.$$

Since the surface is regular, $\det(g_{ij}) \neq 0$ and thus $\frac{\partial g_{11}}{\partial v} = 0 = \frac{\partial g_{22}}{\partial u} = 0$. Therefore, g_{11} and g_{22} are independent of u and v and thus the arc-length of the coordinate curves is simply

$$u \to \int_0^u g_{11}^{\frac{1}{2}}(t)\,dt \text{and } v \to \int_0^v g_{22}^{\frac{1}{2}}(t)\,dt,$$

and thus inverting this relationship will yield a parametrization with unit speed coordinate curves in the asymptotic directions. □

Theorem 3.1.2. Let S be a surface of constant Gaussian curvature $K_0 = -1$ with a C-net parametrization $\mathbf{x} : \mathcal{D} \to S$ with coordinates (u, v). If ϕ is the corresponding generating angle ϕ then ϕ satisfies the sine-Gordon equation:

$$\frac{\partial^2\phi}{\partial u\partial v} = \sin(\phi). \tag{3.1.3}$$

Proof. By Biroshi's formula (A.4.4) it follows that

$$\begin{aligned} -1 &= \frac{1}{\sin^4(\phi)}\det\begin{pmatrix} \frac{\partial^2}{\partial u\partial v}\sin(\phi) & 0 & \frac{\partial}{\partial u}\sin(\phi) \\ \frac{\partial}{\partial v}\sin(\phi) & 1 & \sin(\phi) \\ 0 & \sin(\phi) & 1 \end{pmatrix} \\ &= \frac{1}{\sin^4(\phi)}\left[\left(-\cos(\phi)\frac{\partial\phi}{\partial u}\frac{\partial\phi}{\partial v} - \sin(\phi)\frac{\partial^2\phi}{\partial u\partial v}\right)\sin^2(\phi) + \sin^2(\phi)\cos(\phi)\frac{\partial\phi}{\partial u}\frac{\partial\phi}{\partial v}\right] \\ &= -\frac{\frac{\partial^2\phi}{\partial u\partial v}}{\sin(\phi)}. \end{aligned}$$

□

Now the condition that there must be two distinct asymptotic curves at each point in S implies that ϕ must satisfy the constraint

$$0 < \phi(u, v) < \pi. \tag{3.1.4}$$

Therefore, solutions to the sine-Gordon satisfying (3.1.4) generate hyperbolic surfaces. In fact Hilbert proved that there is no smooth immersion of $\mathbb{H}^2$ by showing that there is no smooth solution to (3.1.3) that satisfies (3.1.4) in the entire $u - v$ plane. The points on the surface where $\phi = n\pi$ are precisely the boundaries where the immersion fails to be smooth. In figure 3.1 this degeneracy of the coordinate curves occurs at the singular rim.

3.1.2 Geometry of C-nets

For the rest of the section assume that $\mathbf{x} : \mathcal{D} \to S$ is a C-net parametrization by asymptotic curves of a surface with constant negative Gaussian curvature $K = -1$ with generating angle ϕ and first and second fundamental forms $\mathbf{g}'$ and $\mathbf{h}$ respectively. Since the coordinate curves are asymptotic it follows that $h_{11} = h_{22} = 0$. By (A.4.2) it follows that

$$-1 = \frac{\det(h_{ij})}{\det(g'_{ij})} = -\frac{h_{12}}{\sin^2(\phi)},$$

and consequently $h_{12} = \pm \sin(\phi)$.

Since the second and first fundamental forms only depend on the generating angle ϕ it follows that all of the relevant geometric quantities of the surface can be found as well. From (A.4.2) and (A.4.3) it follows that the principal curvatures k_1 and k_2 satisfy

$$k_1 + k_2 = -\tan(\phi) \text{ and } k_1 k_2 = -1.$$

Therefore,

$$k_1^2 = \tan^2(\phi/2) \text{ and } k_2^2 = \cot^2(\phi/2). \tag{3.1.5}$$

Furthermore, by (A.5.2) the Christoffel symbols satisfy

$$\begin{array}{ll} \Gamma^1_{11} = \cot(\phi)\dfrac{\partial \phi}{\partial u}, & \Gamma^2_{11} = -\csc(\phi)\dfrac{\partial \phi}{\partial u}, \\ \Gamma^1_{12} = 0, & \Gamma^2_{12} = 0, \\ \Gamma^1_{22} = -\csc(\phi)\dfrac{\partial \phi}{\partial v}, & \Gamma^2_{22} = \cot(\phi)\dfrac{\partial \phi}{\partial v}, \end{array} \tag{3.1.6}$$

which by (A.6.1) gives us the following differential equations satisfied by the components $(u(t), v(t))$ of a geodesic:

$$\begin{aligned} \frac{d^2u}{dt^2} + \left(\frac{du}{dt}\right)^2 \cot(\phi)\frac{\partial \phi}{\partial u} - \left(\frac{dv}{dt}\right)^2 \csc(\phi)\frac{\partial \phi}{\partial v} = 0, \\ \frac{d^2v}{dt^2} - \left(\frac{du}{dt}\right)^2 \csc(\phi)\frac{\partial \phi}{\partial u} + \left(\frac{dv}{dt}\right)^2 \cot(\phi)\frac{\partial \phi}{\partial v} = 0. \end{aligned} \tag{3.1.7}$$

By (3.1.5) it follows that

$$\mathcal{W}[\mathbf{x}] = \int_0^{2\pi} \int_0^R \sinh(r)(\tan^2(\phi/2) + \cot^2(\phi/2))\, dr\, d\Psi. \tag{3.1.8}$$

Therefore, the bending content diverges if $\phi = n\pi$, precisely where the asymptotic curves become degenerate.

3.1.3 C-nets of the Second Kind

We conclude this section by pointing out that a closely related parametrization of S, that is sometimes easier to make calculations with, is a parametrization by curves of principal curvature or a **C-net of the second kind** (Gray et al., 2006). If $\mathbf{x}$ is a C-net, then a C-net of the second kind $\mathbf{y}$ is given by $\mathbf{y}(\eta, \xi) = \mathbf{x}\left(\frac{\eta+\xi}{2}, \frac{\eta-\xi}{2}\right)$. The components of the metric $\mathbf{g}'$ corresponding to $\mathbf{y}$ are

$$g'_{11} = \cos^2(\theta),\ g'_{12} = g'_{21} = 0,\ g'_{22} = \sin^2(\theta). \tag{3.1.9}$$

Since $g'_{12} = g'_{21} = 0$, the parameter curves of this parametrization are orthogonal and in fact they bisect the asymptotic curves. Therefore, $\theta = \phi/2$ and thus we can determine the generating angle by such a parametrization.

3.2 Elastic Energy of the Pseudosphere

In this section we illustrate how isometric immersions of geodesic disks in the hyperbolic plane can be constructed from a surface of constant negative Gaussian curvature by fixing a point $p \in S$ and "cutting" out a subset $U = \{q \in S : d(p, q) < R\}$. To

illustrate this process we consider a commonly known hyperbolic surface, the pseudosphere. The pseudosphere is parametrized by the following C-net of the second kind

$$\mathbf{y}(\eta,\xi)=\left(\frac{\cos(\xi)}{\cosh(\eta)},\frac{\sin(\xi)}{\cosh(\eta)},\eta-\tanh(\eta)\right), \tag{3.2.1}$$

(Gray et al., 2006). The mapping is singular on the curve $\eta=0$, which is where the surface fails to be a smooth immersion, and consequently we will only consider the "upper half" $\eta>0$ of the pseudosphere. Furthermore, since the sheets we are modelling have the topology of a plane and not a tubular surface we will think of the pseudosphere as a multi-sheeted surface.

Directly calculating, the metric coefficients are given by the following simple expressions:

$$\begin{aligned} g'_{11} &= \frac{\partial\mathbf{y}}{\partial\eta}\cdot\frac{\partial\mathbf{y}}{\partial\eta}=\tanh^2(\eta),\\ g'_{12} &= g'_{21}=\frac{\partial\mathbf{y}}{\partial\eta}\cdot\frac{\partial\mathbf{y}}{\partial\xi}=0,\\ g'_{22} &= \frac{\partial\mathbf{y}}{\partial\xi}\cdot\frac{\partial\mathbf{y}}{\partial\xi}=\frac{1}{\cosh^2(\eta)}. \end{aligned}$$

Consequently, by equation (3.1.9) the generating angle has the form

$$\phi(\eta,\xi)=4\arctan(e^{-\eta}), \tag{3.2.2}$$

and thus by (3.1.5) the principal curvatures are

$$k_1^2=\tan^2(2\arctan(e^{-\eta}))=\frac{1}{\sinh^2(\eta)}\text{ and }k_2^2=\cot^2(2\arctan(e^{-\eta})=\sinh^2(\eta). \tag{3.2.3}$$

Therefore, by equation (3.1.8) the elastic energy of a disk U centered at $\mathbf{x}(\eta_0,0)$ and lying in the pseudosphere is simply

$$\mathcal{W}[\mathbf{y}]=\int_0^{2\pi}\int_0^R\sinh(r)\left(\sinh^2(\eta(r,\Psi))+\frac{1}{\sinh^2(\eta(r,\Psi))}\right)dr\,d\Psi. \tag{3.2.4}$$

Now, to determine the dependency between η,ξ and r,Ψ we need to calculate the arclength of geodesics on the pseudosphere. The arclength of a curve $\mathbf{x}(\eta,\xi(\eta))$

starting at $\mathbf{x}(\eta_0, 0)$ and terminating at $\mathbf{x}(\eta_f, \xi_f)$ is given by the functional

$$L[\xi(\eta)] = \int_{\eta_0}^{\eta_f} \sqrt{\tanh^2(\eta) + \sinh^2(\eta) \left(\frac{d\xi}{d\eta}\right)^2}\, d\eta. \tag{3.2.5}$$

Since the integrand does not explicitly depend on ξ, the Euler-Lagrange equation of this functional is

$$\frac{d}{d\eta} \frac{\operatorname{sech}^2\eta}{\sqrt{\tanh^2(\eta) + \operatorname{sech}^2(\eta)\frac{d\xi}{d\eta}}} = 0. \tag{3.2.6}$$

This can be integrated once, with a constant of integration $\pm\frac{1}{\sqrt{D}}$. This generates a first order separable differential equation that can be integrated with a constant of integration C. The solution curves, and thus the geodesics, are given by the family of curves implicitly defined by

$$\cosh^2(\eta) + (\xi + C)^2 = D. \tag{3.2.7}$$

The constants C and D are determined by the condition that the geodesic passes through $(\eta_0, 0)$ and (η_f, ξ_f):

$$C = \frac{\cosh(\eta_0)^2 - \cosh^2(\eta_f) - \xi_f^2}{2\xi_f}, \tag{3.2.8}$$

$$D = \cosh^2(\eta_0) + \frac{(\cosh^2(\eta_0) - \cosh^2(\eta_f) - \xi_f^2)^2}{4\xi_f^2}. \tag{3.2.9}$$

Define the function $\mathcal{L}(\eta, \xi)$ to be arclength of the geodesic starting at $\mathbf{y}(\eta_0, 0)$ and terminating at $\mathbf{y}(\eta, \xi)$. Since the geodesics fail to be a function of η at the critical values

$$\begin{aligned} \eta^* &= \operatorname{arccosh}\left(\sqrt{D}\right), \\ \xi^\star &= \sqrt{\cosh^2(\eta_0) - \cosh^2(\eta_f)}, \end{aligned}$$

the arclength of a geodesic will have to be computed over both branches of a square root. Assuming $\eta_0 < \eta$ we have by equation (3.2.5) that

$$\mathcal{L}(\eta, \xi) = \begin{cases} \int_{\eta_0}^{\eta} \sqrt{\frac{D\tanh^2(t)}{D-\cosh^2(t)}}\, dt & \text{if} \quad 0 < \xi^2 < (\xi^*)^2 \\ \int_{\eta_0}^{\eta^*} \left(\sqrt{\frac{D\tanh^2(t)}{D-\cosh^2(t)}} + \sqrt{\frac{D\tanh^2(t)}{D-\cosh^2(t)}}\right)\, dt & \text{if} \quad \xi^2 > (\xi^*)^2 \\ \ln\left(\frac{\cosh(\eta)}{\cosh(\eta_0)}\right) & \text{if} \quad \xi = 0 \end{cases} \tag{3.2.10}$$

If $\eta_0 > \eta$ then $\mathcal{L}(\eta, \xi)$ can be computed by switching η_0 and η. By making the substitution $z = \operatorname{sech}(t)$, and taking into account the case $\eta_0 > \eta$, the integrals can be explicitly evaluated and simplified into the form

$$\mathcal{L}(\eta,\xi) = \begin{cases} \left| \ln\left(\frac{\operatorname{sech}(\eta_0)+\sqrt{\operatorname{sech}^2(\eta_0)-\frac{1}{D}}}{\operatorname{sech}(\eta)+\sqrt{\operatorname{sech}^2(\eta)-\frac{1}{D}}} \right) \right| & \text{if} \quad 0 < \xi^2 < (\xi^*)^2 \\ \left| \ln\left(D \frac{\operatorname{sech}(\eta_0)+\sqrt{\operatorname{sech}^2(\eta_0)-\frac{1}{D}}}{\left(\operatorname{sech}(\eta)+\sqrt{\operatorname{sech}^2(\eta)-\frac{1}{D}}\right)^{-1}} \right) \right| & \text{if} \quad \xi^2 > (\xi^*)^2 \\ \left| \ln\left(\frac{\cosh(\eta_0)}{\cosh(\eta)} \right) \right| & \text{if} \quad \xi = 0 \end{cases} . \tag{3.2.11}$$

The contour $\mathcal{L}(\eta, \xi) = R$ forms the boundary of the disk U (see figure 3.2).

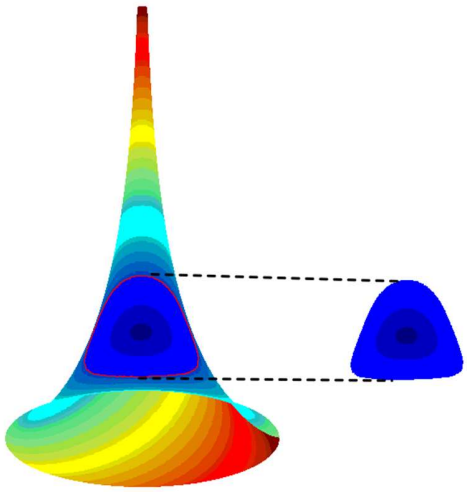

FIGURE 3.2. The pseudosphere colored by the geodesic distance from an arbitrary point p lying on the surface. Geodesic disks of constant negative curvature can be formed from the contour data of the arclength of geodesics originating at p and correspond to isometric immersions of geodesic disks in the hyperbolic plane.

Furthermore, the geodesics on the pseudosphere itself are given by the following curves:

$$\gamma(\xi) = \mathbf{x}(\operatorname{arccosh}\left(D - (\xi + C)^2\right), \xi)$$

The angle Ψ a geodesic makes with respect to the basis $\left(\frac{\partial \mathbf{x}(\eta,\xi)}{\partial \xi}, \frac{\partial \mathbf{x}(\eta,\xi)}{\partial \eta}\right)$ of the tangent

plane at the center of the disk can then be found by

$$\left.\frac{d}{d\xi}\mathbf{x}(\eta(\xi),\xi)\right|_{\eta=\eta_0} \cdot \left.\frac{\partial \mathbf{x}}{\partial \xi}\right|_{\eta=\eta_0} = \left\|\left.\frac{d}{d\xi}\mathbf{x}(\eta(\xi),\xi)\right\|_{\eta=\eta_0}\right\| \left\|\left.\frac{\partial \mathbf{x}}{\partial \xi}\right\|_{\eta=\eta_0}\right\| \cos(\Psi).$$

By making the substitution $D = \cosh(\eta_0)^2 + C^2$, this calculation gives us that the angle Ψ satisfies

$$\cos(\Psi) = \frac{\sqrt{2}\mathrm{csch}(\eta_0)}{1 + 2C^2 + \cos(2\xi_0)}. \tag{3.2.12}$$

Consequently, by specifying a value for Ψ we can calculate C and therefore use equation (3.2.10) to determine η for a particular value of r and Ψ. This allows us to color the disk by bending energy density (see figure 3.3) and numerically integrate (3.2.4) over the disk to determine how the bending energy scales with R for various values of η_0 (see figure 3.4).

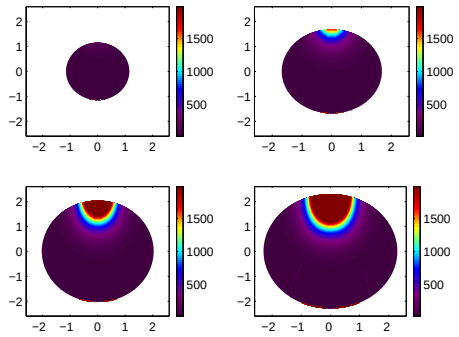

FIGURE 3.3. A representation of the geodesic disks colored by $k_1^2 + k_2^2$ in which the radius and polar angle correspond to the geodesic radius r and polar angle Ψ. These disks are centered at $\mathbf{y}(\eta_0, 0)$ for the values $\eta_0 = 1.94, 2.54, 2.92, 3.21$ respectively. The concentration of energy at the top of the disk arises from the large amount of bending in the "skinny" part of the pseudosphere. The narrow region of concentrated energy near the bottom of the disc corresponds to the divergence of the principal curvatures near the singular rim.

Now, a disk centered at $\mathbf{x}(\eta_0, 0)$ cannot be made arbitrarily large since it will eventually meet the singular curve corresponding to $\eta = 0$. We can prove that the

largest disk on the pseudosphere with this center has a critical radius of

$$R_{\eta_0} = \ln(\cosh(\eta_0)).$$

To prove this, note that the curve $\xi = 0$ is a geodesic, it trivially solves the Euler-Lagrange equation, and therefore

$$\mathcal{L}(0,0) = \int_0^{\eta_0} \tanh(u)\, d\eta = \ln(\cosh(\eta_0)). \tag{3.2.13}$$

Now, let $\xi(\eta)$ be another geodesic that terminates at a point $(0, \eta^*)$ on the boundary. Then,

$$\begin{aligned}\mathcal{L}(0,\xi^*) &= \int_0^{\eta_0} \sqrt{\tanh^2(\eta) + \sinh^2(\eta)\left(\frac{d\xi}{d\eta}\right)^2}\, d\xi \\ &> \int_0^{\eta_0} \tanh(\eta)\, d\eta = \ln(\cosh(\eta_0)).\end{aligned}$$

Consequently, the contour $\mathcal{L}(\eta,\xi) = \ln(\cosh(\eta_0))$ meets the curve $\eta = 0$ at only one point and thus $\ln(\cosh(\eta_0))$ is the radius of the largest possible disk centered at $(\eta_0, 0)$. Therefore, we can see that for arbitrary R we can find a value η_0 such that D is isometric to U, and thus by varying the center of the disk we can create arbitrarily large isometric immersions. This proves the following proposition

Proposition 3.2.1. Let D be a disk of radius R in the hyperbolic plane. There exists a smooth isometric immersion $\mathbf{x} : \mathcal{D} \to U \subset \mathbb{R}^3$ such that U is a subset of the pseudosphere.

3.3 Lower Bounds for the Curvature of Smooth Isometric Immersions

In this section we use the C-net structure to explore numerically how the principal curvatures of smooth isometric immersions scale with the size of the disk. In particular, we show that the maximum principal curvature on the disk grows exponentially in $\sqrt{-K_0}R$.

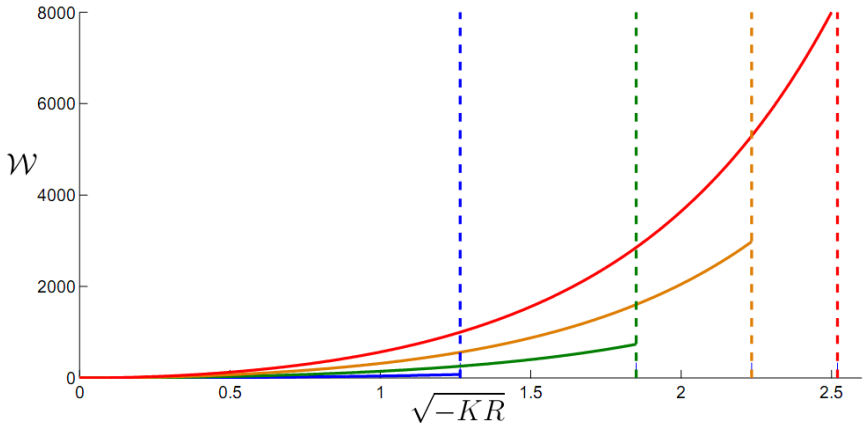

FIGURE 3.4. Plot of the energy $\mathcal{W}$ of isometric immersions of $(\mathcal{D}, \mathbf{g})$ cut from the pseudosphere for disks centered at $\mathbf{y}(\eta_0, 0)$ for the values $\eta_0 = 1.94, 2.54, 2.92, 3.21$ respectively. The dashed lines correspond to the critical radius when the isometric immersion fails to be smooth.

Let p denote the center of the disk, and let us choose the asymptotic coordinates u and v such that p is the point $(0, 0)$. If $|u_0| + |v_0| < R$, it follows easily that there exists p' in D with coordinates (u_0, v_0) since $d(p, p') \leq |u_0| + |v_0| < R$. Let q, r, s and t denote the vertices of a "square" denoted $[qrst]$ in asymptotic coordinates given by the intersections of the asymptotic lines $u = -R/(2+\nu), v = -R/(2+\nu), u = R/(2+\nu), v = R/(2+\nu)$ for some given $\nu > 0$.

We redefine the variables

$$u' = \frac{1}{2} + \frac{(2+\eta)u}{2R}, \quad v' = \frac{1}{2} + \frac{(2+\eta)v}{2R}, \quad \lambda = \frac{4|K_0|R^2}{(2+\eta)^2}, \quad \phi'(u', v') = \phi(u, v),$$

and then drop the primes to transform equation (3.1.3) into

$$\frac{\partial^2 \phi}{\partial u \partial v} = \lambda \sin(\phi) \quad \text{on the domain } (0,1) \times (0,1). \tag{3.3.1}$$

A smooth isometric immersion corresponds to a smooth function $\phi : (0,1)^2 \to (0, \pi)$ satisfying the Sine-Gordon equation (3.3.1).

We want to consider the variational problem for minimizing the L^p norms of the principal curvatures. The natural mode of converge is then L^p convergence which

does not preserve the class of smooth functions. We thus enlarge the admissible set. Let $\mathcal{M}$ denote the set of all measurable functions on the unit square with values in $[0,\pi]$ and let $\mathcal{A} \subseteq \mathcal{M}$ be the set of measurable functions $\phi : [0,1]^2 \to [0,\pi]$ that are distributional solutions of the sine-Gordon equation, *i.e.*,

$$\int_{[0,1]^2} \phi \frac{\partial^2 g}{\partial u \partial v} du dv = \lambda \int_{[0,1]^2} \sin(\phi) g du dv, \qquad \forall g \in C_c^\infty((0,1)^2).$$

Clearly $\mathcal{A} \subseteq L^p([0,1]^2)$ for all $1 \leq p \leq \infty$.

Proposition 3.3.1. $\mathcal{A}$ is a closed subset of $L^p([0,1]^2)$ for all $1 \leq p \leq \infty$.

Proof. Let ϕ_n be a sequence in $\mathcal{A}$ such that $\phi_n \to \phi$ in L^p. The mean value theorem implies that $\|\sin(\phi_n) - \sin(\phi)\|_p \leq \|\phi_n - \phi\|_p \to 0$. Therefore by the dominated convergence theorem it follows that for all $g \in C_c^\infty((0,1)^2)$ we have that

$$\begin{aligned} \lambda \int_{[0,1]^2} \sin(\phi) g du dv &= \lim_{n\to\infty} \lambda \int_{[0,1]^2} \sin(\phi_n) g du dv \\ &= \lim_{n\to\infty} \int_{[0,1]^2} \phi_n \frac{\partial^2 g}{\partial u \partial v} du dv \\ &= \int_{[0,1]^2} \phi \frac{\partial^2 g}{\partial u \partial v} du dv \end{aligned}$$

implying that $\phi \in \mathcal{A}$. Consequently, $\mathcal{A}$ is a closed subset of $L^p([0,1]^2)$ for all $1 \leq p \leq \infty$. □

Remark 3.3.2. (Compactness) Since $\mathcal{M}$ consists of bounded measurable functions, for every sequence $\phi_n \in \mathcal{M}$, there exists a subsequence ϕ_{n_k} and a limit point $\phi^* \in \mathcal{M}$ such that $\phi_{n_k} \rightharpoonup \phi^*$ weakly in all $L^p([0,1])^2$ for $1 \leq p < \infty$ and $\phi_{n_k} \overset{*}{\rightharpoonup} \phi^*$ (converges weak-$*$) in $L^\infty([0,1]^2)$. Note that the limit ϕ^* is independent of p. In fact, on $\mathcal{M}$, the weak L^p topologies for $1 \leq p < \infty$ and the weak-$*$ L^∞ topology are all the same (Evans, 1990).

We are interested in a lower bound for the principal curvatures of a *Chebyshev patch*, *i.e.*, a portion of a surface of constant negative curvature covered by a single

coordinate system given by a Chebyshev net. We thus define

$$M(\lambda) = \inf_{\phi \in \mathcal{A}} \sup_{x \in [0,1]\times[0,1]} \max \left[\cot\left(\frac{\phi}{2}\right), \tan\left(\frac{\phi}{2}\right) \right].$$

While we can estimate $M(\lambda)$ by direct numerical computation, we use a slightly different approach that yields some more information. Since $\cot(\phi/2) + \tan(\phi/2) = 2\csc(\phi)$, we get $k_1^2 + k_2^2 = 4\csc^2(\phi) - 2 = 4\cot^2(\phi) + 2$. This motivates the definition

$$I_p(\lambda) = \inf_{\phi \in \mathcal{A}} \| \cot^2(\phi) \|_p$$

where $\|.\|_p$ denotes the L^p norm. This corresponds to the variational problem for functionals $F_p : \mathcal{M} \to [0, \infty]$ given by

$$F_p(\phi) = \begin{cases} \| \cot^2 \phi \|_p, & \phi \in \mathcal{A}. \\ +\infty, & \text{otherwise.} \end{cases}$$

Note that $M(\lambda)$ and $I_p(\lambda)$ are for a unit square in asymptotic coordinates, and this is not the same thing as a geodesic disk, although the two can be related.

For all $p < \infty$, the map $f \mapsto \|f\|_p$ is differentiable at $f \neq 0$. Also, for any function $f : [0,1] \times [0,1] \to \mathbb{R}$, the p-norm $\|f\|_p$ is a nondecreasing function of p. It is easy to see that, as a consequence, I_p is non-decreasing in p.

A natural question is whether there exists a minimizer for F_p. In this context we have the following proposition.

Proposition 3.3.3. Let ϕ_n be a minimizing sequence for F_p, *i.e.*, $\phi_n \in \mathcal{A}$ and $F_p(\phi_n) \to I_p$. If ϕ_n (or a subsequence) converges pointwise to ϕ^*, ϕ^* is a minimizer for F_p.

Proof. If ϕ_n (or a further subsequence) converges pointwise, it follows from dominated convergence that $\|\phi_n - \phi^*\|_p \to 0$. Since $\mathcal{A}$ is closed in L^p, it follows that $\phi^* \in \mathcal{A}$. Also, by Fatou's lemma, we have

$$I_p \leq F_p(\phi^*) \leq \liminf F_p(\phi_n) = I_p$$

showing that the minimum is attained. □

Remark 3.3.4. The function $\theta \mapsto -\lambda \sin(\theta)$ is convex on $(0, \pi)$. Therefore, the map

$$\mathcal{M} \ni \phi \mapsto -\lambda \int_{[0,1]^2} \sin(\phi) g du dv, \quad g \in C_c^\infty((0,1)^2),\, g \geq 0,$$

is weakly lower semi-continuous. If $\phi_n \in \mathcal{A}$ is any sequence and $\phi_n \rightharpoonup \phi^*$ weakly in some $L^p, 1 \leq p < \infty$ or converges weak-$*$ in L^∞, $\phi_n \overset{*}{\rightharpoonup} \phi^*$ it follows that

$$\int_{[0,1]^2} \phi^* \frac{\partial^2 g}{\partial u \partial v} du dv - \lambda \int_{[0,1]^2} \sin(\phi^*) g du dv \leq 0, \qquad \forall g \in C_c^\infty((0,1)^2),\, g \geq 0.$$

So, in general, $\phi^* \notin \mathcal{A}$, and thus, the functionals F_p are not lower semi-continuous with respect to weak or weak-$*$ convergence. Thus, it is not enough to have weak convergence of the minimizing sequence for the existence of a minimizer. The pointwise convergence in the proposition is also necessary for using the direct method to show the existence of a minimizer for F_p.

The previous remark suggests considering the problem of minimizing the relaxed energy $\tilde{F}_p$, namely the largest weakly lower semi-continuous function less than or equal to F_p on $\mathcal{M}$ (Pedregal, 1999; Müller, 1999). Let $\overline{\mathcal{A}}$ denote the weak closure of $\mathcal{A}$ in some $L^{p'}$. The relaxation of F_p is defined by

$$\tilde{F}_p(\phi) = \begin{cases} \inf\{\liminf_n F_p(\phi_n) : \phi_n \rightharpoonup \phi\} & \phi \in \overline{\mathcal{A}}. \\ +\infty, & \text{otherwise} \end{cases}$$

where the infimum is over all sequences which converge weakly to ϕ. Clearly, $\mathcal{A} \subseteq \overline{\mathcal{B}} \subseteq \mathcal{M}$ and $\tilde{F}_p$ is weakly lower semi-continuous by construction. It thus follows from Remark 3.3.2 that we can prove the existence of a minimizer for $\tilde{F}_p$ by the direct method in the calculus of variations.

The question of the existence of a minimizer for F_p can thus be posed in terms of the nature of the minimizer of $\tilde{F}_p$ which always exists. If there exists $\phi^* \in \mathcal{A}$ which is a minimizer for $\tilde{F}_P$, then ϕ^* is also a minimizer for F_p. Conversely, if all the minimizers of $\tilde{F}_p$ are in $\overline{\mathcal{A}} \backslash \mathcal{A}$, it follows that F_p does not have a minimizer. Studying this question involves computing the relaxation $\tilde{F}_p$ which in turn needs a careful analysis of the potential oscillations in weakly convergent sequences of solutions of the sine-Gordon equation.

3.3.1 A Numerical Investigation of Lower Bounds for the Curvature

We can discretize the sine-Gordon equation on a $N \times N$ grid covering the unit square, and minimize the l^p norms of $\cot^2 \phi$ over all solutions of this discrete sine-Gordon equation. This is a finite dimensional problem with a coercive energy, so there always exists a minimizer ϕ^N on the $N \times N$ grid. Figure 3.3.1 displays the numerically obtained results for this minimization. Observe the lack of high frequency oscillations in the numerically obtained minimizers. In fact, increasing the mesh size suggests that as $N \to \infty$, the numerically obtained minimizers converge pointwise on $[0,1]^2$. If this were indeed the case, Proposition 3.3.3 implies the existence of minimizers for the functionals F_p on the admissible set $\mathcal{A}$.

We will henceforth assume that the infimum is attained, *i.e.*, for any given p and λ, there is an admissible function $\phi_p(\lambda) \equiv \phi_p \in \mathcal{A}$ such that $I_p = \| \cot^2(\phi_p)\|_p$, it follows that

$$I_p \leq I_\infty \leq \| \cot^2(\phi_p)\|_\infty.$$

Thus, numerically determining the function ϕ_p which minimizes the p-norm of $\cot^2(\phi)$ in the admissible set, gives both lower and upper bounds for I_∞, and the difference between these bounds gives an estimate for the error in a numerical determination of I_∞.

Once we determine $I_\infty(\lambda)$, we can compute $M(\lambda)$ as the following argument shows:

$$\begin{aligned}
\max(|k_1|,|k_2|) &= \frac{|k_1|+|k_2|}{2} + \frac{||k_1|-|k_2||}{2} \\
&= \sqrt{\frac{k_1^2 + 2|k_1 k_2| + k_2^2}{4}} + \sqrt{\frac{k_1^2 - 2|k_1 k_2| + k_2^2}{4}} \\
&= \sqrt{\frac{k_1^2 + 2 + k_2^2}{4}} + \sqrt{\frac{k_1^2 - 2 + k_2^2}{4}} \\
&= \sqrt{\cot^2(\phi) + 1} + \sqrt{\cot^2(\phi)} \equiv g(\cot^2(\phi))
\end{aligned}$$

where $g(x) = \sqrt{x} + \sqrt{1+x}$ is a monotone function with a monotone inverse. Conse-

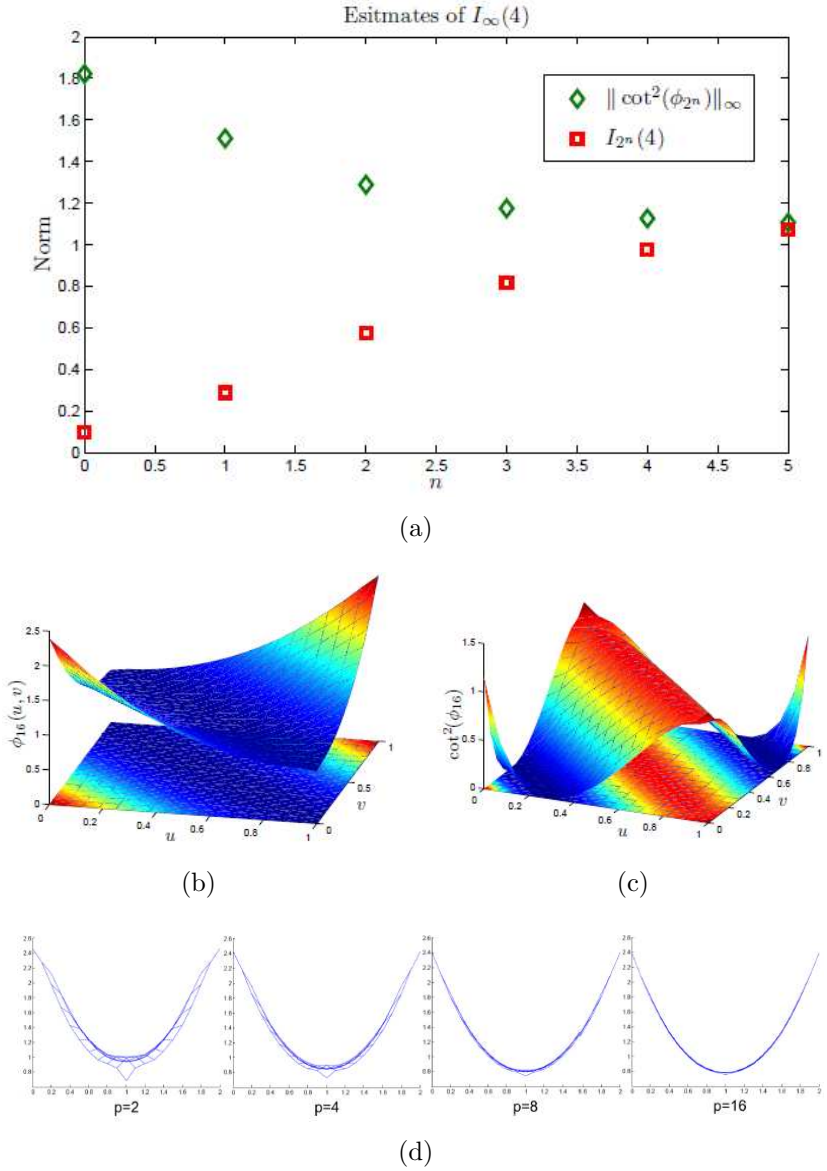

FIGURE 3.5. (a) Plot of I_{2^n} and $\|\cot^2(\phi_{2^n})\|$ as a function of n with $\lambda = 4$. The collapse of these data points onto a single line confirms that these two quantities are valid approximations to I_∞ for large enough n. (b) Plot of ϕ_{16} as a function of u and v with the contour plot of ϕ_{16} underneath the surface. We can see from the contour plot that it appears that lines $u + v =$ constant form the contours suggesting that ϕ_∞ is a function of $u + v$. (c) $\cot^2(\phi_{16})$ plotted as a function of u and v again with the contour plot $\cot^2(\phi_{16})$ plotted underneath the surface. (d) Plot of $\phi_p(u, v)$ as a function of $u+v$ for $p = 2, 4, 8, 16$ the collapse into a single curve again indicates that ϕ_∞ is a function of $u + v$ only.

quently,

$$M(\lambda) = g(I_\infty(\lambda)) = \sqrt{I_\infty(\lambda)} + \sqrt{I_\infty(\lambda)+1},$$

and the value of $M(\lambda)$ is attained on ϕ_∞, the extremizer for I_∞.

The same argument can be applied to any function $\zeta(\phi)$ with the property that there is a continuous monotone function h with a continuous monotone inverse such that $h(\zeta(\phi)) = \cot^2(\phi)$. In particular, if $\zeta(\phi) = (\phi - \pi/2)^2$, there is such a function h, and it follows that

$$\begin{aligned}
\phi_\infty &\equiv \arg\min_{\phi\in\mathcal{A}} \max_{x\in D} \cot^2(\phi) \\
&= \arg\min_{\phi\in\mathcal{A}} \max_{x\in D} \max[\tan(\phi/2), \cot(\phi/2)] \\
&= \arg\min_{\phi\in\mathcal{A}} \max_{x\in D} \left[\phi - \frac{\pi}{2}\right]^2 . \qquad (3.3.2)
\end{aligned}$$

We can solve any of these minimax problems to determine the extremizing function ϕ_∞. For our numerics, we use the third formulation of the problem, *i.e.*, finding the minimax for the square of the deviation of ϕ from $\pi/2$. Also, we note that, I_∞ directly estimates the maximum bending energy density $k_1^2 + k_2^2$ and I_1 estimates the total bending energy.

Figure 3.5(a) shows the numerically computed values of I_p and $\|\cot^2(\phi_p)\|_\infty$ as a function of $p = 2^n$, $n \in \mathbb{N}$, for $\lambda = 4$. Figure 3.5(b) and figure 3.5(c) shows the numerically determined extremizers ϕ_p as well as the quantity $\cot^2(\phi_p)$ for $\lambda = 4$ and $p = 16$. The figures for other values of λ are similar in character. The key observation from these figures is that as p gets large $\phi_p(u, v)$ numerically approaches a limit that is purely a function of the combination $u + v$ (see figure 3.5(d)). This motivates the ansatz $\phi_\infty(u, v) = \psi(u + v)$.

Substituting this ansatz in equation (3.3.1) yields $\psi'' = \lambda \sin(\psi)$, which is the Hamiltonian motion of a unit mass in a potential $V(\psi) = \lambda \cos(\psi)$. The trajectories in phase space (ψ, ψ') are given by conservation of the energy, $\psi'^2/2 + \lambda \cos(\psi) = E$ (see figure 3.3.1). Now, it known that there are only three distinct types of surfaces of

revolution of constant negative curvature and for each of these surfaces ϕ is a function of $u+v$ only (Rozendorn, 1989). Therefore, the three distinct trajectories in the phase plane correspond to the three types of surfaces of revolution. The pseudosphere corresponds to the separatrix, hyperboloid surfaces correspond to closed orbits, and conical surfaces correspond to unbounded orbits.

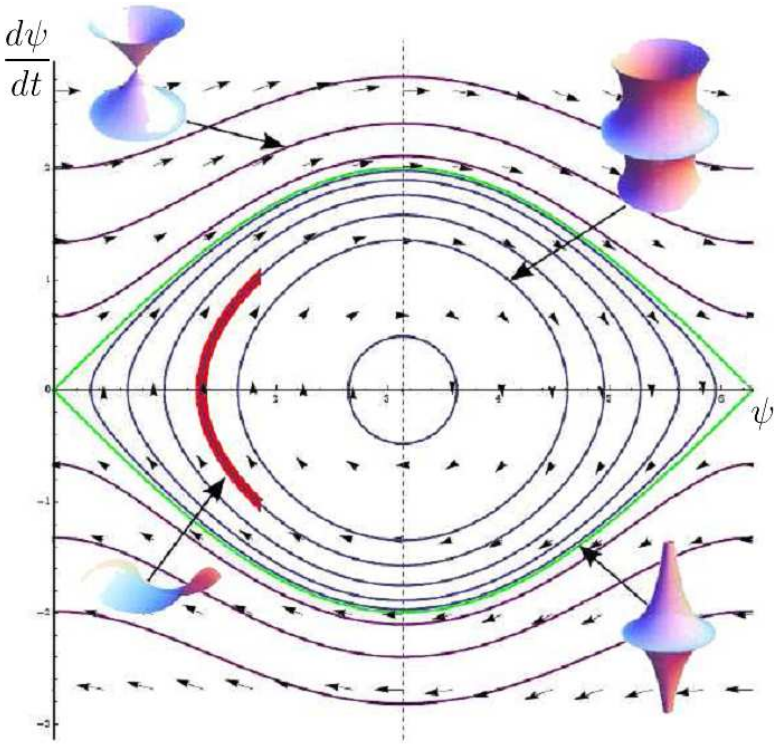

FIGURE 3.6. Phase portrait of the differential equation $\psi'' = \lambda \sin(\psi)$. The three different types of orbits correspond to the three different types of surfaces of revolution of constant negative curvature. The piece of the orbit outlined in bold is the trajectory $\psi : [0, 2] \to (0, \pi)$ that minimizes the value of $\cot^2(\psi)$ over all trajectories in the phase plane defined over the same time domain.

We seek solutions on the unit square, $0 \leq t \equiv u + v \leq 2$, that are bounded away from $\psi = \pi$ on the interval $[0, 2]$. If we want trajectories that minimize the maximum value of $\cot^2(\psi)$, it is clear from the symmetry of $\cot(\psi)$ we are interested in the closed orbits. Furthermore, we seek a piece of these trajectories that satisfies the

further symmetry requirement $\psi(0) = \psi(2) = \pi - \delta, \psi(1) = \delta,$ and $\psi'(1) = 0$ since if these conditions are not met we could select a different piece of the trajectory that could further minimize $\cot^2(\phi)$. This trajectory is depicted in bold in figure 3.3.1.

The value E of a minimizing trajectory can be computed as $E = [\psi'(1)]^2/2 + \lambda\cos(\psi(1)) = \lambda\cos(\delta)$, and the relation between δ and λ is determined by requiring that the time it takes to get from $\psi = \pi - \delta$ to $\psi = \delta$ is 1, *i.e.*,

$$\int_{\delta}^{\pi-\delta} \frac{d\theta}{\sqrt{2\lambda(\cos(\delta) - \cos(\theta))}} = 1 \tag{3.3.3}$$

We can solve this equation numerically, and thereby determine $\phi_\infty(u, v) = \psi(u + v)$, provided that our ansatz is valid.

Generating an asymptotic series for (3.3.3), we have for small δ that

$$\frac{-\log(\delta) + \log(8) + O(\delta)}{\sqrt{\lambda}} = 1.$$

Rearranging, we obtain

$$\cot(\delta) \sim \delta^{-1} + O(\delta) = \frac{1}{8}\exp[\sqrt{\lambda}] + O[e^{-\sqrt{\lambda}}] \tag{3.3.4}$$

This implies $I_\infty(\lambda) \sim \frac{1}{64}\exp[2\sqrt{\lambda}] + O(1)$. Finally, if we set $\nu = 0$ we have in terms of $\sqrt{-K_0}R$ that

$$I_\infty(\sqrt{-K}R) \sim \frac{1}{64}e^{2\sqrt{-K_0}R} + O(1). \tag{3.3.5}$$

3.3.2 Elastic Energy of Hyperboloids of Revolution

We conclude this section by comparing the bending energy of disks cut from hyperboloids of revolution with the pseudosphere. The family of hyperboloids are parametrized by the following family of C-nets of the second kind

$$\mathbf{y}(\eta, \xi) = \frac{1}{b}\left(\mathrm{dn}(\eta, b^2)\cos(bv), \mathrm{dn}(\eta, b^2)\sin(b\xi), u - E(\mathrm{am}(\eta, b^2)|b^2)\right), \tag{3.3.6}$$

where dn, am, sn denote the usual Jacobi elliptic functions, E is the elliptic function of the second kind, and $0 < b < 1$ (Abramowitz & Stegun, 1964; Gray et al., 2006).

The metric and principal curvatures are given by

$$g'_{11} = b^4\mathrm{sn}^2(\eta, b^2),\ g'_{12} = g'_{21} = 0,\ g'_{22} = 1 - b^4\mathrm{sn}^2(\eta, b^2) \tag{3.3.7}$$

$$k_1^2 = \frac{g'_{22}}{g'_{11}} = \frac{1 - b^4\mathrm{sn}^2(\eta, b^2)}{b^4\mathrm{sn}^2(\eta, b^2)},\ k_2^2 = \frac{b^4\mathrm{sn}^2(\eta, b^2)}{1 - b^4\mathrm{sn}^2(\eta, b^2)}. \tag{3.3.8}$$

The Christoffel symbols for this parameterization are

$$\begin{array}{ll} \Gamma^1_{11} = \frac{\mathrm{cn}(\eta,b^2)\mathrm{dn}(\eta,b^2)}{\mathrm{sn}(\eta,b^2)}, & \Gamma^2_{11} = 0 \\ \Gamma^1_{12} = 0, & \Gamma^2_{12} = \frac{-b^4\mathrm{sn}(\eta,b^2)\mathrm{cn}(\eta,b^2)\mathrm{dn}(\eta,b^2)}{1-b^4\mathrm{sn}(\eta,b^2)}, \\ \Gamma^1_{22} = -\frac{\mathrm{cn}(\eta,b^2)\mathrm{dn}(\eta,b^2)}{\mathrm{sn}(\eta,b^2)} & \Gamma^2_{22} = 0, \end{array} \tag{3.3.9}$$

Therefore, the geodesic equations are

$$0 = \frac{d^2\eta}{dt^2} + \frac{\mathrm{cn}(\eta, b^2)\mathrm{dn}(\eta, b^2)}{\mathrm{sn}(\eta, b^2)}\left[\left(\frac{d\eta}{dt}\right)^2 + \left(\frac{d\xi}{dt}\right)^2\right] \tag{3.3.10}$$

$$0 = \frac{d^2\xi}{dt^2} + \frac{2b^4\mathrm{sn}(\eta, b^2)\mathrm{cn}(\eta, b^2)\mathrm{dn}(\eta, b^2)}{1 - b^4\mathrm{sn}^2(\eta, b^2)}. \tag{3.3.11}$$

It is easy to see that the principal curvatures diverge when $\pi = \mathrm{am}(\eta, b^2)$. Consequently, the center of the disk is located at the coordinate $\eta_0 = F(\pi/2, b^2)$, where F is the elliptic function of the first kind, and thus the relationship between δ and b is given by

$$\frac{\delta}{2} = \arctan\left(\sqrt{\frac{1 - b^4\sin^2(\mathrm{am}(F(\pi/2, b^2))}{b^4\sin^2(\mathrm{am}(F(\pi/2, b^2))}}\right) = \arctan\left(\sqrt{\frac{1 - b^4}{b^4}}\right). \tag{3.3.12}$$

Solving this equation yields

$$b = \sqrt{\cos(\delta/2)}. \tag{3.3.13}$$

Therefore, for a particular radius R we can numerically solve equation (3.3.3) to obtain b. Once, we determine b we can then numerically integrate the bending energy

$$\mathcal{W}[\mathbf{y}] = \int_0^{2\pi}\int_0^R \left(\frac{1 - b^4\mathrm{sn}^2(\eta, b^2)}{b^4\mathrm{sn}^2(\eta, b^2)} + \frac{b^4\mathrm{sn}^2(\eta, b^2)}{1 - b^4\mathrm{sn}^2(\eta, b^2)}\right)\sinh(r)\, dr d\Psi, \tag{3.3.14}$$

following a similar procedure as we did with the pseudosphere. These results are summarized in figure 3.3.2.

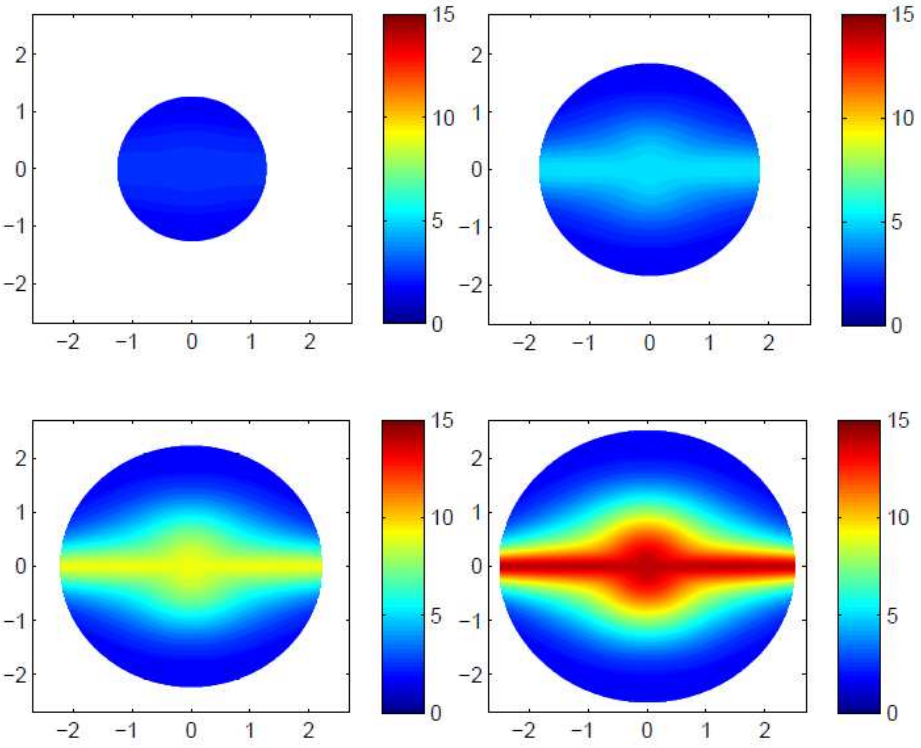

(a)

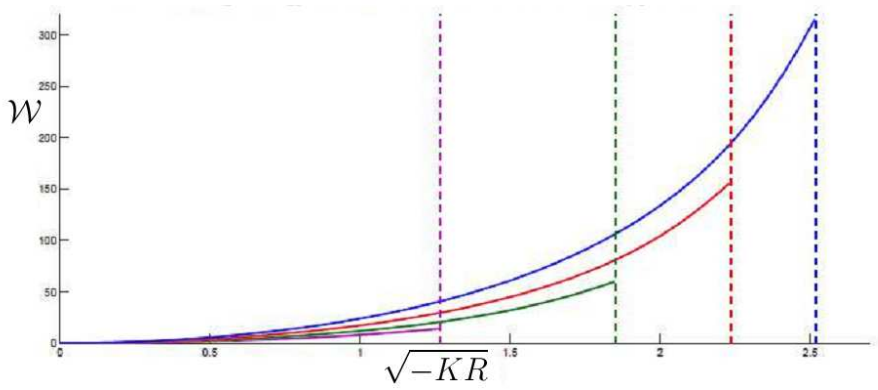

(b)

FIGURE 3.7. (a) A representation of the geodesic disks cut out of hyperboloid surfaces colored by $k_1^2 + k_2^2$. The radius and polar angle of these disks correspond to the geodesic radius r and polar angle Ψ. These disks each have a maximum radii of $R = 1.2654, 1.8505, 2.2342, 2.5199$. (b) The Willmore energy of disks cut from hyperboloids plotted versus geodesic radius. The dashed lines correspond to where the isometric immersions fails to be smooth.

3.4 Isometric Immersions with a Periodic Profile

In this section we extend the periodic isometric immersions in the FvK ansatz created in section 2.4.3 to create exact isometric immersions with a periodic profile. The key to this construction will be the existence of a hyperbolic surface that has two asymptotic curves that are straight lines that intersect at the origin of U. Hyperbolic surfaces satisfying this property exist, they are called Amsler surfaces (Bobenko & Eitner, 2000), and form a one parameter family of surfaces $\mathcal{A}_\theta$ that are uniquely determined by the angle θ between the asymptotic lines (Amsler, 1955). As in the construction of surfaces in the FvK ansatz, if the angle θ between the asymptotic lines satisfies $\theta = \frac{\pi}{n}$ we can take the odd periodic extension of the piece of the Amsler surface bounded between the asymptotic lines and form a periodic profile with n waves. We call the surfaces constructed in this manner **periodic Amsler surfaces** .

3.4.1 Construction of Periodic Amsler Surfaces

The generating angle for the C-net of an Amsler surface is found by the similarity transformation $z = 2\sqrt{uv}$, $\varphi(z) = \phi(u, v)$ which transforms (3.1.3) into a Painlevé III equation in trigonometric form:

$$\varphi''(z) + \frac{1}{z}\varphi'(z) - \sin(\varphi(z)) = 0, \tag{3.4.1}$$

where $'$ denotes differentiation with respect to z (Amsler, 1955; Bobenko & Eitner, 2000). By imposing the initial conditions $\varphi(0) = \frac{\pi}{n}$ and $\varphi'(0) = 0$ solutions to (3.4.1), denoted by $\varphi_n(z)$, generate surfaces such that the u and v axis in $\mathcal{D}$ correspond to the asymptotic lines of the surface. Moreover, the asymptotic lines intersect at the origin at an angle $\varphi_n(0) = \frac{\pi}{n}$ and the angle between the coordinate curves along the lines $u = 0$ and $v = 0$ is given by $\varphi_n(0) = \frac{\pi}{n}$ as well.

To generate the parametrization $\mathbf{x} : \mathcal{D} \to \mathbb{R}^3$ from the generating angle ϕ, one could use the Frenet-Serret formulas to relate the second fundamental form and tan-

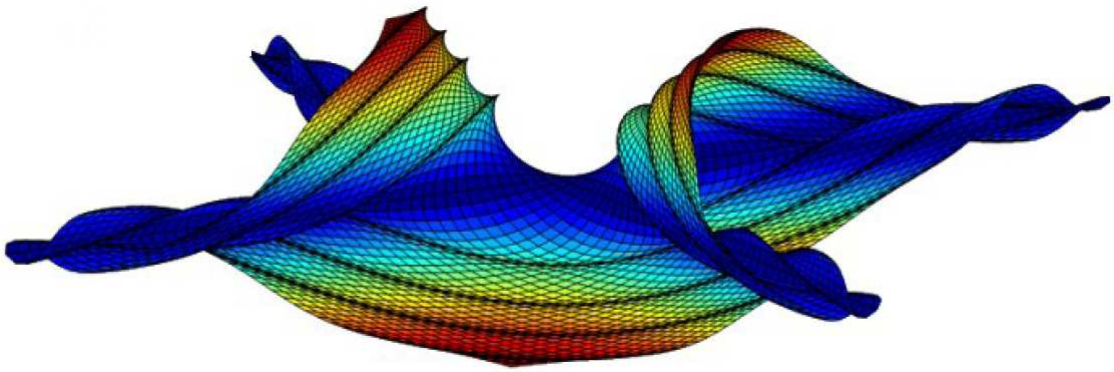

FIGURE 3.8. Amsler surface with a C-net parametrization. This surface is not in fact a true Amsler surface but is a discrete Amsler that is generated by a discretization of the sine-Gordon equation (Bobenko & Pinkall, 1999).

gent vectors to the asymptotic curves and numerically solve the resulting differential equation (Amsler, 1955). Unfortunately, this direct approach is numerically unstable. Instead, a theory of discrete surfaces of constant negative Gaussian curvature has been developed that naturally discretizes a surface from its C-net that is numerically stable and preserves the intrinsic and extrinsic geometry of the surface (Bobenko & Pinkall, 1999). In this method, if the parametrization $\mathbf{x}$ is discretized by $F : \mathbb{Z}^2 \to \mathbb{R}^3$ then

$$F_{i+1,j} - F_{i,j} = N_{i+1,j} \times N_{i,j} \tag{3.4.2}$$

$$F_{i,j+1} - F_{i,j} = -N_{i,j+1} \times N_{i,j}, \tag{3.4.3}$$

where $N_{i,j}$ is the normal to the surface at the lattice point $\{i, j\}$. The normals are then determined by the following relationship

$$N_{i,j+1} = -N_{i+1,j} + \frac{< N_{i+1,j}, N_{i,j} + N_{i+1,j+1} >}{1 + < N_{i,j}, N_{i+1,j+1} >}(N_{i,j} + N_{i+1,j+1}), \tag{3.4.4}$$

where $< \cdot, \cdot >$ denotes the standard Euclidean product in $\mathbb{R}^3$.

To construct a discrete Amsler surface for the quadrant $u > 0$ and $v > 0$ we use a lattice $\{i, j\}$ in which $\{i, 1\}$ corresponds to the u-axis and $\{1, j\}$ corresponds to the v-axis. Furthermore, we assume a uniform spacing δ between lattice points.

Now, since the u and v axis are mapped to lines in $\mathbb{R}^3$ we have the following initial conditions

$$N_{1,1} = (0,0,1) \tag{3.4.5}$$

$$F_{i,1} = (\delta \cdot i, 0, 0) \tag{3.4.6}$$

$$F_{1,j} = (\delta \cdot j \cos(\pi/n), \delta \cdot j \sin(\pi/n), 0). \tag{3.4.7}$$

Furthermore, by the Weingarten equations (A.5.3) and the fact that $\mathbf{x}(u,0) = (u,0,0)$ and $\mathbf{x}(0,v) = (\cos(\pi/n)v, \sin(\pi/n)v, 0)$ it follows that

$$\left.\frac{\partial \mathbf{N}}{\partial u}\right|_{v=0} = \frac{1}{\sin\left(\frac{\pi}{n}\right)} \left.\frac{\partial \mathbf{x}}{\partial v}\right|_{v=0} \tag{3.4.8}$$

$$\left.\frac{\partial \mathbf{N}}{\partial v}\right|_{v=0} = \frac{1}{\sin\left(\frac{\pi}{n}\right)} \left.\frac{\partial \mathbf{x}}{\partial u}\right|_{u=0}. \tag{3.4.9}$$

Therefore,

$$\left\|\frac{\partial \mathbf{N}}{\partial u}\right\|_{v=0} = \frac{1}{\sin(\pi/n)} \text{ and } \left\|\frac{\partial \mathbf{N}}{\partial v}\right\|_{u=0} = \frac{1}{\sin(\pi/n)} \tag{3.4.10}$$

Consequently, initial conditions for the normal can be specified:

$$\begin{aligned} N_{i,1} &= \left(0, -\sin\left(\tfrac{1}{\sin(\pi/n)}\right), \cos\left(\tfrac{1}{\sin(\pi/n)}\right)\right) \delta \cdot i \\ N_{1,j} &= \left(-\sin\left(\tfrac{\pi}{n}\right)\sin\left(\tfrac{1}{\sin(\pi/n)}\right), \cos\left(\tfrac{\pi}{n}\right)\sin\left(\tfrac{1}{\sin(\pi/n)}\right), \cos\left(\tfrac{1}{\sin(\pi/n)}\right)\right) \delta \cdot j. \end{aligned} \tag{3.4.11}$$

Therefore, equations (3.4.3-3.4.4) along with the initial conditions (3.4.6-3.4.7) and (3.4.11) form a complete system of equations that can be solved by "stair casing" from the lattice point $i = 1, j = 1$. In figure 3.8 we plot a discrete Amsler surface generated by this algorithm. A periodic Amsler surface can then be constructed by periodic reflecting the piece of the surface bounded between the lines $u = 0$ and $v = 0$ as we did in section 2.4.3. In figure 3.9 we plot these surfaces.

3.4.2 Maximum Radius of Periodic Amsler Surfaces

As in the case with the pseudosphere, the Amsler surfaces become singular when $\varphi_n(z) = n\pi$. In figure 3.10 we plot φ_n versus z which indicates that $\varphi^{-1}(\pi)$ grows

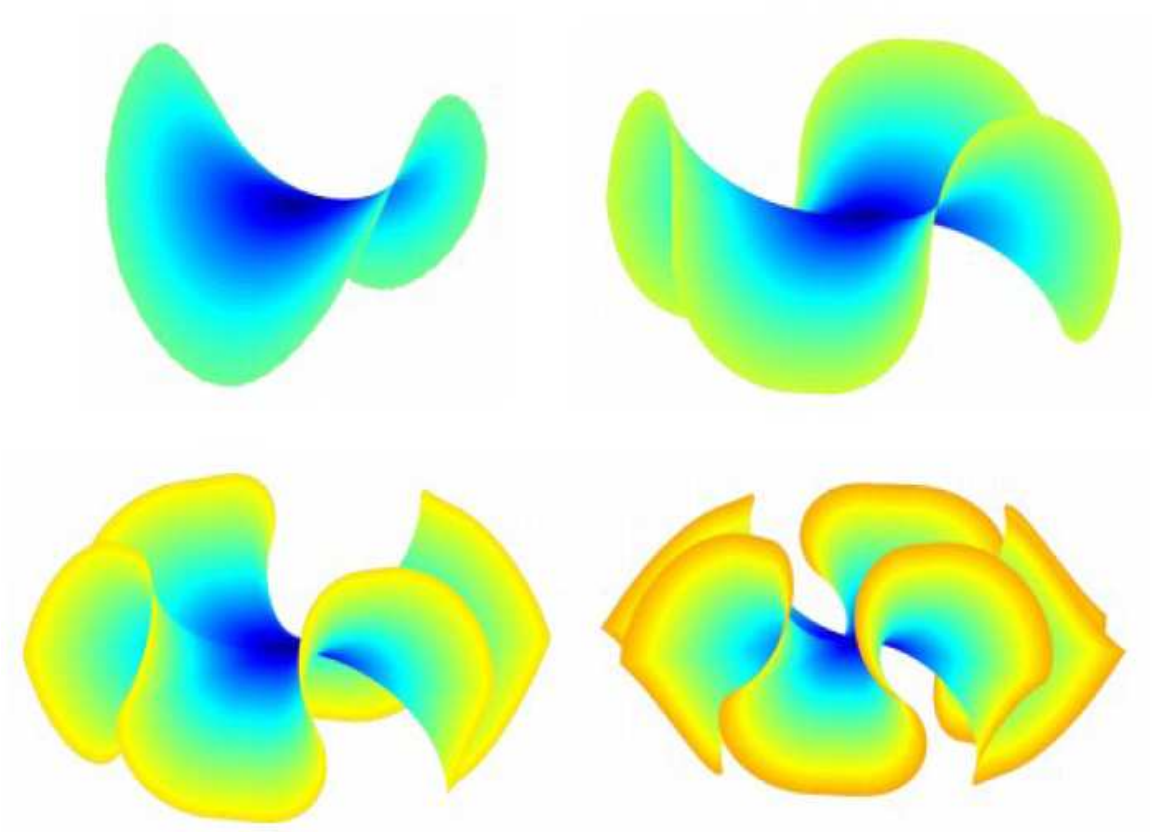

FIGURE 3.9. Periodic Amsler surfaces with $n = 2, 3, 4$ and 5 waves respectively. These surfaces are not drawn to scale, but are close to the maximum radii presented in figure **??**. The coloring of the disks corresponds to contours of arclength data and indicate how the different geodesic circles cut from these surfaces would appear. These surfaces are in fact not true Amsler surfaces but are discrete Amsler surfaces creating using the algorithm presented in Bobenko & Pinkall (1999).

approximately logarithmically with increasing n. The following proposition makes this scaling precise.

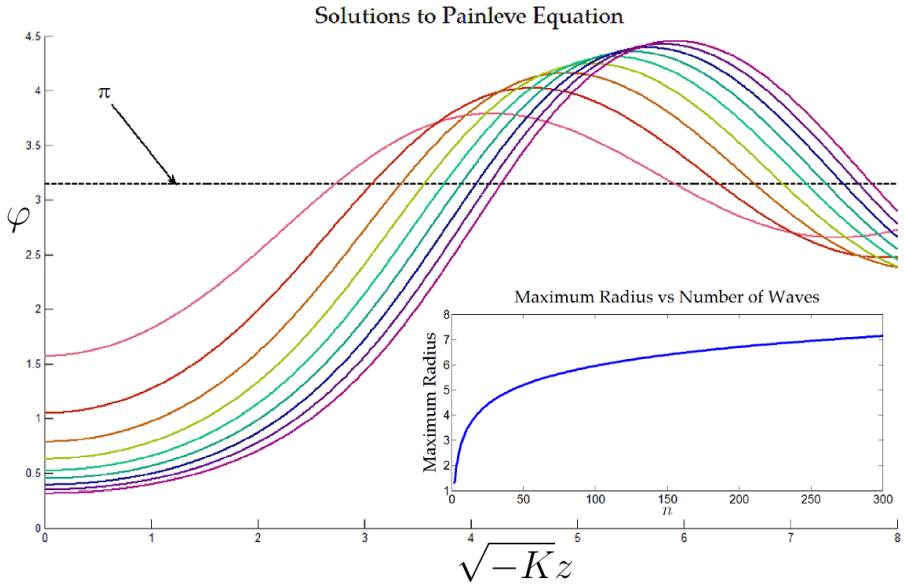

FIGURE 3.10. A plot of φ versus r satisfying the initial conditions $\varphi(0) = \pi/n$ for $n = 2, \ldots 10$. The dashed horizontal line corresponds to where $\varphi(r) = \pi$. At this point a principal curvature diverges and by choosing a higher value of n a larger disk can be created. The inset plot illustrates how the maximum radius scales with n. We can see that the radius grows very slowly with n and it looks to be growing approximately at a logarithmic rate.

Proposition 3.4.1.

$$\ln\left(\cot\left(\frac{\pi}{4n}\right)\right) \leq \varphi_n^{-1}(\pi). \tag{3.4.12}$$

Proof. Multiplying equation (3.4.1) by $\varphi'(z)$ we get that

$$\frac{1}{2}\frac{d(\varphi')^2}{dz} = -\frac{d\varphi}{dz}\frac{d\cos(\varphi)}{d\varphi} - \frac{1}{z}\varphi'(z)^2 \leq -\frac{d\cos(\varphi)}{dz}.$$

Integrating, and assuming $\varphi'(0) = 0$ and $\varphi(0) = \pi/n$, we have that

$$\frac{1}{2}(\varphi')^2 = \frac{1}{2}\int_0^z \frac{d}{dz}(\varphi'(z))^2 dz \leq -\int_0^z \frac{d}{dz}\cos(\varphi)dz = \cos(\pi/n) - \cos(\varphi).$$

and therefore it follows that

$$\int_{\pi/n}^{\pi} \frac{d\varphi}{\sqrt{2(1-\cos(\varphi))}} \leq \int_{\pi/n}^{\pi} \frac{d\varphi}{\sqrt{2(\cos(\pi/n)-\cos(\varphi)}} \leq \varphi_n^{-1}(\pi).$$

Therefore,

$$\ln\left(\cot\left(\frac{\pi}{4n}\right)\right) \leq \varphi_n^{-1}(\pi).$$

□

The geodesic equations (3.1.7) for geodesics starting at the origin with corresponding angle function $\varphi_n(z)$ take the form:

$$\begin{aligned} \tfrac{d^2u}{dt^2} + \tfrac{1}{\sqrt{uv}}\tfrac{d\varphi_n}{dz}\left(\cot(\varphi_n)v\left(\tfrac{du}{dt}\right)^2 - \csc(\varphi_n)u\left(\tfrac{dv}{dt}\right)^2\right) = 0, \\ \tfrac{d^2v}{dt^2} + \tfrac{1}{\sqrt{uv}}\tfrac{d\varphi_n}{dz}\left(\cot(\varphi_n)u\left(\tfrac{dv}{dt}\right)^2 - \csc(\varphi_n)v\left(\tfrac{du}{dt}\right)^2\right) = 0, \end{aligned} \tag{3.4.13}$$

with initial conditions $u(0) = v(0) = 0$, $\frac{du}{dt}(0) = \cos(\psi)$, and $\frac{dv}{dt}(0) = \sin(\psi)$ for $\psi \in [0, \pi/2]$. As expected, the differential equations are singular on the curve $\varphi_n^{-1}(\pi)$ which can be found by numerically solving (3.4.1). Once the singular curve is determined we can calculate the maximum radius of a periodic Amsler surface with n waves by determining the shortest geodesic that intersects the singular curve. Now, it follows from proposition 3.4.1 that by adding more waves this singular curve can be arbitrarily far from the origin. Thus we have the following proposition.

Proposition 3.4.2. Let D be a disk of radius R in the hyperbolic plane. There exists a $W^{2,2}$ isometric immersion $\mathbf{x} : D \to U \subset \mathbb{R}^3$ such that U is a subset of a periodic Amsler surface.

Proof. The same argument used to prove (3.4.1) implies that $\lim_{n\to\infty} \varphi_n^{-1}(\pi/2) = \infty$. Now, let $\alpha(t) = \mathbf{x}((u(t), v(t)))$ be a geodesic lying on a periodic Amsler surface with generating angle $\theta = \pi/n$. Suppose $\alpha(t)$ starts at the origin and travels to the curve $\sqrt{v} = \dfrac{\varphi_n^{-1}(\pi/2)}{2\sqrt{u}}$ terminating at the point (u_f, v_f) and without loss of generality assume that $u(t)$ is a function of $v(t)$. Then, the arclength of $\alpha(t)$ satisfies:

$$d(0,(u_f,v_f)) = \int_0^{u_f} \sqrt{1 + 2\cos(\varphi)\frac{du}{dv} + \left(\frac{du}{dv}\right)^2}\, dv > \int_0^{u_f} dv = u_f. \tag{3.4.14}$$

Thus, since $u_f \to \infty$ as $n \to \infty$ it follows that

$$\lim_{n\to\infty} (0, (u_f, v_f)) = \infty.$$

□

3.4.3 Elastic Energy of Periodic Amsler Surfaces

To compute the elastic energy using equation (3.1.8) we need to determine the dependence of u and v on r and Ψ. Let j_1 and j_2 denote unit vectors in the $u-v$ plane that are aligned with the u and v axis respectively. If we let $\mathbf{x}$ denote the parameterization of the Amsler surface, then the pushforward or differential of $\mathbf{x}$, denoted $\mathbf{x}_*$, is a linear map. Furthermore, since $\mathbf{x}$ is an isometry and the images of j_1 and j_2 under $\mathbf{x}_*$ make an angle of π/n we have without loss of generality that

$$\mathbf{x}_* j_1 = e_1 \text{ and } \mathbf{x}_* j_2 = \cos(\pi/n)e_1 + \sin(\pi/n)e_2, \tag{3.4.15}$$

where e_1 and e_2 are the standard basis elements for the tangent plane at $\mathbf{x}(0,0)$. Consequently, if we let $\alpha(t) = (u(t), v(t))$ be a geodesic defined in the $u-v$ plane satisfying $\alpha'(0) = \cos(\psi)j_1 + \sin(\psi)j_2$ then by linearity we have that

$$\mathbf{x}_*(\alpha'(0)) = (\cos(\theta) + \sin(\theta)\cos(\pi/n))\, e_1 + \sin(\theta)\sin(\pi/n)e_2. \tag{3.4.16}$$

Therefore, we can conclude that the polar angle Ψ for this geodesic is given by

$$\Psi = \arctan\left(\frac{\sin(\psi)\sin(\pi/n)}{\cos(\psi) + \sin(\psi)\cos(\pi/n)}\right). \tag{3.4.17}$$

Now, we can numerically integrate the elastic bending energy for the periodic Amsler surfaces. First, by specifying Ψ and numerically solving (3.4.17) for ψ we can generate initial conditions for equations (3.4.13) which can then be numerically solved to determine $u(t)$ and $v(t)$. Then, by fixing r and numerically solving the arclength equation

$$r = \int_0^T \sqrt{\left(\frac{du}{dt}\right)^2 + 2\cos(\varphi)\frac{du}{dt}\frac{dv}{dt} + \left(\frac{dv}{dt}\right)^2}\, dt, \tag{3.4.18}$$

for T we can calculate the values $u(T)$ and $v(T)$ which correspond to the coordinates (Ψ, r). Finally by setting up a mesh on the rectangle $(\Psi, r) \in [0, 2\pi] \times [0, R]$ and using the above process to determine u and v we can numerically integrate equation (3.1.8).

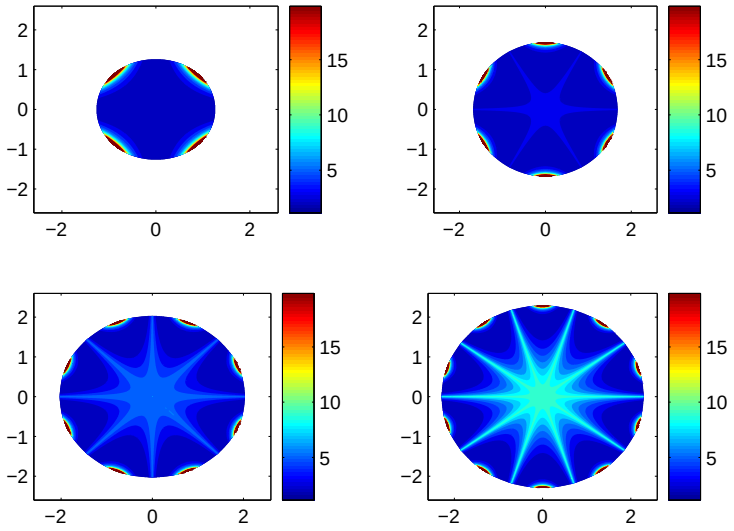

FIGURE 3.11. A representation of the geodesic disks cut out of Amsler surfaces with $n = 2, \ldots, 5$ waves colored by $k_1^2 + k_2^2$ in which the radius and polar angle correspond to the geodesic radius r and polar angle Ψ. These disks each have a maximum radii of $R = 1.2654, 1.8505, 2.2342, 2.5199$ beyond which one of the principal curvatures diverges. The energy of these disks is concentrated in small regions near the singular edge of the disk.

In figure 3.11 we plot the contour data of $k_1^2 + k_2^2$ in geodesic polar coordinates for periodic Amsler surfaces. The radius of the disk is chosen to be near the critical value where the immersions fails to be smooth. We can see that the bending energy is concentrated in small regions near this singular edge. Moreover, for small radii we can see that $k_1^2 + k_2^2$ is approximately constant. In this region of the disk, the quantity $k_1^2 + k_2^2$ is well approximated by the corresponding term $\left(\frac{\partial^2 \eta}{\partial x^2}\right)^2 + \left(\frac{\partial^2 \eta}{\partial y^2}\right)^2$ in the FvK ansatz. Therefore, Amsler surfaces are indeed the natural extensions of the periodic

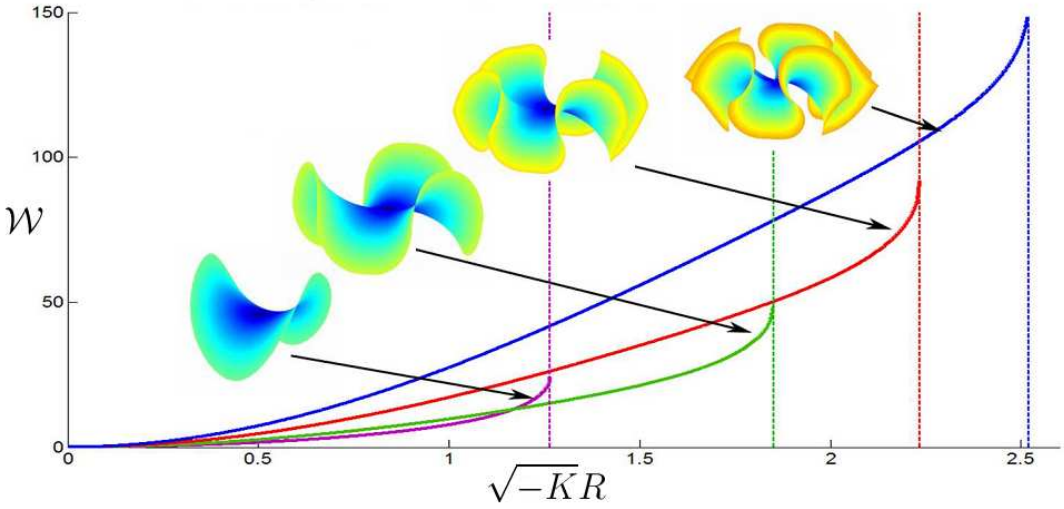

FIGURE 3.12. The scaled bending energy of periodic Amsler surfaces with $n = 2, \ldots, 5$ waves plotted versus geodesic radius. We can see that these disks have lower energy than there counterparts lying in the hyperboloid of revolution. Moreover, the The vertical dashed lines correspond to the radius where the surface with n waves can no longer be isometrically embedded.

surfaces constructed in section 2.4.3.

In figure 3.12 we plot the Willmore energy of periodic Amsler surface. These periodic Amsler surfaces have a lower Willmore energy than the smooth immersions given by subsets of the pseudosphere and hyperboloids of revolution with constant Gaussian curvature. Furthermore, we can see that for each $n \geq 2$, there is a radius $R_n \sim \log(n)$ such that the n-periodic Amsler surfaces only exist for a radius $0 < R < R_n$. This gives a natural mechanism for the refinement of the wavelength of the buckling pattern with increasing radius of the disk.

Chapter 4

Conclusion

Free non-Euclidean elastic sheets arise in a variety of physical and biological systems. The morphology of these sheets is usually modelled as the equilibrium deformations for an appropriate elastic energy. One approach is to model the sheet as a Riemannian manifold $(\mathcal{D}_{3d}, \mathbf{g}_{3d})$ with a prescribed metric $\mathbf{g}_{3d}$, which is then used to define strains and hence an elastic energy for a configuration.

In this dissertation we presented a study of two reduced theories of non-Euclidean sheets, the Föppl-von Kármán and Kirchhoff models, for metrics with constant negative Gaussian curvature K_0. Specifically, to obtain a better understanding of the morphology of swelling hydrogels (Klein et al., 2011), we focused on radially symmetric domains and deformations with a periodic profile with n waves.

4.1 Discussion of Results from the FvK Model

In the FvK approximation, we proved that global minimizers of the bending energy over the set of isometric immersions in the FvK ansatz are given by a quadratic saddle $\eta = xy$. We thus expect that, with decreasing thickness, the configuration of the sheet will converge to a two wave profile. This is not what is observed experimentally, where the number of waves increases with decreasing thickness (Klein et al., 2011). Consequently, the physically realized configurations *are not* given by the global minimizers of this model energy. Note however, that the periodic, non-smooth profiles that we construct in section 2.4.3 do agree qualitatively, and in scaling behavior, with the experimental observations. This is surprising since these periodic, non-smooth profiles *are not* global minimizers of the energy, and we need a different selection mechanism if these profiles do indeed represent the experimental configurations.

The second main result from chapter 2 is theorem 2.6.6, which gives rigorous upper and lower bounds for the elastic energy of minimizing deformations. This theorem allows us to construct regions in the $\tau - n$ plane in which minimizers of the elastic energy with n-waves behave either like a flat deformation or an isometric immersion. The critical thickness t^* in which an $n-$periodic deformation transitions from a flat deformation into an approximate $n-$periodic isometric immersion scales like $t^* \sim \sqrt{-K_0}R^2 n^{-1/2}$. Moreover, theorem 2.6.6 allows us to prove quantitatively in the FvK ansatz that there can be no refinement with decreasing thickness of the number of waves for a sequence of minimizing deformations.

The third main result from chapter 2 is the scaling with τ of the width of boundary layers in which stretching energy is concentrated. In these localized regions of stretching, the total elastic energy of an isometric immersion is lowered by allowing some stretching to reduce the bending energy. Near the edge of the annulus the contributions to the bending energy coming from the Gaussian and mean curvatures is reduced in overlapping boundary layers that scale with the thickness like $t^{1/2}|K_0|^{-1/4}$. Furthermore, for $n \geq 3$ boundary layers form along the lines of inflection in which the mean curvature of an isometric immersion is reduced by removing a jump discontinuity in the curvature along the azimuthal direction. The width of these boundary layers scales with the radius and thickness like $\rho^{1/3}t^{1/3}|K_0|^{-1/6}$.

It is important to note that the FvK elastic energy is valid in an asymptotic limit in which the metric becomes increasingly flat with decreasing thickness, that is $\epsilon \sim t/R$. In this dissertation we took ϵ fixed and t decreasing and in particular we showed that the energy of minimizers scales like τ^2. Consequently, when $\tau \ll 1$ it is perhaps more appropriate to consider the Kirchhoff model. But, the Kirchhoff model is rigid in the sense that there is no competition between stretching and bending energies and thus there is no possibility of the Kirchohff model alone explaining the refinement of the number of waves with decreasing thickness.

4.2 Discussion of Results from the Kirchhoff Model

In chapter 3 we considered the geometric problem of finding exact $W^{2,2}$ isometric immersions of $\mathbf{g}_{K_0}$. We showed that there exists smooth isometric immersions $\mathbf{x} : \mathcal{D} \to \mathbb{R}^3$ for geodesic disks of arbitrarily large radii. Now, for complete surfaces of constant negative curvature (or surfaces whose curvature is bounded above by a negative constant), Hilbert's theorem (Hilbert, 1901) (resp. Efimov's theorem (Efimov, 1964)) show that there are no analytic (resp. C^2) solutions of $\mathbb{H}^2$ in its entirety. In elucidating the connection between these non-existence results and the existence of isometric immersions for bounded domains, we provided numerical evidence that the maximum principal curvature of such immersions is bounded below by a bound which grows exponentially in $\sqrt{-K_0}R$. This is a geometric feature that is in contrast with the FvK model in which $|D^2\eta|$ does not grow with the size of the domain.

The existence of smooth, and thus also $W^{2,2}$ immersions of arbitrarily large disks have consequences for the modeling of free non-Euclidean sheets. In particular, the mid-surface of minimizers for the three dimensional elastic energy E_{3d} must converge as $t \to 0$ to a minimizer of E_{Ki} (Lewicka & Pakzad, 2011). This is again an apparent contradiction with experimental observations where the bending energy of the minimizer scales with the thickness t and is well fit by a power law, t^{-1}, which diverges as $t \to 0$ (Klein et al., 2011).

The smooth immersions $\mathbf{x} : D_R \to \mathbb{R}^3$ constructed in sections 3.2 and 3.3 do not have the rotational n-fold symmetry ($\Psi \to \Psi + 2\pi/n$ for the geodesic polar angle Ψ) of the underlying energy functional, which is also seen in the experimentally observed configurations. In section 3.4 we generalize the construction of the non-smooth, n-periodic isometric immersions in the linearized geometry constructed in section 2.4.3 to construct exact $W^{2,2}$ isometric immersions which are also non-smooth and have the same symmetry/morphology as the experimentally observed configurations. These periodic Amsler surfaces *have lower bending energy* than the smooth immersions given

by subsets of the pseudosphere and hyperboloids with constant negative curvature.

For each $n \geq 2$, there is a radius $R_n \sim \log(n)$ such that the n-periodic Amsler surfaces only exist for a radius $0 < R < R_n$. This gives a natural mechanism for the refinement of the wavelength of the buckling pattern with increasing radius of the disk. However, it does not, at least directly, explain the observed refinement with decreasing thickness.

4.3 Future Directions

From this work and it is clear that the FvK and Kirchhoff models of non-Euclidean elasticity cannot completely explain the periodic shapes in experiments. The periodic shapes we have constructed in both the FvK and Kirchhff models are qualitatively similar to the experimental shapes but are only local minimizers of the FvK energy. A major goal of future works is to connect the existence of these local minimizers to the observed patterns in experiments. Below we discuss a short list of mathematical questions and avenues for future research that could shed light on these issues.

1. The exact isometric immersions with a periodic profile constructed in section 4.3 are similar to the n-periodic isometric immersions in the FvK approximation but have highly localized regions of bending energy near the edge of the disk and along the lines of inflection. Therefore, in these regions, as in the boundary layers in the FvK ansatz, it is conceivable that it would be energetically favourable to allow some stretching to reduce this localized bending energy. These observations illustrate the multiple scale behavior of this problem and it may be more appropriate to consider a combination of different reduced theories in various regions of the domain. A hierarchy of such reduced theories has recently been conjectured to exist and further research in this direction may explain the complex morphologies of non-Euclidean plates (Lewicka et al., 2011).

2. The periodic shapes in swelling hydrogels are the result of dynamical processes. It may be more appropriate to model this type of differential growth dynamically, perhaps as a gradient flow of the elastic energy. The pattern could then be selected for dynamical reasons and not by global minimization of an energy functional. This might explain why local but not global extrema for the energy functional seem to describe the observed patterns.

3. Chebyshev nets give a natural discretization of surfaces with constant negative curvature that respects both the intrinsic and the extrinsic geometry of the surface. This idea has already been used for constructing discrete isometric immersions (K-surfaces) for such surfaces (Bobenko & Pinkall, 1999). Developing a numerical methods for minimizing the variational problem exploiting this structure could increase our understanding of the complex interaction between geometry and elasticity.

4. Our results in chapter 3 strongly use the fact that the target metric on the surface has constant negative curvature, which then allows us to naturally associate a Chebyshev net with each isometric immersion through an asymptotic parameterization (Gray et al., 2006). However, we believe that our results, in particular the lower bound for the maximum principal curvature (3.3.5), and the construction of $C^{1,1}$ and piecewise smooth isometric immersions can also be extended to other target metrics whose curvature is bounded above by a negative constant. It is natural to study these questions, in particular the difference between smooth and $C^{1,1}$ immersions using the ideas in Chen et al. (2010).

5. For the periodic Amsler surfaces in section 4.3, the global structure, *i.e.* the number n of waves is determined by the local structure at the origin. The origin is a *bifurcation point* for the Chebyshev net induced by the immersion in the sense that, every point in the complement of the origin has precisely

two asymptotic directions, while the origin has n asymptotic directions with $n > 2$ (Burago et al., 2005). For surfaces whose total positive curvature is bounded by 2π, it is always possible to find a global Chebyshev net, except it can have multiple bifurcation points (Burago et al., 2005). This suggests the following natural questions: Are there non-smooth immersions ($C^{1,1}$ or even $W^{2,2}$ immersions) with multiple bifurcation points?

Appendix A

Differential Geometry of Surfaces

Here we place in one location the definitions and equations from the elementary differential geometry of surfaces that are relevant to this dissertation. The material presented here is a survey of some of the standard results from the classical theory of surfaces and is compiled from Spivak (1979), McCleary (1995), Lee (1997), Frankel (2003), and Gray et al. (2006). For a more complete understanding of this material the reader is encouraged to obtain these references.

In this appendix and in some locations in this dissertation we make use of the so called Einstein summation convention of summation over repeated indices. That is, for any duplicate occurrence of a superscript and a subscript summation over these indices is implied. For example,

$$\begin{aligned} v_i v^i &= \sum_i v_i v^i, \\ v_{ij} v^{ik} &= \sum_i v_{ij} v^{ik}, \\ v_{ij} v^{ij} &= \sum_i \sum_j v_{ij} v^{ij}. \end{aligned}$$

A.1 Tangent and Normal Vectors to a Surface

Let $\mathbf{x} : \mathcal{D} \to \mathbb{R}^3$ be a **local parametrization** of a surface S, with parametrization variables (u, v). That is, as a vector valued function in $\mathbb{R}^3$ we have that

$$\mathbf{x}(u, v) = (\mathbf{x}_1(u, v), \mathbf{x}_2(u, v), \mathbf{x}_3(u, v)) . \tag{A.1.1}$$

In the terminology of continuum mechanics the variables (u, v) are called the **material coordinates** . For fixed v_0 or fixed u_0 the curves $u \to \mathbf{x}(u, v_0)$ and $v \to \mathbf{x}(u_0, v)$ form

the **coordinate curves** on the surface. At a fixed point $P \in S$ the vectors $\frac{\partial \mathbf{x}}{\partial u}$ and $\frac{\partial \mathbf{x}}{\partial v}$ are tangential to the surface and lie in the directions of the coordinate curves. Thus if the surface is regular the vectors $\frac{\partial \mathbf{x}}{\partial u}$ and $\frac{\partial \mathbf{x}}{\partial v}$ form a basis for the tangent plane T_pS and there exists a unit normal vector that can be defined from the structure of $\mathbb{R}^3$:

$$\mathbf{N} = \frac{\frac{\partial \mathbf{x}}{\partial u} \times \frac{\partial \mathbf{x}}{\partial v}}{\left\| \frac{\partial \mathbf{x}}{\partial u} \times \frac{\partial \mathbf{x}}{\partial v} \right\|}. \tag{A.1.2}$$

Remark A.1.1. In instances where summation over the coordinates is needed we will use the variables (u^1, u^2) to denote the parametrization variables.

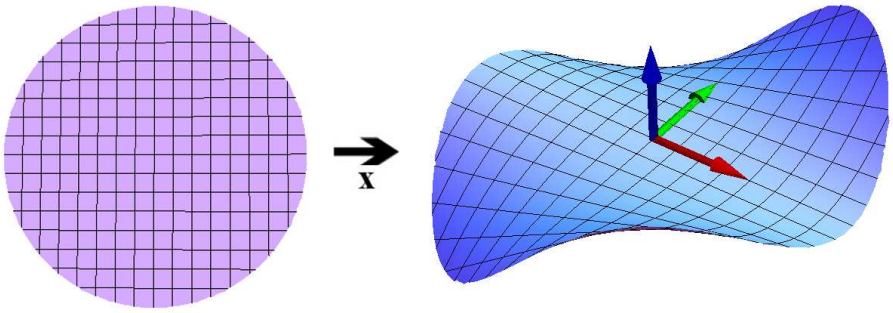

FIGURE A.1. A surface parametrized by a map $\mathbf{x}(u, v) \to \mathbb{R}^3$. The black curves are the coordinate curves on the surface. The green and red arrows illustrate tangent vectors in the direction of the coordinate curves and the blue arrow corresponds to the normal vector to the surface.

A.2 First Fundamental Form and the Induced Riemannian Metric

The **first fundamental form** or the **induced Riemannian metric** $\mathbf{g}$ (classically written as $\mathbf{I}$) is a symmetric positive definite tensor $\mathbf{g} : T_pS \times T_pS \to \mathbb{R}$ defined by

$$\mathbf{g}(\mathbf{v}, \mathbf{w}) \;=\; \mathbf{v} \cdot (\nabla \mathbf{x})^T \cdot \nabla \mathbf{x} \cdot \mathbf{w}^T.$$

As the following calculations show, the metric encodes how the mapping $\mathbf{x}$ distorts lengths, angles, and areas:

1. Let $\alpha : [a, b] \to \mathcal{D}$ be a differentiable curve. The length $L(\alpha)$ of the image of the curve on S can be found from the chain rule:

$$\begin{aligned} L(\alpha) &= \int_a^b \sqrt{\frac{d\mathbf{x}(\alpha(s))}{ds} \cdot \frac{d\mathbf{x}(\alpha(s))}{ds}} ds = \int_a^b \sqrt{\frac{d\alpha}{ds} \cdot (\nabla \mathbf{x})^T \cdot \nabla \mathbf{x} \cdot \left(\frac{d\alpha}{ds}\right)^T} ds \\ &= \int_a^b \sqrt{\mathbf{g}\left(\frac{d\alpha}{ds}, \frac{d\alpha}{ds}\right)} ds. \end{aligned}$$

2. Let $\alpha, \beta : [a, b] \to \mathcal{D}$ be differentiable curves with unit speed whose images on S intersect at a point $P \in S$. The angle θ between the curves at this intersection point can be calculated:

$$\cos(\theta) = \frac{\partial \mathbf{x}(\alpha(s))}{ds} \cdot \frac{\partial \mathbf{x}(\beta(s))}{ds} = \frac{d\alpha}{ds} \cdot (\nabla \mathbf{x})^T \cdot \nabla \mathbf{x} \cdot \left(\frac{\partial \alpha}{ds}\right)^T = \mathbf{g}\left(\frac{d\alpha}{ds}, \frac{d\beta}{ds}\right).$$

3. The area $A(\mathbf{x}(\mathcal{D}))$ of the image of $\mathcal{D}$ is given by

$$A(\mathcal{D}) = \int_{\mathcal{D}} \left\| \frac{\partial \mathbf{x}}{\partial u} \times \frac{\partial \mathbf{x}}{\partial v} \right\| dudv. = \int_{\mathcal{D}} \det(\mathbf{g}) dudv = \int_{\mathcal{D}} dA_{\mathbf{g}}, \tag{A.2.1}$$

where the area form $\det(\mathbf{g})dudv = dA_{\mathbf{g}}$.

A.3 Basic Riemannian Geometry

Since the metric $\mathbf{g}$ is coordinate independent and does not depend on the outward normal $\mathbf{N}$, a metric $\mathbf{g}$ can be defined on $\mathcal{D}$ independent of the existence of a corresponding parametrization. A domain $\mathcal{D}$ equipped with a symmetric positive definite tensor $\mathbf{g}$, written $(\mathcal{D}, \mathbf{g})$, is called an **abstract surface** or more generally a two dimensional **Riemannian manifold**. On a Riemmanian manifold the notions of the length of a curve, angle between vectors, and area can be defined in terms of $\mathbf{g}$ by

taking items 1-3 above as definitions. Additional, a Riemannanian $(\mathcal{D}, \mathbf{g})$ is a metric space with the **distance function** $d : \mathcal{D} \times \mathcal{D} \to \mathbb{R}$ defined by

$$d(p, q) = \inf\{L(\alpha) : \alpha \text{ is a piecewise smooth curve in } \mathcal{D} \text{ joining } p \text{ and } q\}. \quad \text{(A.3.1)}$$

The metric also allows us to identify when two abstract manifolds have the same intrinsic geometric properties by defining two manifolds $(\mathcal{D}_1, \mathbf{g}_1)$ and $(\mathcal{D}_2, \mathbf{g}_2)$ to be **isometric** if there exists a diffeomorphism $f : \mathcal{D}_1 \to \mathcal{D}_2$ such that $\mathbf{g}_1(u, v) = \mathbf{g}_2(f(u, v), f(u, v))$. The mapping f is called an **isometry**. An **isometric invariant** is any quantity that is preserved by an isometry. Examples of isometric invariants are length, area, and angle. An **isometric immersion** of a Riemannian manifold $(\mathbf{x}, \mathcal{D})$ is a mapping $\mathbf{x} : \mathcal{D} \to \mathbb{R}^3$ such that the induced Riemmanian metric $(\nabla\mathbf{x})^T \cdot \nabla\mathbf{x}$ satisfies $(\nabla\mathbf{x})^T \cdot \nabla\mathbf{x} = \mathbf{g}$.

Also, the Riemannian metric creates a richer structure on a manifold by allowing one to define the notion of an inner product $< \cdot, \cdot >: T_p\mathcal{D} \times T_p\mathcal{D} \to \mathbb{R}$ by:

$$< \mathbf{v}, \mathbf{w} >= \mathbf{g}(\mathbf{v}, \mathbf{w}) = \mathbf{v} \cdot \mathbf{g} \cdot \mathbf{w}^T.$$

Therefore, if we fix a vector $\mathbf{v} \in T_p\mathcal{D}$ we can naturally associate a covector in $T_p^*\mathcal{D}$, where $T_p^*\mathcal{D}$ is the dual space of $T_p\mathcal{D}$, to $\mathbf{v}$ by

$$\mathbf{v} \to < \mathbf{v}, \cdot > .$$

If we let $\mathbf{e}_i$ denote a basis for the tangent plane and $\mathbf{e}^j$ it corresponding dual basis, that is $\mathbf{e}^j(\mathbf{e}_i) = \delta_i^j$, then the components v_i of the covector associated with $\mathbf{v}$ can be found by a simple calculation:

$$v_i = g_{ij}v^j,$$

which we call the **covariant components of the contravariant vector v**. If we now denote the components of the matrix $\mathbf{g}^{-1}$ by g^{ij} we then have that

$$v^i = g^{ij}v_i.$$

Therefore, the metric $\mathbf{g}$ allows one to naturally associate covectors and vectors and thus identifies the tangent and cotangent planes of the Riemannian manifold. The process of using $\mathbf{g}$ to convert a vector into a covector and vice versa is colloquially called "lowering" and "raising" indices and can be applied to higher order mixed tensors as well.

Another key property of Riemannian manifolds is that it allows one to identify rank two tensors with linear transformations, which is important if we want to make meaningful definitions of quantities such as the determinant and trace of a tensor. To show this identification we will first show that rank two mixed tensors can be identified with linear transformations. Let E be a vector space, E^* its dual space and $A : E \to E$ a linear transformation. We can define a mixed tensor $W_A : E^* \times E \to \mathbb{R}$ by $W_A(\alpha, A(\mathbf{v})) = \alpha(\mathbf{v})$. If we let $\mathbf{e}_i$ denote a basis for E and $\mathbf{e}^j$ its corresponding dual basis for E^* then in components

$$W_A{}^i_j = W_A(\mathbf{e}^i, \mathbf{e}_j) = \mathbf{e}^i(A(\mathbf{e}_j)) = \mathbf{e}^i(\mathbf{e}_k A^k_j) = \delta^i_k A^k_j = A^i_j.$$

That is, the components of W_A correspond precisely with the components of A. Conversely, given a mixed tensor $W : A : E^* \times E \to \mathbb{R}$ we define a $A : E^* \times E \to \mathbb{R}$ to be the unique linear transformation such that $W(\alpha, \mathbf{v}) = \alpha(A\mathbf{v})$, where the existence and uniqueness of A follows from the bilinearity of W. Now, in a Riemannian manifold $(\mathcal{D}, \mathbf{g})$ if $W : T^*_p\mathcal{D} \times T^*_p\mathcal{D}$ is a rank two tensor then we can associate it with a mixed tensor by raising its index. The associated mixed tensor has the components

$$W^j_i = g^{ik} W_{kj},$$

from which quantities like the determinant and trace can be calculated.

A.4 Second Fundamental Form and Curvature

The **second fundamental form h** (classically denoted **II**) is the tensor $\mathbf{h} : T_pS \to T_pS$ defined by

$$\mathbf{h}(\mathbf{v}, \mathbf{w}) \;\; = \;\; -\mathbf{v} \cdot (d\mathbf{N})^T \cdot \nabla\mathbf{x} \cdot \mathbf{w}^T.$$

Using the fact that $\mathbf{N} \cdot \frac{\partial \mathbf{x}}{\partial u} = 0$ and $\mathbf{N} \cdot \frac{\partial \mathbf{x}}{\partial v} = 0$ we have that the components of $\mathbf{h}$ satisfy

$$h_{11} = -\frac{\partial \mathbf{N}}{\partial u} \cdot \frac{\partial \mathbf{x}}{\partial u} = \mathbf{N} \cdot \frac{\partial^2 \mathbf{x}}{\partial u^2},$$
$$h_{12} = -\frac{1}{2}\left(\frac{\partial \mathbf{N}}{\partial u} \cdot \frac{\partial \mathbf{x}}{\partial v} + \frac{\partial \mathbf{N}}{\partial v} \cdot \frac{\partial \mathbf{x}}{\partial u}\right) = \mathbf{N} \cdot \frac{\partial^2 \mathbf{x}}{\partial u \partial v},$$
$$h_{22} = -\frac{\partial \mathbf{N}}{\partial v} \cdot \frac{\partial \mathbf{x}}{\partial v} = \mathbf{N} \cdot \frac{\partial^2 \mathbf{x}}{\partial v^2}.$$

To provide a geometric interpretation of $\mathbf{h}$, let $\alpha : [a, b] \to \mathcal{D}$ be a curve such that $\mathbf{x}(\alpha(s))$ defines a unit speed curve C on S with normal $\mathbf{n}$ and tangent vector $\mathbf{t}$ and let (u^1, u^2) denote the parametrization variables. Differentiating, we have that

$$\mathbf{t} = \frac{d\mathbf{x}(\alpha(s))}{ds} = \frac{\partial \mathbf{x}}{\partial u^i}\frac{d\alpha^i(s)}{ds}.$$

Differentiating again and using the fact that curve is unit speed, we have that

$$\kappa\mathbf{n} = \frac{\partial^2 \mathbf{x}}{\partial u^i \partial u^j}\frac{d\alpha^i(s)}{ds}\frac{d\alpha^j(s)}{ds} + \frac{\partial \mathbf{x}}{\partial u^i}\frac{\partial^2 d\alpha^i(s)}{ds},$$

where κ is the curvature of the curve. Now, since $\frac{\partial \mathbf{x}}{\partial u^1}$ and $\frac{\partial \mathbf{x}}{\partial u^2}$ are orthogonal to $\mathbf{N}$ it follows that

$$\kappa\mathbf{N} \cdot \mathbf{n} = \frac{d\alpha(s)}{ds} \cdot D^2\mathbf{x} \cdot \left(\frac{d\alpha(s)}{ds}\right)^T = \mathbf{h}(\mathbf{t}, \mathbf{t}).$$

Now, let $\mathbf{v} \in T_pS$ have unit length and Π be the plane spanned by $\mathbf{v}$ and $\mathbb{N}$. The intersection of Π and S forms a plane curve C on S with a unit tangent vector $\mathbf{v}$ at p and thus

$$\mathbf{h}(\mathbf{v}, \mathbf{v}) = \pm\kappa, \tag{A.4.1}$$

where κ is the plane curvature of C at p. That is $\mathbf{h}(\mathbf{v}, \mathbf{v})$ measures the curvature of S in the direction of $\mathbf{v}$ (see figure A.2). Define the **principal curvatures** of S at p by

$$k_1 = \max_{\|\mathbf{v}\|=1} \mathbf{h}(\mathbf{v}, \mathbf{v}) \text{ and } k_2 = \min_{\|\mathbf{v}\|=1} \mathbf{h}(\mathbf{v}, \mathbf{v}).$$

By compactness there are two vectors that obtain this maximum and minimum and we call them the **principal directions**. Furthermore, since $\mathbf{h}$ is symmetric the following theorem follows from linear algebra:

Theorem A.4.1 (Euler)**.** k_1 and k_2 are the eigenvalues of the linear transformation H corresponding to $\mathbf{h}$ and the principal directions are the eigenvectors. If $k_1 \neq k_2$ then the principal directions are orthogonal.

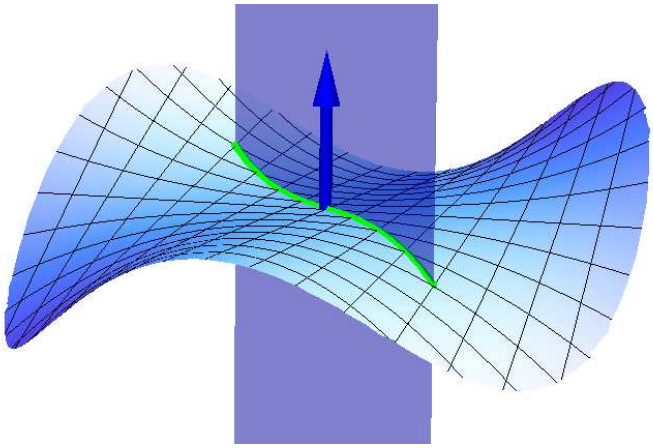

FIGURE A.2. The second fundamental form measures the curvature of the plane curve formed by the intersection of a plane parallel to the unit normal N and a tangent vector.

There are two measures of curvature for a point on a surface that correspond to the two principal invariants of $\mathbf{h}$.

1. The **Gaussian curvature** K is defined by:

$$K = \det(\mathbf{h}) = \det(g^{ij} h_{ik}) = \frac{\det(h_{ij})}{\det(g_{ij})} = k_1 k_2. \tag{A.4.2}$$

2. The **mean curvature** H is defined by:

$$H = \frac{1}{2}\mathrm{tr}(\mathbf{h}) = \frac{1}{2}\mathrm{tr}(g^{ij}h_{jk}) = \frac{1}{2}\left(k_1 + k_2\right). \tag{A.4.3}$$

The Gaussian curvature can be interpreted as follows, if $K > 0$ in the neighborhood of a point the neighborhood is elliptic or bowl shaped while if $K < 0$ the neighborhood is hyperbolic or saddle shaped. The mean curvature is a measure of the bending of the surface and surfaces with $H = 0$ are called **minimal surfaces**.

The definitions of the mean and Gaussian curvature are defined above in terms of the second fundamental form which depends on the normal N and relies on the surface being immersed in $\mathbb{R}^3$. It is a remarkable and surprising fact that the Gaussian curvature can be calculated in terms of $\mathbf{g}$ alone. This was first stated and proved by Gauss in the form of his famous Theorema Egregium (Spivak, 1979).

Theorem A.4.2. (Gauss's Theorema Egregium) The Gauss curvature $K = k_1 k_2$ is an isometric invariant.

This result implies that if a surface is bent without stretching the principal curvatures may change but their product will not. Moreover, this provides a simple necessary condition to check if two surfaces are isometric.

Corollary A.4.3. Isometric surfaces have the same Gaussian curvatures at corresponding points.

The exact formula for the Gaussian curvature in terms of the components of $\mathbf{g}$ is provided by Biroshi's formula:

$$\begin{aligned} K &= \det(g_{ij}) \det \begin{pmatrix} -\frac{1}{2}\frac{\partial^2 g_{11}}{\partial v^2} + \frac{\partial^2 g_{12}}{\partial u \partial v} - \frac{1}{2}\frac{\partial^2 g_{22}}{\partial u^2} & \frac{1}{2}\frac{\partial g_{11}}{\partial u} & \frac{\partial g_{12}}{\partial u} - \frac{1}{2}\frac{\partial g_{11}}{\partial v} \\ \frac{\partial g_{12}}{\partial v} - \frac{1}{2}\frac{\partial g_{22}}{\partial u} & g_{11} & g_{12} \\ \frac{1}{2}\frac{\partial g_{22}}{\partial v} & g_{12} & g_{22} \end{pmatrix} \\ &\quad - \det(g_{ij}) \det \begin{pmatrix} 0 & \frac{1}{2}\frac{\partial g_{11}}{\partial u} & \frac{1}{2}\frac{\partial g_{22}}{\partial u} \\ \frac{1}{2}\frac{\partial g_{11}}{\partial v} & g_{11} & g_{12} \\ \frac{1}{2}\frac{\partial g_{22}}{\partial u} & g_{12} & g_{22} \end{pmatrix}. \end{aligned} \tag{A.4.4}$$

The above equation allows one to define Gaussian curvature K on abstract surfaces regardless if there exists an isometric immersion of the abstract surface into $\mathbb{R}^3$.

A.5 Compatibility Conditions

Let (u^1, u^2) denote the parametrization variables. The **Gauss equations** for a surface are obtained by decomposing $\frac{\partial^2 \mathbf{x}}{\partial u^i \partial u^j}$ into tangential and normal components:

$$\frac{\partial^2 \mathbf{x}}{\partial u^i \partial u^j} = \Gamma_{ij}^k \frac{\partial \mathbf{x}}{\partial u^k} + h_{ij}\mathbf{N}, \tag{A.5.1}$$

where the **Christoffel symbols** Γ_{ij}^k are defined by

$$\Gamma_{jk}^l = \frac{g^{il}}{2}\left(\frac{\partial g_{jl}}{\partial u^k} + \frac{\partial g_{kl}}{\partial u^j} - \frac{\partial g_{ik}}{\partial u^l}\right). \tag{A.5.2}$$

The **Weingarten equations** are

$$\frac{\partial \mathbf{N}}{\partial u^i} = g^{jk} h_{ki} \frac{\partial \mathbf{x}}{\partial u^j}. \tag{A.5.3}$$

From the identities $\frac{\partial^3 \mathbf{x}}{\partial u^i \partial u^j \partial u^k} = \frac{\partial^3 \mathbf{x}}{\partial u^i \partial u^k \partial u^j}$ the following equations - also called the Gauss equations - can be derived:

$$g_{11}K = \frac{\partial \Gamma_{11}^2}{\partial u^2} - \frac{\partial \Gamma_{12}^2}{\partial u^1} + \Gamma_{11}^1\Gamma_{12}^2 + \Gamma_{11}^2\Gamma_{22}^2 - \Gamma_{12}^1\Gamma_{11}^2 - \Gamma_{12}^2\Gamma_{12}^2, \tag{A.5.4}$$

$$g_{22}K = \frac{\partial \Gamma_{22}^2}{\partial u^1} - \frac{\partial \Gamma_{12}^1}{\partial u^2} + \Gamma_{22}^1\Gamma_{11}^1 + \Gamma_{22}^2\Gamma_{12}^1 - \Gamma_{12}^1\Gamma_{12}^1 - \Gamma_{12}^2\Gamma_{12}^1, \tag{A.5.5}$$

$$g_{12}K = \frac{\partial \Gamma_{12}^1}{\partial u^1} - \frac{\partial \Gamma_{11}^1}{\partial u^2} + \Gamma_{12}^2\Gamma_{12}^1 - \Gamma_{11}^2\Gamma_{22}^1, \tag{A.5.6}$$

$$g_{12}K = \frac{\partial \Gamma_{12}^2}{\partial v} - \frac{\partial \Gamma_{22}^2}{\partial u^2} + \Gamma_{12}^1\Gamma_{12}^2 - \Gamma_{22}^1\Gamma_{11}^2. \tag{A.5.7}$$

The **Mainardi-Codazzi equations** follow from the relationship $\frac{\partial \mathbf{N}}{\partial u^i \partial u^j} = \frac{\partial \mathbf{N}}{\partial u^j \partial u^i}$:

$$\frac{\partial h_{11}}{\partial u^2} - \frac{\partial h_{12}}{\partial u^1} = h_{11}\Gamma_{12}^1 + h_{12}\left(\Gamma_{12}^2 - \Gamma_{11}^1\right) - h_{22}\Gamma_{11}^2, \tag{A.5.8}$$

$$\frac{\partial h_{12}}{\partial u^2} - \frac{\partial h_{22}}{\partial u^1} = h_{11}\Gamma_{22}^1 + h_{12}\left(\Gamma_{22}^2 - \Gamma_{12}^1\right) - h_{22}\Gamma_{12}^2. \tag{A.5.9}$$

The equations (A.5.4-A.5.9) are the compatibility conditions for a surface and are necessary and sufficient conditions for the existence of a local parametrization of a surface with first and second fundamental forms $\mathbf{g}$ and $\mathbf{h}$ respectively (Bonnet, 1865).

A.6 Geodesics and Geodesic Polar Coordinates

A geodesic is an extension of the concept of a line to a curved manifold or surface and as such it should retain some familiar properties:

1. A geodesic should be the curve of shortest length between two points.

2. A geodesic should have plane curvature identically zero.

To satisfy item 2, a **geodesic** on a surface S is defined to be a unit speed curve whose normal is aligned with the surface normal N. Therefore, if $\alpha : [a, b] :\to \mathcal{D}$ is a curve whose image on S is a geodesic then

$$\frac{d^2\alpha(s)}{ds^2} = \kappa\mathbf{N},$$

where κ is the curvature of α. Consequently, as measurable from the surface, the curve has zero curvature. If we again let (u^1, u^2) denote the parametrization variables of the surface then it follows from Gauss's equations (A.5.1) that

$$\begin{aligned}\frac{d^2\mathbf{x}(\alpha(s))}{ds^2} &= \frac{\partial^2\mathbf{x}}{\partial u^i \partial u^j}\frac{d\alpha^i(s)}{ds}\frac{d\alpha^j(s)}{ds} + \frac{\partial\mathbf{x}}{\partial u^j}\frac{\partial^2\alpha^j(s)}{ds^2} \\ &= \left(\frac{\partial\mathbf{x}}{\partial u^k}\Gamma^k_{ij} + \mathbf{h}_{ij}\mathbf{N}\right)\frac{d\alpha^i(s)}{ds}\frac{d\alpha^j(s)}{ds} + \frac{\partial\mathbf{x}}{\partial u^k}\frac{\partial^2\alpha^k(s)}{ds^2}.\end{aligned}$$

Therefore, a unit speed curve $\alpha(s)$ is a geodesic if and only if its components satisfy the following coupled system of differential equations

$$\frac{d^2\alpha^k(s)}{ds^2} + \Gamma^k_{ij}\frac{d\alpha^i(s)}{ds}\frac{d\alpha^j(s)}{ds} = 0. \tag{A.6.1}$$

The above differential equations are also the Euler-Lagrange equations corresponding to variation of the arc-length. Therefore, we have the following theorem which satisfies condition 1.

Theorem A.6.1. If $\alpha : [-\epsilon, \epsilon] \to \mathcal{D}$ is a unit-speed curve such that for any $a, b \in (-\epsilon, \epsilon)$, with $\mathbf{x}(\alpha(a)) = p$ and $\mathbf{x}(\alpha(b)) = q$, $\mathbf{x}(\alpha)$ is the curve of shortest distance joining p and q in S, then α is a geodesic.

Since the differential equations for a geodesic equations involve only the Christoffel symbols which only depend on the metric $\mathbf{g}$ it follows that geodesics are isometric invariants as well. Moreover, geodesics can also be defined on abstract surfaces independent of the existence of an isometric immersion.

The concept of a circle and polar coordinates can also be extended to a Riemannian manifold. For a Riemannian manifold $(\mathcal{D}, \mathbf{g})$, **geodesic polar coordinates** centered at $p \in \mathcal{D}$ are the natural analogs of the radial and polar coordinates defined on a Riemannian manifold. In these coordinates a neighborhood around p is parametrized by the coordinates (r, Ψ) which map to a point q satisfying $d(p, q) = r$ and q lies on a geodesic whose initial velocity vector makes an angle Ψ with a respect to a basis of the tangent plane at p. In these coordinates the metric $\mathbf{g}$ has components

$$g_{11} = 1, \quad g_{12} = g_{21} = 0, \quad g_{22} = G(r, \Psi),$$

where the function $G(r, \Psi)$ satisfies the following differential equation

$$K = -\frac{1}{\sqrt{G(r, \Psi)}} \frac{\partial^2 \sqrt{G(r, \Psi)}}{\partial r^2}. \tag{A.6.2}$$

If $K = K_0$ is constant and negative then the above differential equation can be solved to yield

$$G\,(r, \Psi) = \sinh(\sqrt{-K_0} r). \tag{A.6.3}$$

Additionally a **geodesic circle** of radius R centered at $p \in \mathcal{D}$ is defined to be the set $B_R(p) = \{q \in \mathcal{D} : d(p, q) = R\}$.

Appendix B

Fourth Order Finite Difference Approximations

Approximation to $\frac{df}{dx}$	Error
$\frac{3f(x-4h)-16f(x-3h)+36f(x-2h)-48f(x-h)+25f(x)}{12h}$	$-\frac{1}{5}h^4\frac{d^5f}{dx^5}$
$\frac{-f(x-3h)+6f(x-2h)-18f(x-h)+10f(x)+3f(x+h)}{12h}$	$\frac{1}{12}h^4\frac{d^5f}{dx^5}$
$\frac{f(x-2h)-8f(x-h)+8f(x+h)-f(x+2h)}{12h}$	$-\frac{1}{30}h^4\frac{d^5f}{dx^5}$
$\frac{-3f(x-h)-10f(x)+18f(x+h)-6f(x+2h)+f(x+3h)}{12h}$	$\frac{1}{20}h^4\frac{d^5f}{dx^5}$
$\frac{-25f(x)+48f(x+h)-36f(x+2h)+16f(x+3h)-3f(x+4h)}{12h}$	$-\frac{1}{5}h^4\frac{d^5f}{dx^5}$

Table B.1. Backward, centered, and forward approximations to the first derivative of a function $f(x)$ on a stencil of uniform width h.

Approximation to $\frac{d^2f}{dx^2}$	Error
$\frac{-10f(x-5h)+61f(x-4h)-156f(x-3h)+214f(x-2h)-154f(x-h)+45f(x)}{12h^2}$	$-\frac{137}{180}h^4\frac{d^6f}{dx^6}$
$\frac{f(x-4h)-6f(x-3h)+14f(x-2h)-4f(x-h)-15f(x)+10f(x+h)}{12h^2}$	$\frac{13}{180}h^4\frac{d^6f}{dx^6}$
$\frac{-f(x-2h)+16f(x-h)-30f(x)+16f(x+h)-f(x+2h)}{12h^2}$	$-\frac{1}{90}h^4\frac{d^6f}{dx^6}$
$\frac{10f(x-h)-15f(x)-4f(x+h)+14f(x+2h)-6f(x+3h)+f(x+4h)}{12h^2}$	$\frac{13}{180}h^4\frac{d^6f}{dx^6}$
$\frac{45f(x)-154f(x+h)+214f(x+2h)-156f(x+3h)+61f(x+4h)-10f(x+5h)}{12h^2}$	$-\frac{137}{180}h^4\frac{d^6f}{dx^6}$

Table B.2. Backward, centered, and forward approximations to the second derivative of a function $f(x)$ on a stencil of uniform width h.

Index

References

Abramowitz, M., & Stegun, I. A. (1964). *Handbook of mathematical functions with formulas, graphs, and mathematical tables*, vol. 55 of *National Bureau of Standards Applied Mathematics Series*. For sale by the Superintendent of Documents, U.S. Government Printing Office, Washington, D.C.

Alben, S., & Brenner, M. P. (2007). Self-assembly of flat sheets into closed surfaces. *Phys. Rev. E*, *75*, 056113.

Amar, M. B., & Goriely, A. (2005). Growth and instability in elastic tissues. *Journal of the Mechanics and Physics of Solids*, *53*(10), 2284 – 2319.

Amsler, M.-H. (1955). Des surfaces à courbure négative constante dans l'espace à trois dimensions et de leurs singularités. *Math. Ann.*, *130*, 234–256.

Arndt, K.-F., Kuckling, D., & Richter, A. (2000). Application of sensitive hydrogels in flow control. *Polymers for Advanced Technologies*, *11*(8-12), 496–505.

Audoly, B., & Boudaoud, A. (2002). 'Ruban à godets': an elastic model for ripples in plant leaves. *Comptes Rendus Mecanique*, *330*(12), 831 – 836.

Audoly, B., & Boudaoud, A. (2003). Self-similar structures near boundaries in strained systems. *Phys. Rev. Lett.*, *91*(8), 086105.

Bobenko, A., & Pinkall, U. (1999). Discretization of Surfaces and Integrable Systems. In *Discrete Integrable Geometry and Physics*, (pp. 3–58). Oxford: Clarendon Press.

Bobenko, A. I., & Eitner, U. (2000). *Painlevé equations in the differential geometry of surfaces*, vol. 1753 of *Lecture Notes in Mathematics*. Berlin: Springer-Verlag.

Bonnet, O. (1865). *Mémoire sur la théorie des surfaces applicables sur une surface donnée*. Gauthier-Villars.

Braides, A. (2002). Γ-*Convergence for Beginners*. Oxford University Press Inc., New York.

Brndsted, H., & Kopecek, J. (1991). Hydrogels for site-specific oral drug delivery: synthesis and characterization. *Biomaterials*, *12*(6), 584 – 592.

Burago, Y. D., Ivanov, S. V., & Malev, S. G. (2005). Remarks on Chebyshev coordinates. *Zap. Nauchn. Sem. S.-Peterburg. Otdel. Mat. Inst. Steklov. (POMI)*, *329*(Geom. i Topol. 9), 5–13, 195.

Carpi, F., & Smela, E. (2009). *Biomedical Applications of Electroactive Polymer Actuators*, (p. 476). John Wiley and Sons, Ltd.

Cerda, E., & Mahadevan, L. (2003). Geometry and physics of wrinkling. *Phys. Rev. Lett.*, *90*, 074302.

Chebychef, P. L. (1878). Sur la coupe des vetements.

Chen, G., Slemrod, M., & Wang, D. (2010). Isometric Immersions and Compensated Compactness. *Communications in Mathematical Physics*, *294*, 411–437.

Chen, Y.-c., & Hoger, A. (2000). Constitutive functions of elastic materials in finite growth and deformation. *Journal of Elasticity*, *59*, 175–193. 10.1023/A:1011061400438.

Ciarlet, P. G. (1980). A justification of the von kármán equations. *Arch. Rational Mech. Anal.*, *73*(4), 349–389.

Conti, S., & Maggi, F. (2008). Confining thin elastic sheets and folding paper. *Archive for Rational Mechanics and Analysis*, *187*, 1–48.

Davidovitch, B., Schroll, R. D., Vella, D., Adda-Bedia, M., & Cerda, E. A. (2011). Prototypical model for tensional wrinkling in thin sheets. *Proceedings of the National Academy of Sciences*, *108*(45), 18227–18232.

Dervaux, J., & Ben Amar, M. (2008). Morphogenesis of growing soft tissues. *Phys. Rev. Lett.*, *101*(6), 068101.

DiCarlo, A., & Quiligotti, S. (2002). Growth and balance. *Mechanics Research Communications*, *29*(6), 449 – 456.

Efimov, N. V. (1964). Generation of singularites on surfaces of negative curvature. *Mat. Sb. (N.S.)*, *64 (106)*, 286–320.

Efrati, E., Klein, Y., Aharoni, H., & Sharon, E. (2007). Spontaneous buckling of elastic sheets with a prescribed non-Euclidean metric. *Physica D: Nonlinear Phenomena*, *235*(1-2), 29 – 32. Physics and Mathematics of Growing Interfaces - In honor of Stan Richardson's discoveries in Laplacian Growth and related free boundary problem.

Efrati, E., Sharon, E., & Kupferman, R. (2009). Elastic theory of unconstrained non-Euclidean plates. *J. Mech. Phys. Solids*, *57*(4), 762–775.

Evans, L. C. (1990). *Weak convergence methods for nonlinear partial differential equations*. Published for the Conference Board of the Mathematical Sciences, Washington, DC.

Feil, H., Bae, Y. H., Feijen, J., & Kim, S. W. (1992). Mutual influence of ph and temperature on the swelling of ionizable and thermosensitive hydrogels. *Macromolecules*, *25*(20), 5528–5530.

Föppl, A. (1907). *Vorlesungen über technische Mechanik*. B.G. Teubner, Leipzig.

Frankel, T. (2003). *The Geometry of Physics: An Introduction, Second Edition*. Cambridge University Press, 2 ed.

Friesecke, G., James, R., & Muller, S. (2006). A hierarchy of plate models derived from nonlinear elasticity by gamma-convergence. *Arch. Rat. Mech. Analysis*, *180*, 183–236.

Goriely, A., & Ben Amar, M. (2005). Differential growth and instability in elastic shells. *Phys. Rev. Lett.*, *94*, 198103.

Goriely, A., Vandiver, R., & Destrade, M. (2008). Nonlinear euler buckling. *Proceedings of the Royal Society A: Mathematical, Physical and Engineering Science*, *464*(2099), 3003–3019.

Gray, A., Abbena, E., & Salamon, S. (2006). *Modern differential geometry of curves and surfaces with Mathematica*. Studies in Advanced Mathematics. Chapman & Hall/CRC, Boca Raton, FL, third ed.

Han, Q., & Hong, J.-X. (2006). *Isometric embedding of Riemannian manifolds in Euclidean spaces*, vol. 130 of *Mathematical Surveys and Monographs*. American Mathematical Society, Providence RI.

Hazzidakis, J. (1880). Ueberienge Iegenshaften der Flachen mit Constatem Krummungsmaass. *J. Reine Angew. Math. (Crelle)*, *88*.

Hilbert, D. (1901). Ueber Flächen von constanter Gaussscher Krümmung. *Trans. Amer. Math. Soc.*, *2*(1), 87–99.

Hoger, A. (1997). Virtual configurations and constitutive equations for residually stressed bodies with material symmetry. *Journal of Elasticity*, *48*, 125–144. 10.1023/A:1007459331524.

Holmes, D. P., Roche, M., Sinha, T., & Stone, H. A. (2011). Bending and twisting of soft materials by non-homogenous swelling. *Soft Matter*, *7*, 5188–5193.

Holmgren, E. (1902). Sur les surfaces á courbure constante négative. *C.R. Acad. Sci. Paris*, *134*, 740–743.

Hunter, J. K., & Nachtergaele, B. (2001). *Applied analysis*. River Edge, NJ: World Scientific Publishing Co. Inc.

Jin, W., & Sternberg, P. (2001). Energy estimates for the von Kármán model of thin-film blistering. *Journal of Mathematical Physics*, *42*, 192–199.

Jin, W., & Sternberg, P. (2002). In-plane displacements in thin-film blistering. *Proceedings of the Royal Society of Edinburgh, Section: A Mathematics*, *132*(04), 911–930.

Juodkazis, S., Mukai, N., Wakaki, R., Yamaguchi, A., Matsuo, S., & Misawa, H. (2000). Reversible phase transitions in polymer gels induced by radiation forces. *Nature*, *408*, 178–181.

Klein, Y., Efrati, E., & Sharon, E. (2007). Shaping of elastic sheets by prescription of non-Euclidean metrics. *Science*, *315*(5815), 1116–1120.

Klein, Y., Venkataramani, S., & Sharon, E. (2011). Experimental study of shape transitions and energy scaling in thin non-euclidean plates. *Phys. Rev. Lett.*, *106*(11), 118303.

Koenderink, J., & van Doorn, A. (1998). Shape from Chebyshef Nets. In *Burkhardt, H., Neumann, B. ECCV*, vol. 1407, (pp. 215–225). Springer, Heidelberg.

Kuiper, N. H. (1955). On C^1-isometric imbeddings. I, II. *Nederl. Akad. Wetensch. Proc. Ser. A.* **58** = *Indag. Math.*, *17*, 545–556, 683–689.

Lamb, H. (1889). On the deformation of an elastic shell. *Proceedings of the London Mathematical Society*, *s1-21*(1), 119–146.

Landau, L. D., & Lifshitz, E. M. (1986). *Course of theoretical physics. Vol. 7*. Oxford: Pergamon Press, third ed. Theory of elasticity, Translated from the Russian by J. B. Sykes and W. H. Reid.

Lee, J. (1997). *Riemannian manifolds: an introduction to curvature*. Graduate texts in mathematics. Springer.

Lewicka, M., Mahadevan, L., & Pakzad, M. R. (2011). The Föppl-von Kármán equations for plates with incompatible strains. *Proc. R. Soc. Lond. Ser. A Math. Phys. Eng. Sci.*, *467*(2126), 402–426.

Lewicka, M., & Pakzad, R. M. (2011). Scaling laws for non-euclidean plates and the $\mathrm{w}^{2,2}$ isometric immersions of riemannian metrics. *ESAIM: Control, Optimisation and Calculus of Variations*, *FirstView*.

Liang, H., & Mahadevan, L. (2009). The shape of a long leaf. *Proceedings of the National Academy of Sciences*, *106*(52), 22049–22054.

Lobkovsky, A. E. (1996). Boundary layer analysis of the ridge singularity in a thin plate. *Phys. Rev. E*, *53*, 3750–3759.

Lubarda, V., & Hoger, A. (2002). On the mechanics of solids with a growing mass. *International Journal of Solids and Structures*, *39*(18), 4627 – 4664.

Marder, M., & Papanicolaou, N. (2006). Geometry and elasticity of strips and flowers. *J. Stat. Phys.*, *125*(5-6), 1069–1096.

Marder, M., Sharon, E., Smith, S., & Roman, B. (2003). Theory of edges of leaves. *EPL (Europhysics Letters)*, *62*(4), 498.

MATLAB (2010). *version 7.10.0 (R2010a)*. Natick, Massachusetts: The MathWorks Inc.

Maz'ya, V. (2011). *Sobolev Spaces: With Applications to Elliptic Partial Differential Equations*. Grundlehren der mathematischen Wissenschaften Series. Springer.

McCleary, J. (1995). *Geometry from a Differentiable Viewpoint*. Cambridge University Press.

McLachlan, R. (1994). A gallery of constant-negative-curvature surfaces. *Math. Intelligencer*, *16*(4), 31–37.

McMahon, J. (2009). *Geometry and Mechanics of Growing, Nonlinearly Elastic Plates and Membranes*. Ph.D. thesis, The University of Arizona, Tucson, Arizona.

Minding, F. (1839). Wie sich entscheiden läBt, ob zwei gegebene krumme Flächen auf einander abwickelbar sind oder nicht; nebst Bemerkungen über die Fláchen von unveränderlichem Krümmungsmabe. *(Crelle) Journal der Mathematic*, *1*, 370–87.

Mora, T., & Boudaoud, A. (2006). Buckling of swelling gels. *The European Physical Journal E: Soft Matter and Biological Physics*, *20*, 119–124.

Müller, S. (1999). Variational models for microstructure and phase transitions. In *Calculus of variations and geometric evolution problems (Cetraro, 1996)*, (pp. 85–210). Berlin: Springer.

Nash, J. (1954). C^1 isometric imbeddings. *Ann. of Math. (2)*, *60*, 383–396.

Payne, L., & Weinberger, H. (1960). An optimal poincar inequality for convex domains. *Archive for Rational Mechanics and Analysis*, *5*, 286–292.

Pedregal, P. (1999). Optimization, relaxation and Young measures. *Bull. Amer. Math. Soc. (N.S.)*, *36*(1), 27–58.

Polyanin, A. D., & Zaitsev, V. F. (2004). *Handbook of nonlinear partial differential equations*. Chapman & Hall/CRC, Boca Raton, FL.

Poznyak, E. G. (1973). Isometric immersions of two-dimensional riemannian metrics in euclidean space. *Russian Mathematical Surveys*, *28*(4), 47.

Richter, A., Klenke, C., & Arndt, K.-F. (2004). Adjustable low dynamic pumps based on hydrogels. *Macromolecular Symposia*, *210*(1), 377–384.

Richter, A., Paschew, G., Klatt, S., Lienig, J., Arndt, K.-F., & Adler, H.-J. P. (2008). Review on hydrogel-based ph sensors and microsensors. *Sensors*, *8*(1), 561–581.

Rodriguez, E. K., Hoger, A., & McCulloch, A. D. (1994). Stress-dependent finite growth in soft elastic tissues. *Journal of Biomechanics*, *27*(4), 455 – 467.

Rowley, J. A., Madlambayan, G., & Mooney, D. J. (1999). Alginate hydrogels as synthetic extracellular matrix materials. *Biomaterials*, *20*(1), 45 – 53.

Rozendorn, E. (1989). Surfaces of Negative Curvature. In V. Z. Y.D. Burago (Ed.) *Encylcopedia of Mathematical Sciences: Geometry III*, vol. 48, (p. 113). Springer-Verlag.

Santangelo, C. D. (2009). Buckling thin disks and ribbons with non-euclidean metrics. *EPL (Europhysics Letters)*, *86*(3), 34003.

Schmidt, O. G., & Eberl, K. (2001). Nanotechnology: Thin solid films roll up into nanotubes. *Nature*, *410*, 168–+.

Sharon, E., Marder, M., & Swinney, H. (2004). Leaves, flowers and garbage bags: Making waves. *American Scientist*, *92*(3), 254–261.

Sharon, E., Roman, B., Marder, M., Shin, G., & Swinney, H. (2002). Buckling cascades in free sheets. *Nature*, *419*(5), 579–579.

Spivak, M. (1979). *A comprehensive introduction to differential geometry. Vol. II*. Wilmington, Del.: Publish or Perish Inc., second ed.

Szilard, R. (2004). *Theories and applications of plate analysis: classical, numerical, and engineering methods*. John Wiley.

Trejo, M., Amar, M. B., & Müller, M. M. (2009). Hamiltonian formulation of surfaces with constant gaussian curvature. *Journal of Physics A: Mathematical and Theoretical*, *42*(42), 425204.

Vandiver, R., & Goriely, A. (2008). Tissue tension and axial growth of cylindrical structures in plants and elastic tissues. *EPL (Europhysics Letters)*, *84*(5), 58004.

Venkataramani, S. C. (2004). Lower bounds for the energy in a crumpled elastic sheet a minimal ridge. *Nonlinearity*, *17*(1), 301.

Willmore, T. J. (1982). *Total curvature in Riemannian geometry*. Ellis Horwood Series: Mathematics and its Applications. Chichester: Ellis Horwood Ltd.

Yu, C., Mutlu, S., Selvaganapathy, P., Mastrangelo, C. H., Svec, F., & Frchet, J. M. J. (2003). Flow control valves for analytical microfluidic chips without mechanical parts based on thermally responsive monolithic polymers. *Analytical Chemistry*, *75*(8), 1958–1961.

Zhang, X., Guo, T., & Zhang, Y. (2010). Formation of gears through buckling multilayered filmhydrogel structures. *Thin Solid Films*, *518*(21), 6048 – 6051.